Cronfa
Swansea University's Research Repository

Enhanced Osteogenesis by Combining Exogenous BMPs with Hydroxyapatite/Calcium Carbonate Bone Grafts: *In Vitro* and *In Vivo* Study

Swansea University
Prifysgol Abertawe

Medical School
Ysgol Feddygaeth

Lu Hong

Submitted to Swansea University in fulfilment of the requirements for the Degree of Doctor of Medicine

Swansea University

2024

Copyright: The Author, Lu Hong, 2024. Licensed under the terms of a Creative Commons Attribution-No-Derivatives (CC-BY-ND) license. Third party content is excluded for use under the license terms.

Abstract

Bone grafts play a crucial role in the restoration of substantial bone defects. However, the scarcity of natural sources necessitated alternative solutions. Hydroxyapatite/calcium carbonate (HA/CC) scaffolds, while biocompatible and resorbable, lack the inherent growth factors and associated osteogenic properties found in natural grafts. Therefore, this study focused on evaluating the suitability of bone graft substitute (BGS) made of HA and CC for osteogenesis after incorporating bone morphogenetic protein (BMP)-2/7. It is hypothesized that artificial allografts can be developed through the decellularization of BGS scaffolds cocultured with human umbilical mesenchymal stem cells (HUMSCs) and human embryonic kidney 293T (HEK-293T) cells expressing BMP-2/7. The hypothesis was tested using objectives (1) Develop tissue engineering products using HA/CC and MSCs and BMP-2/7, (2) Assess osteogenesis enhancement by HEK cells expressing BMP-2/7, (3) Decellularisation of the constructed HA/CC scaffold cocultured with MSCs and the modified HEK cells to produce artificial allograft (4) *In vivo* assessment of the osteogenic potential of the artificial allograft.

Initially, HUMSCs were isolated form umblical cord and subcultured successfully. The HUMSCs and immortalised MSCs (MSC-TERT) were cultured with HA/CC particles and attached to the HA/CC scaffold, which was observed by scanning electron microscopy (SEM) and analysed by AlarmarBlue and Cell Counting Kit-8 (CCK-8). Nodules formed by culturing MSCs and particles were confirmed for the biocompatibility of the particles through calcin staining observed by confocal microscopy.

HEK-293T cells were transfected successfully with plasmids which carry the BMP-2&BMP-7 genes, which could induce cells produce proteins for promoting bone formation. The transfected HEK-293T cells were assessed using ELISA, demonstrating that they could produce and release BMP-2 at 10 ng/ml and BMP-7 at 5 ng/ml into the media. This concentration is much higher than normal osteocytes can provide. Confocal fluorescence microscopy and scanning electron microscopy (SEM) analysis revealed the nodules formed after coculturing MSCs with modified HEK-293T cells and the HA/CC scaffolds. When BMP-2 and BMP-7 levels were analysed by ELISA in the constructed HA/CC after decellularisation, they showed that the nodules formed contained BMP-2 and BMP-7 which are sufficient for bone formation.

The constructed MSCs + HEK-293T-BMP 2/7+ HA/CC modifiued nodules were implanted between the tibia and fibula of mice and analysed for osteogenesis at specific time points. The micro-computer tomography (CT) results revealed that the HA/CC scaffolds cocultured with MSCs and HEKs facilitated the formation of more new bone callous in mice when compared to groups cultured with only MSCs or no cells at all. This resulted in a significant increase in new bone volume and osteogenic marker gene expression. Osteogenesis and osteogenic marker gene expression were assessed by histochemical staining (Toluidine Blue and Masson-Goldner's trichrome stainings) and qPCR, respectively. In conclusion, the findings of this study revealed that bioactive factors (BMP-2, BMP-7 and extracellular matrix) could be incorporated into the BGS scaffolds by attaching to the HA/CC and promoting the osteogenesis process.

Declaration and Statements

DECLARATION
This work has not previously been accepted in substance for any degree and is not being concurrently submitted in candidature for any degree.

Signed ..... [redacted] ..... Date .....01/02/2024.....

STATEMENT 1
This thesis is the result of my own investigations, except where otherwise stated. Where correction services have been used, the extent and nature of the correction is clearly marked in a footnote(s).
Other sources are acknowledged by footnotes giving explicit references. A bibliography is appended.

Signed ..... [redacted] ..... Date ..... 01/02/2024.....

STATEMENT 2
I hereby give consent for my thesis, if accepted, to be available for photocopying and for inter-library loans after expiry of a bar on access approved by the Swansea University.

Signed ..... [redacted] ..... Date ..... 01/02/2024.....

Acknowledgement

The day has finally arrived.

Firstly, this MD would not have been possible without the funding from the Life Sciences Research Network Wales.

I extend my deepest appreciation to my supervisor, Prof Venkat, for your guidance and support throughout my research work in the UK.

To Dao, thank you for imparting the knowledge I needed; this achievement would not have been possible without you! To James, my co-supervisor, I am immensely grateful for your assistance during my work; your training was crucial to the vital aspects of my research.

Emma, your constant presence and friendship have been invaluable. Words cannot express my gratitude for your help in my study and work in the UK. I feel fortunate to have gained lifelong friends in all of you. I will miss our coffees and dinner parties, and I will never forget the support and collaboration during challenging times.

Victoria, a special thank you for your endless patience in the lab and for helping me find medicines for Covid-19. I will miss our coffees and conversations.

To Yuexi Guo and Xiao Li, I cannot thank you enough for your support during the entire COVID-19 period. As colleagues and friends, your encouragement and the numerous dinner parties and hotpots helped me get through the tough times.

Finally, to my family, friends, and colleagues who provided unwavering support back home. A special thanks to my wife, Qiuyuan Wang, and my son, Ryan, for your spiritual and material support throughout my overseas studies. Please forgive me for being away for so long. I hope to make you all proud!

Table of Contents

Abstract ***2***

Declaration and Statements ***4***

Acknowledgement ***5***

List of Figures ***10***

List of Tables ***11***

Abbreviations ***12***

Chapter 1:General Introduction ***16***

1.1 Background **17**

1.2 Objectives of this study: **19**

Chapter 2: Literature Review ***22***

2.1 Introduction **23**

2.2 Bone tissue engineering **26**

2.2.1 Design methods for porous structures 26

2.2.2 The porosity of scaffolds 30

2.2.3 Fabrication of scaffolds 33

2.2.4 Bio-factors binding with scaffold to promote osteogenesis 35

2.2.5 Perspectives of artificial bone allografts 40

2.3 Mesenchymal stem cells **41**

2.4 Decellularisation **41**

2.4.1 Decellularisation through Physical Means 43

2.4.2 Biological enzymes for decellularisation 44

2.4.3 Chemical methods for decellularisation 44

2.5 Process of Bone Healing **45**

2.6 Undecalcified Tissue Section **46**

2.7 Transformation **48**

2.8 Transduction **48**

2.9 Transfection **49**

2.10 Conclusion **49**

Chapter 3: Material and Methods ***51***

3.1 Materials **52**

3.1.1 Chemical and reagents 52

3.1.2 Double distilled water (ddH_2O) 53

3.1.3 Umbilical Cord Tissue Samples 53

3.1.4 Cell Lines 53

3.1.4.1 MSC-TERT 53

3.1.4.2 HEK293T 53

3.1.5 Plasmids 53

3.1.5.1 The plasmids from Addgene 53

3.1.5.2 The plasmids from Vector Builder 54

3.1.6 Gene Sequences 55

3.1.6.1 Human BMP-2 (Accession: NM_001200 [https://www.ncbi.nlm.nih.gov/]) 55

3.1.6.2 Human BMP-7 56
3.1.7 Primers 56

3.2 Methods 57
3.2.1 Umbilical Cord Tissue Dissection 57
3.2.2 Mesenchymal Stem Cells Culture 57
3.2.2.1 Cell Preservation 57
3.2.2.2 Reviving of Frozen Cells 58
3.2.2.3 Cell Viability 58
3.2.2.4 Cryopreservation 59
3.2.3 Scaffold Preparation 60
3.2.4 Alamar Blue Assay 60
3.2.5 CCK-8 Assay 60
3.2.6 Scanning Electron Microscopy 61
3.2.7 Osteogenic differentiation 61
3.2.8 ALP Staining 62
3.2.9 Oil Red Stain 62
3.2.10 Alizarin Red Stain 63
3.2.11 qPCR 63
3.2.11.1 RNA and Protein Extraction 63
3.2.11.2 Bicinchoninic Acid Assay (BCA) 64
3.2.11.3 cDNA Synthesis 65
3.2.11.4 qPCR Composition 65
3.2.11.5 Flow cytometry 67
3.2.12 Purification of Plasmid DNA 68
3.2.12.1 Transformation 68
3.2.12.2 Mini-prep 68
3.2.12.3 Midi-prep 69
3.2.12.4 Restrict Digestion of Plasmid DNA 71
3.2.12.5 Agarose gel electrophoresis 71
3.2.13 Transfection 72
3.2.13.1 Chemical method 72
3.2.13.2 Neon™ Electroporation 72
3.2.14 Transduce 74
3.2.15 Enzyme-linked immunosorbent assay (ELISA) 75
3.2.16 Cells Selection for Stable Cell Line 76
3.2.17 Confocal Microscopy 76
3.2.18 Histology of Undecalcificated Samples 76
3.2.19 Statistical Analysis 77

Chapter 4: 78

Culturing of Mesenchymal Stem cells and Preparation of Artificial Allograft 78

4.1 Introduction 79
4.1.1 Isolation and Culture of MSCs 79
4.1.2 Scaffold Biocompatibility Assessment 80
4.1.3 MSC Differentiation 80
4.1.4 Analysis of Osteogenic Genes Expression Level 81
4.1.5 Aim and Objective 81

4.2 Methods 83
4.2.1 Isolation of MSCs from Umbilical Cord (HUMSCs) 83
4.2.2 MSCs growth curve producing 83
4.2.3 Biocompatibility Assay 83
4.2.4 Osteogenic differentiation 85
4.2.5 Alkaline Phosphatase (ALP) Staining 85
4.2.6 Oil Red O Stain 86

4.2.7 Alizarin Red Stain 86
4.2.8 q-PCR 86

4.3 Results 88
4.3.1 HUMSC Isolation and Culturing 88
4.3.2 MSC growth curve 88
4.3.3 Scaffold Biocompatibility 89
4.3.4 Analysing Osteogenic Differentiation of HUMSCs 92
4.3.5 Analysis of HUMSCs differentiation to adipocytes and Osteocytes 95

4.4 Discussion 97
4.4.1 Isolation, Culture, and Growth Characteristics of HUMSCs 97
4.4.2 Biocompatibility of HA/CC 98
4.4.3 Osteogenetic differentiation potential of MSCs 99

4.5 Summary 102

CHAPTER 5: Osteogenesis Enhancement by Constructs for Osteogenetic Bone Allografts 103

5.1 Introduction 104

5.2 Hypothesis and Objectives 106

5.3 Materials and methods 107
5.3.1 Materials 107
5.3.2 Methods 107

5.4 Results 113
5.4.1 Restriction Digestion 113
5.4.2 Transduced MSC cells 114
5.4.3 The transduced MSCs expression of BMPs 116
5.4.4 Transfection of HEK-293T cells 117

5.5 Discussion 119

5.6 Summary 124

5.7 Conclusion 124

Chapter 6: 125

In vivo Assessment of the Osteogenic Potential of Exogenous BMP-enhanced HA/CC in Mice 125

6.1 Introduction 126

6.2 Materials and Methods 129
6.2.0. Materials 129
The materials required for this chapter are detailed in **Chapter 3**. 129
6.2.1. Preparation of MSC+HEK+HA/CC bone graft for implantation 129
6.2.2 Animal preparation 130
6.2.3 Implantation 130
6.2.4 Sample Harvesting 131
6.2.5 Micro-CT Scan 131
6.2.6 q-PCR 131
6.2.7 Histology of Undecalcified Samples 132
6.2.8 Statistical Analysis 132

6.3 Results 133
6.3.1 Characterisation of the MSC+HEK+HA/CC bone graft by confocal microscopy 133
6.3.2 The effect of decellularisation 133

6.3.3 Analysis of gross appearance and micro CT of the implanted MSC+HEK+HA/CC bone graft 134
6.3.4 Histological observations.....139
6.3.5 Expression of osteogenic markers: RUNX2, BMP-2 and BMP-7.....142
6.4 Discussion.....145
6.5 Summary 148
6.6 Conclusion 149
Chapter 7: General Discussion 150
7.1 Biocompatibility of HA/CC Scaffolds for Tissue Engineering 151
7.2 Differentiation Potential of BMP-2 152
7.3 Exogenus Expression of BMP-2 and BMP-7 in HEK293T and MSCs 152
7.4 *In Vivo* Assessment of Exogenous BMP Enhanced Osteogenesis of HA/CC in Mice.....154
7.5 Limitations of the Study 155
7.7 Summary 157
7.8 Conclusion 157
***Appendix 1*.....159**
***Appendix 2*.....160**
***Reference*.....161**

List of Figures

Figure 1.1 The figure illustrates the production of artificial allografts and the evaluation of the materials. 20
Figure 1.2 The figure illustrates the protocol for Osteogenic scaffold preparation and the precise implantation site in the mouse. 21
Figure 2.1 The physiological effect and binding location of BPs.....39
Figure 3.1. The plasmid map of BMP-expression vectors.....54
Figure 3.2. The plasmid map of BMP-expressing lentiviral vectors.....55
Figure 4.1. Visualisation of the umbilical cord, its dissection and isolation of MSCs from it.....88
Figure 4.2. The growth of MSCs with varying initial cell seeding densities over 6 days.....89
Figure 4.3 Visualising the HA/CC scaffold surface structure using SEM. 90
Figure 4.4 Effect of HA/CC scaffold on the viability of HUMSCs. 91
Figure 4.5. Assessing time-dependent differentiation of HUMSCs by ALP staining.....93
Figure 4.6. Analysis of the expression of Runx2 and Osteocalcin genes in osteogenically differentiated HUMSCs. 94
Figure 4.7. Osteogenic and adipogenic differentiation of HUMSC cells. 95
Figure 5.1 Plasmid transformed bacteria growth on LB-agar+kanamycin plate and restricted digestion results. 114
Figure 5.2 Expression of BMP-2 & BMP-7 in MSCs through lentiviral transduction. 115
Figure 5.3 Analysing the expression of BMP-2/7 in MSCs by ELISA. 116
Figure 5.4 Analysis of BMP-2 and BMP-7 expression in HEK-293T cells. 118
Figure 6.1 The protocol for osteogenic scaffold preparation, showing the precise implantation site in the mouse..... ***Error! Bookmark not defined.***
Figure 6.2 Morphological changes of HUMSCs adhering to scaffolds grown in cell culture medium. 133
Figure 6.3 SEM images of the surface of MSC-HEK+HA/CC before and after decellularisation.....134
Figure 6.4 Gross observations of new bone formation in mice. 135
Figure 6.5 Bone and calluses of mice post-operation scanned by micro-CT. 136
Figure 6.6 Analysis of quality of bone formation through micro-CT in mice implanted with HA/CC+MSC+HEK bone grafts. 137
Figure 6.7 Analysing time-dependent osteogenesis by Masson Goldner's trichrome-staining. 140
Figure 6.8 Toluidine Blue-staining of the implanted Tibial scaffolds. 142
Figure 6.9 Analysis of the expression of the osteogenic markers RUNX2, BMP-2 and BMP-7 in implanted tissues. 144

List of Tables

Table 2.1 Different structures design methods *29*
Table 2.2 Porosities and pore sizes of scaffolds for bone regeneration (pores are denoted either as range or as average pore size) *31*
Table 3.1. Human BMP-2 Forward and Reverse Primers. *56*
Table 3.2. Human BMP-7 Forward and Reverse Primers. *56*
Table 3.3. qPCR Forward and Reverse Primers Used in qPCR. *56*
Table 3.4. cDNA Synthesis Incubations. *65*
Table 3.5. RT-PCR Forward and Reverse Primers. *66*
Table 3.6. qPCR Running Conditions. *66*
Table 3.7. Transduce Reagents Amounts. *75*
Table 5.1 Transduce Reagents Amounts for this study *110*
Table 6.1 Experimental mouse groups *130*

Abbreviations

°C	Degrees Centigrade
μg	Microgram
μL	Microliter
μm	Micrometer
μM	Micromolar
α	Alpha
β	Beta
ATCC	American Type Culture Collection
BCA	Bicinchoninic Acid
BglII	Bacillus globigii II
BSA	Bovine Serum Albumin
Ca^{2+}	Calcium ions
CCK-8	Cell Counting Kit-8
cm	Centimeter
Co.	Company
CO_2	Carbon Dioxide
DAPI	4′, 6-Diamidio-2-Phenylindole
ddH_2O	Double Distilled Water
dL.	Deciliter
DMEM	Dulbecco's Modified Eagle's Medium
DMSO	Dimethyl Sulfoxide
DNA	Deoxyribonucleic Acid
E. *Coli*	*Escherichia coli*
ECM	Extracellular Matrix
EDTA	Ethylenediaminetetraacetic Acid
ELISA	Enzyme-Linked Immunosorbent Assay
ERK	Extracellular Signal-Related Kinase
FACS	Fluorescent Activated Cell Sorting
FBS	Fetal Bovine Serum
FDA	Food and Drug Administration

FSM	Full Serum Medium
FT	Flow-Through
g	Gram
GFP	Green Fluorescent Protein
GLP	Good Laboratory Practice
GTP	Guanosine Triphosphate
H+	Hydrogen
H_2O	Water
Hb	Haemoglobin
HCI	Hydrochloric Acid
HCT	Haematocrit
HEK293	Human Embryonic Kidney 293
HRP	Horseradish Peroxidase
HS	Heparan Sulphate
HUVEC	Human Umbilical Vein Endothelial Cell
IgG	Immunoglobulin G
IL	Interleukin
Inc.	Incorporated
IP	Immunoprecipitation
IPA	Isopropanol
kDa	Kilodalton
L	Litre
LAMP	Lysosome associated membrane protein
LB	Luria Broth
LCAT	Lecithin-Cholesterol Acyltransferase
Ltd.	Limited
m	Metre
M	Molar
m/Z	Mass-to-Charge
MFI	Median Fluorescent Intensity
mg	Milligram

MHC-II	Major Histocompatibility Complex Class-II
miRNA	Micro Ribonucleic Acid
mL	Millilitre
MLCK	Myosin Light Chain Kinase
mm	Millimetre
mM	Millimole
mmHg	Millimetres of Mercury
Mn	Molecular Weight
MP	Microparticle
mRNA	Messenger Ribonucleic Acid
ms	Millisecond
MWCO	Molecular Weight Cut Off
Na+	Sodium
Na2CO3	Sodium Carbonate
NaCl	Sodium Chloride
Nco I	Nocardia corallina I
NHS	National Health Service
nm	Nanometre
nM	Nanomolar
NO	Nitric Oxide
No.	Number
ns	Nanosecond
02	Oxygen
PAGE	Polyacrylamide Gel Electrophoresis
PBS	Phosphate Buffered Saline
PC	Phosphatidylcholine
PCR	Polymerase Chain Reaction
PEG	Polyethylene Glycol
PFA	Paraformaldehyde
PLA2	Phospholipase A2
POD	Post-Operative Day

PRE	Preoperative
PS	Phosphatidylserine
P-S	Penicillin-Streptomycin
PVDF	Polyvinylidene Fluoride
R&D	Research and Development
RFP	Red Fluorescent Protein
RIPA	Radioimmunoprecipitation Assay
RNA	Ribonucleic Acid
RPM	Revolutions per Minute
RT-PCR	Reverse Transcription-Polymerase Chain Reaction
RunX2	Runt-related transcription factor 2
SD	Standard Deviation
SDS	Sodium Dodecyl Sulphate
SEM	Scanning Electron Microscopy
SFM	Serum Free Medium
TBS	Tris-Buffered Saline
TEM	Transmission Electron Microscopy
TEMED	N,N,N',N',-Tetramethylethylenediamine
TF	Tissue Factor
TOF	Time of Flight
U	Units
U.K.	United Kingdom
U.S.A.	United States of America
UC	Ultracentrifugation
UF	Ultrafiltrate
UV	Ultraviolet
V	Volume
W	Weight
WBC	White Blood Cell

Chapter 1:General Introduction

1.1 Background

The field of regenerative medicine has witnessed remarkable advances in recent years, offering novel approaches to address substantial bone defects and explore innovative solutions beyond traditional treatments. Among the various strategies, the integration of hydroxyapatite/calcium carbonate (HA/CC) scaffolds with exogenous bone morphogenetic proteins (BMPs) has emerged as a promising avenue for enhancing osteogenesis. This could improve both the quality and speed of bone healing, improving patient outcomes and reducing patient discomfort(Kim et al., 2019; Rogers et al., 2015).

Bone grafts play an impotrant role in the restoration of extensive bone defects resulting from trauma, disease, or surgical interventions. However, the conventional sources of bone grafts, such as autografts and allografts, have limitations, including donor site morbidity and the risk of immunological rejection. This has spurred the exploration of alternative solutions that can overcome these challenges while promoting effective bone regeneration. In this context, the integration of synthetic scaffolds, particularly those composed of hydroxyapatite and calcium carbonate, has garnered attention for their biocompatibility and resorbable nature.

Hydroxyapatite, a key component of natural bone, provides a biomimetic environment that facilitates cell adhesion, proliferation, and differentiation (A. Singh et al., 2018). However, HA could take longer to absorb than required. Calcium carbonate complements this by contributing to the mechanical strength of the scaffold. The combination of these materials forms a scaffold that not only mimics the structural aspects of natural bone but also provides a conducive environment for cellular activities, making it an ideal candidate for tissue engineering applications. Subsequently, calcium carbonate degrades within an appropriate timeframe, allowing space for the proliferation of new bone cells.

The incorporation of exogenous BMPs into such scaffolds adds a layer of complexity and sophistication to the regenerative process (De Biase & Capanna, 2005). BMPs are signalling proteins that play a pivotal role in bone development and repair. They can

induce osteogenic differentiation of mesenchymal stem cells (MSCs) and promote bone matrix formation (García-Gareta et al., 2015). Harnessing the potential of BMPs within the context of tissue engineering offers a unique opportunity to accelerate and enhance the osteogenic capabilities of synthetic scaffolds.

The specific focus on BMP-2 and BMP-7 in this research stems from their well-established roles in bone formation. BMP-2 is known for its ability to stimulate osteoblastic differentiation and enhance bone regeneration, while BMP-7 exhibits multifaceted functions, including promoting osteogenic differentiation and inhibiting adipogenesis. By combining these two BMPs, the research aims to capitalise on their synergistic effects, creating a microenvironment that optimally supports osteogenesis.

The hypothesis underlying this study proposes that artificial allografts can be engineered by decellularising tissue constructs developed with HA/CC scaffolds co-cultured with human umbilical cord-derived MSCs (HUMSCs) and the embryonic kidney -293T (HEK-293T) cell line transfected with BMP-2 and BMP-7 genes. HEK-293T cells are readily transfectable and produce adequate amounts of BMP-2 and BMP-7. In contrast, while HUMSCs are more resistant to transduction, they can serve as the bioactive matrix. This hypothesis is grounded in the belief that the synergy between the scaffold, MSCs, and BMPs can culminate in a regenerative milieu capable of mimicking and, potentially, surpassing the regenerative capacity of natural bone grafts.

Overall, this research aims to develop advanced tissue constructs using HA/CC scaffolds and MSCs for bone regeneration while enhancing osteogenesis through BMP-2 and BMP-7 delivery. Additionally, the research will explore decellularisation to create a biocompatible matrix for regenerative applications and assess the constructs' osteogenic potential *in vitro*.

It is well known that synthetic materials lack bioactivity, while bioactive materials are limited in availability and come with additional constraints. Currently, there is a lack of a material that combines the advantages of synthetic materials with bioactivity. The

research direction in this field focuses on utilizing suitable artifical materials as carriers to incorporate bioactive factors.

1.2 Objectives of this study:

1 Tissue engineering constructs, which include scffolds and cells.

2 Enhancing the osteogenic ability of HA/CC scaffolds by BMP-2/7 transfected HEK cells

3 Decellularisation to MSCs + HEK-293T-BMP 2/7+ HA/CC

4 *In vivo* assessment of the osteogenic potential of the MSCs + HEK-293T-BMP 2/7+ HA/CC

A key aspect of this research involves the isolation and cultivation of MSCs from human umbilical cord tissue. MSCs, known for their multipotency and regenerative potential, serve as crucial contributors to tissue constructs (Lavrentieva et al., 2013; C. Zhang et al., 2022). The successful culture of MSCs together with scaffold particles proves that the scaffolds are biocompatible. An essential criterion for any successful tissue-engineering strategy, biocompatibility was further confirmed by confocal microscopy and AlamarBlue assays.

The transfection of HEK-293T cells with plasmids carrying BMP-2 and BMP-7 genes represents a sophisticated molecular intervention. This genetic modification equips the cells with the ability to produce and release BMP-2 and BMP-7 proteins, acting as potent inducers of bone formation (A. Bandyopadhyay et al., 2006). The subsequent ELISAs quantified the high concentrations of these proteins in the medium, thereby highlighting the success of the transfection process. The reliance on advanced imaging techniques, such as confocal and SEM images, offers a visual narrative of the nodules formed after culturing the scaffold with MSCs.

As the *in vitro* experimental results suggested that the combination of artificially synthesised scaffolds and active biological factors can promote the osteogenic differentiation of MSCs (Prasopthum et al., 2019), it was pertinent to further assess the *in vivo* osteogenic performance of these modified artificial allografts (AAs) through implantation experiments in mice. The *in vivo* experimental segment of this study involves the implantation of AAs in both control and experimental groups (Buser et al., 2016). Evaluation of the *in vivo* osteogenic performance of AAs was conducted through multidimensional assessments, including micro-CT analysis, histological staining of non-decalcified tissue sections, and qPCR evaluation of the expression of osteogenesis-related genes in the newly formed bone callus and surrounding soft tissues.

A general flow chart of this study can be seen in **Figures 1.1** and **1.2**.

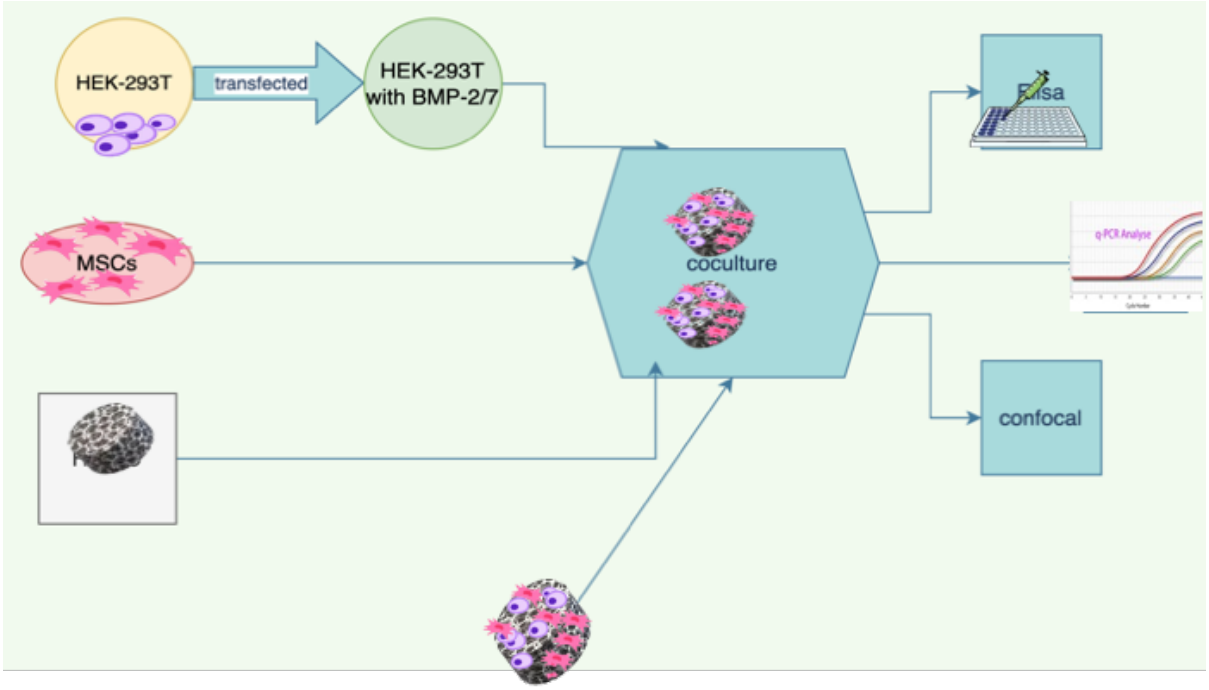

Figure 1.1 The figure illustrates the production of artificial allografts and the evaluation of the materials.

In this study, as depicted in **Figure 1.1**, HEK-293T cells transfected (see **section 3.2.13.1**)with MSC cells were co-cultured on HA/CC particles (see **section 6.2.1**). After 3 days of co-culture, MSC-HEK-293T-HA/CC complexes were subjected to ELISA (see **section 6.2.1**), qPCR , and observation under confocal microscopy to assess cell attachment to the particles (see **section 6.3.1**).

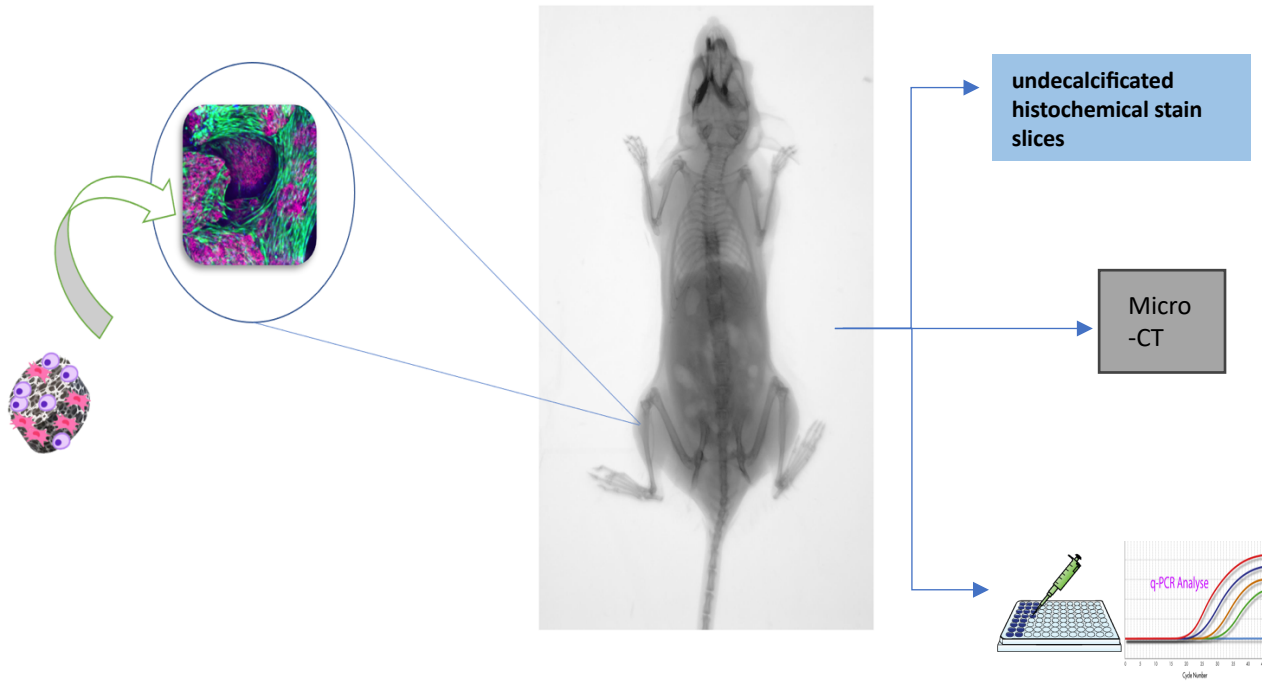

Figure 1.2 The figure illustrates the protocol for Osteogenic scaffold preparation and the precise implantation site in the mouse.

As illustrated in **Figure 1.2**, in the second part of the study, the MSC-HEK-293T-HA/CC particles obtained from the first part were decellularized (see **section 6.2.1** and section **6.3.2**), sterilized, and implanted into the anterior tibia of mice in an animal experiment (see **section 6.2.3**). Specimens were harvested on postoperative days 7, 14, and 28 (see **section 6.2.4**). Micro-CT evaluation was performed to assess bone formation around the implanted particles (see **section 6.2.5** and section **6.3.3**). Surrounding tissue samples were subjected to qPCR analysis (see **section 6.2.6**), and tibia specimens were embedded in poly(methyl methacrylate) (PMMA) resin for non-decalcified sectioning (see **section 6.2.7**). Masson-Goldner trichrome staining and toluidine blue staining were performed on the sections to evaluate bone formation (see **section 6.2.7** and **section 6.3.4**).

Chapter 2: Literature Review

2.1 Introduction

Currently, patients with bone defects may present with various medical conditions such as severe open and closed fractures, bone tumours, and chronic inflammation. The treatment of bone defects and non-unions requires suitable implants to fill the voids and facilitate bridging bone tissue growth(Brydone et al., 2010).

2.1.1 Challenges and Potential of Autologous Bone Grafts

As known, the skeletal system is an essential part of the human body. In the past, the role of human bones was considered to support body and protect human organs. With the deepening of research, researchers found that the complexity of the skeletal system itself and the role it plays in life activities are far beyond the previous imagination. Bone tissues are not static scaffolds after they are built. Instead, they are always in a slow dynamic equilibrium of old and new. The adult osteogenic tissue system, which appears to be stationary, can continue to maintain the strong support of bones in a slow metabolism. Bone tissue has many roles in the body's function, including mechanical, and chemical functions (Clarke, 2008). The skeletal system is also responsible for hematopoiesis and is an excellent repository of very large minerals and various growth factors. The solid bone possesses a self-healing ability, but defects beyond a certain size can complicate bone formation and lead to nonunion of the fracture. Under these certain situations, substitute materials that mimic bone tissue are required to treat the remarkable bone defects.

The autologous bone graft is most commonly used for bone regeneration. Because of its bioactivity, the autologous bone graft has osteoconductivity (Daniel et al., 2019; Z. Liu et al., 2020), osteoinductivity (García-Gareta et al., 2015; Ji et al., 2020), and biocompatibility, which makes the autograft an ideal choice for the treatment of bone defects. Clinically, many surgeons recommend autologous bone grafts as the “gold standard” for the treatment of bone defects (Damien & Parsons, 1991). During the procedure of autograft resorption, newly formed blood capillaries deliver mesenchymal stem cells into the area where they differentiate into osteogenic, chondrogenic, or other cell lines(Prasopthum et al., 2019; Stamnitz & Klimczak, 2021; White & Wallis, 2001). At the same time, these cells provide or produce cytokines such as bone morphogenetic proteins (BMPs), insulin-like growth factors (IGFs) and transforming growth factors (TGFs) which recruit more progenitor

cells for bone formation (Centrella et al., 1989; Groeneveld et al., 1999; Yakar et al., 2018). The biggest difficulty with autologous bone grafting is the limited source. Larger bone defects cannot be addressed because of the volume and mass of bone that can be provided. Additionally, the surgical injury and subsequent complications of the bone harvesting area also limit its clinical application. Additionally, the live replacement should be transplanted immediately, necessitating that the bone harvest and implantation happens in one operation, which expends both the time course of the procedure and the risk of infection.

2.1.2 Allografts and Xenografts

Two other options for the clinical treatment of bone defects are allografts(Baldwin et al., 2019; Buser et al., 2016; Lomas et al., 2013) and xenografts(Buser et al., 2016; McGovern et al., 2018; Perić Kačarević et al., 2018). Allografts are scaffolds obtained from living or dead human donors. The disadvantages of allografts lie in their limited availability and immuno-incompatibility (X. Shi et al., 2021; J. Wu et al., 2021). While allografts are decellularized, remaining antigens can cause an immune response. The ethical problem of using cadavers could be another issue in some countries. Some patients are apprehensive about the use of human cadavers and prefer a substitute where possible (Cherukuri et al., 2018).

Xenografts are the treated bone tissue from the animals which could bypass ethical issues (Bach et al., 1996; Szostakowski & DeMaio, 2020). It also has an obvious advantage in the source being very abundant. Because of the cross-species transplantation, however, this approach presents a more serious risk of immune rejection than allogeneic bone. There is chance that the disease itself carried by an animal can be transmitted via the implant. For example, bacteria and viruses including the Nguyen virus can be transmitted by animals(Perić Kačarević et al., 2018). Researchers or suppliers use extremely high or low temperatures to achieve strict sterilization, attempting to avoid the spread of the above-mentioned diseases, but this destroys many active factors and organic compounds originally existing in bone tissue, thereby reducing their effectivity and increasing the chances of poor effects after transplanting. Studies about the actual effects of xenografts have generated opposing conclusions (Charalambides et al., 2005; Denner, 2023), which

may deduce the viewpoints from the different aspects of the assay (Savolainen et al., 1994; Siqueira & Kranzler, 1982).

2.1.3 Advances in Synthetic Scaffolds for Bone Regeneration

The huge demand for bone grafts has spawned a massive market, with many available options due to the varying drawbacks and source limitations of natural graft materials (Bakhshandeh et al., 2017; Turco et al., 2018). Seeking and manufacturing various artificial synthetic substitutes has always been a hotspot pursued by many researchers in this field. The optimal synthetic material should simulate the advanced properties of natural materials as much as possible to achieve an osteogenic effect that is no less than that of allogeneic bone and autologous bone (Hettwer, 2017; Van Lieshout & Alt, 2016). Before simulating and fabricating bone materials, it is necessary to understand the structural composition and internalization of bone tissue itself.

Typical bone tissue is a long hollow shape consisting of unevenly distributed solid supporting tissue (Wehrli et al., 2006). Its structures, from outside to inside, are cortex, cancellous bone and marrow (Meyers et al., 2008). Many different cell types together compose bone tissue as a metabolically active tissue. Osteoblasts and osteocytes maintain bone health by sensing mechanical stress, regulating bone remodelling, and controlling mineral exchange, whereas, osteoclasts working to maintain a balance to osteoblasts. Osteoblasts are involved in bone construction and mineralization. The main function of osteoclasts is the reabsorption of old bone tissue, so that it may be rebuilt. Osteoblasts, osteocytes and osteoclasts (Tanaka-Kamioka et al., 1998) are all derived from osteoprogenitor cells. There are several non-osteo cells located in the bone marrow which are confirmed as hematopoietic stem cells (Eaves, 2015). These stem cells can transform into common blood cells which are white blood cells, red blood cells, and platelets. Building on this understanding of bone structure and cellular composition, the development of artificial scaffolds for bone engineering seeks to replicate these natural processes. To meet the vital criteria of skeleton tissue formation. Their physical mechanical properties, biocompatibility and biodegradability in remodelling should be similar to natural bone. To address these requirements, researchers have focused on developing composites with porous structure scaffolds and biofactors that can enhance osteogenesis and initiate self-repair. While progress has been made in creating various structures and

sizes of porous designs using additive manufacturing and CAD, technical issues still need to be addressed to accurately mimic the microstructure of natural bone tissues. Additionally, synthesizing and combining bio factors, such as BMPs, Platelet-derived growth factor (PDGF), and more recently, bisphosphonates (BPs), have shown great potential in enhancing the osteogenesis ability of the scaffolds (Cui et al., 2019). However, there are gaps that need to be bridged to satisfy the complex requirements of BPs combined with scaffolds as *in vivo* implants, such as achieving a controlled release rate to avoid significant impacts from burst release (Seshima et al., 2006). This review highlights the recent trend towards composite scaffolds, advanced computer-assisted techniques, and potent growth factors, which together show great promise for effectively addressing bone defects and improving bone health outcomes in clinical settings.

2.2 Bone tissue engineering

2.2.1 Design methods for porous structures

Aside from the material, a major factor in scaffold effectivity is its structure. The majority of mammals have a porous bone structure. The porosity reduces the weight of bone and allows space for cells and blood vessels, but undermines the strength at the same time (Guoqing et al., 2021; G. Zhang et al., 2019).

With the assistance of computers and specific software, engineers can design different types of porous structures. Duplicating and combining the units together allows researchers to construct complex artificial metal or composite material scaffolds. Zhang et al. (2018) used this method to design and create scaffolds with unique shapes, porosity, pore sizes and surface areas. A variety of standard unit libraries have been designed and collected to simulate the internal structure of real bones by combining and self-organizing assembly of various standard units.

Zhang et al. (2020) constructed 3-dimensional scaffolds via the Triple Periodic Minimal Surface (TPMS) method, which means that the minimal unit structure of the scaffold is periodically duplicated in three directions. Each designed unit could be described using a mathematical formula (Lv et al., 2021). For example, the G (Gyroid) structure of the TPMS equation could be expressed as $\varphi(x,y,z)=sin(\omega_x x)cos(\omega_y y)+sin(\omega_y y)cos(\omega_z z)+sin(\omega_z z)cos(\omega_x$

$x)=C$. By adjusting the threshold value, the pore size and surface area can be accurately regulated. Yoo believed that TMPS could mimic complex structures on microscale and various surfaces. Based on the TMPS, Ma et al. (2020) combined TMPS units with grid units to form a new heterogeneous hexahedral grid scaffold and via finite element analysis, they found that the strength, energy absorption and elastic modulus were promoted in hexahedral grid scaffolds compared to any of the uniform unit scaffolds (Ma et al., 2020).

Voronoi Tessellation is another mathematic application and algorithm in scaffold design (Agrawal et al., 2023). In this method, every duplicated cell is based on a seed or generator, consisting of all points of the plane or space closer to that seed than to any other. The surrounding structure is then generated by filling all the space between every two seeds or generators in any direction. Xiao, F., and Yin, X. have used this method to design scaffolds that more accurately mimic the internal structure and irregular pores of natural bone (F. Xiao & Yin, 2016). Some researchers noted that the difficulty in visualizing the porous scaffold causes the creation of complex structures using this method to be complicated (Su Wang et al., 2020).

Topology Optimization (TO) is another mathematical method which was used for the design of complex spacial material structures (Hassan & Calà Lesina, 2022). The advantage of this method is that it can maximize the system design and characteristics of the scaffold at the given conditions of boundary setting, space design setting, structure layout and so on. Based on finite elements, Xiao et al (2013). succeeded in the construction of scaffolds under limited volume with preconceived stiffness properties and an optimal porous structure via the topology optimization method (D. Xiao et al., 2013). As more detailed structures are generated to better mimic the complex natural bone structure, more calculations are needed. This forms the main disadvantage of the TO method, as a balance is required between structural design and efficient calculation (Chang et al., 2012; Dias et al., 2014).

A very common method is CT imaging, which involves analysis of data obtained through CT or magnetic resonance imaging (MRI) (Feinberg et al., 1999). CT scanning is a procedure in which a computerized X-ray machine emits radiation waves and receives the cross-sectional signals. A computer generates the CT images via the received data (Howell, 2021).

This data can then be used to regenerate 3D microstructures of bones or other kinds of tissues. Due to its usefulness and ease of use, this technique is used by many researchers and engineers. Because the data is obtained digitally, data describing the natural pore structure, size and shape are easily calculated. Ben and Fischer (2015) took advantage of CT images and combined their mathematic algorithms to ameliorate the model reconstructions (Ben Shabat & Fischer, 2015). Zheng et al (2020). regenerated skull models with trabecular structures mimicking the natural skull after scanning many skull samples (Zheng et al., 2020). In *ex vivo* experiments, these scaffolds were shown to have good interactions with cells. The thickness between each slice varies from 1-10 mm according to different models of CT machines. The drawback of CT imaging lies in the restriction of the CT image resolution. More accurate details of tissue need more rotations of X-ray scanning which would be followed by a large amount of data calculation and hazard of exposure to radiation (Earl & Badawy, 2019). Some porosities and pore sizes of scaffolds made are listed in **Table 2.1**.

Table 2.1 Different structures design methods

Construct method	Unit images	Materials	Ref.
CAD	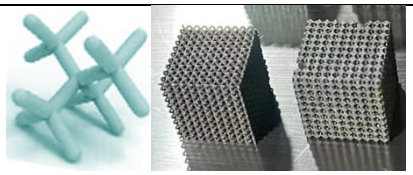	Ti-6Al-4V	(X.-Y. Zhang et al., 2020)
	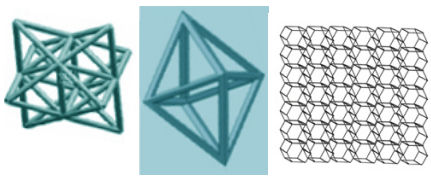	Ti-6Al-4V	(Jamshidinia et al., 2014)
TPMS	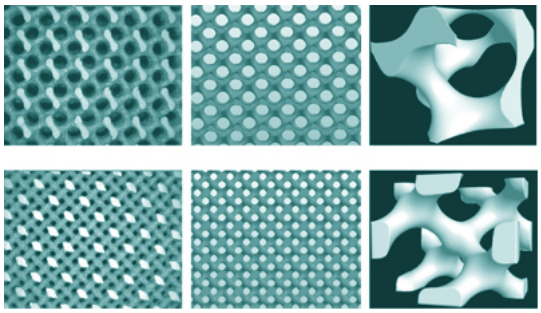	Ti-6Al-4V	(Y. Shi, Pan, et al., 2020)
Voronoi Tessellation	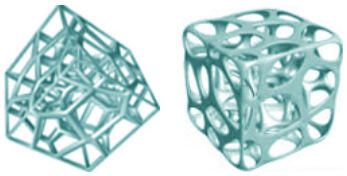	Virtual data	(Gómez et al., 2016)
Topology optimization	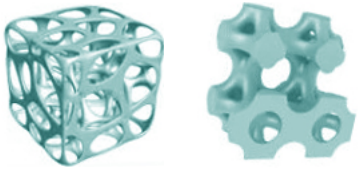	Ti-6Al-4V	(Challis et al., 2010)

CT imaging method	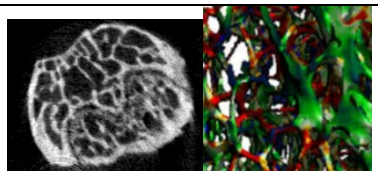	Virtual data	(Ben Shabat & Fischer, 2015)

CAD, Computer Assistant Design; TPMS, Triple Periodic Minimal Surface

2.2.2 The porosity of scaffolds

Among the many mechanical characteristics of scaffolds, the porosity is focused on by engineers. Human bone has a porous structure with various functions. Bone consists of an inorganic and organic matrix. The former is composed of mainly hydroxyapatite ($Ca_{10}(PO_4)_6(OH)_2$) crystals and calcium carbonate, while the organic matrix consists of nearly 95% type I Collagen (Marks & Odgren, 2002). Porosity allows for the use of as little mineralized material as possible to provide sufficient support, while also making the bones less heavy than full solid bone to reduce the burden on the muscles of the whole body. The porous structure is also important for bone vascularisation and innervation. Taking a classic long bone as an example, the pore size decreases sequentially from bone marrow tissue through cancellous bone to cortical bone. Under a pressure of up to 413.6×10^6 Pa, Doktor, T., et al (2011). use the mercury to measure the human trabecular bone by mercury intrusion porosimetry and concluded that the pore size of trabecular bone in the bone marrow ranged between 200μm and 300μm (Doktor et al., 2011). Meanwhile the pore size gradually decreases to 100-200μm (Hulbert et al., 1970) in the cortical bone, a dense zone containing haversian systems. Larger pores (100–150 and 150–200μm) are more likely to support the ingrowth of newly immigrated bone cells. Medium-sized pores (75–100μm)allow unmineralized osteoid tissue to grow while small pores (10–44 and 44–75μm) support the growth of fibrous tissue (van der Linden et al., 2001).

It is worth noting that the porous structure of real bone tissue is non-uniform. Until now it has not been described by any mathematical model, which shows its irregularity. However, the macroscopic arrangement of trabecular bone does follow the direction in which the skeletal tissue is stimulated by stress. In addition to the role of mechanical support, these pore structures are essential for cell growth and migration as well as vascularization

(Kusumbe et al., 2014). Distribution of the capillary network throughout the bones is crucuial for transporting nutrients and taking away metabolic wastes. The haversian systems mentioned above are also grown using this mechanism. Many biologically active factors such as bone morphogenetic proteins, extracellular matrix (ECM) and Insulin-like growth factor (IGF) etc. can freely shuttle and transport through the porous structure. As scaffolds, porous surfaces can provide an interface that facilitates cell anchoring, better supporting cell migration, fixation, and ingrowth. Kuboki et al. compared porous particles of hydroxyapatite with solid particles for BMP-2 delivery, and found that the formerled to more new bone formation than the latter in rat models (Y. Kuboki et al., 1998).

Table 2.2 Porosities and pore sizes of scaffolds for bone regeneration (pores are denoted either as range or as average pore size)

materials	Fabrication technique	Shape	Pore size (μm)	Porosity (%)	Application	References
gelatin	Gas foaming	scaffolds	280		L929 mouse fibroblasts cells *ex vivo*	(Poursamar et al., 2015)
Natural coral	Grinding	Cylinders	500	12± 4	Sheep bone marrow mesenchymal cells *ex vivo* and ectopic bone formation in sheeps	(Manassero et al., 2013)
Alginate hydrogel	3d plotting	Bone defects	210		Resin model of bone with defects	(L. Li et al., 2017)
Polyglycolic acid and tricalcium phosphate	Fused deposition modeling	Cylinders	400 and 5	89.6		(Xiong et al., 2002)
polycaprolactone (PCL)	Fused deposition modeling	Blocks	200	64.7	Osteogenesis in nude mice	(Shor et al., 2009)
Polyglycolic acid and beta-tricalcium phosphate	Solvent-casting and particle leaching	Cylinders	483.3± 113.6	88.4± 0.7%	Repairing of bone defects in rat femoral	(Cao & Kuboyama, 2010)

Polyglycolic acid and beta-tricalcium phosphate	Solvent-casting and particle leaching	Cylinders	504.2 ± 93.5	93.6± 2.0%	Repairing of bone defects in rat femoral	(Cao & Kuboyama, 2010)
Hydroxyapatite/ polylactic acid	3d plotting	Cylinders	500	60	*Ex vivo* coated with rabbit bone marrow mesenchymal cells and implant into rabbits forelimbs	(Z. Liu et al., 2020)
Ti–6Al–4V	Laser melting	Scaffold	560–1600, 480–1450	80-95		(Yan et al., 2015)
Alumina (Al2O3)	Sintering	Scaffold	100-500	50		(Vijayavenkataraman et al., 2020)
NiTi alloy	Laser melting	Scaffold	500	60		(Lv et al., 2022)

When Akay G., et al (2004). seeded primary rat osteoblasts into scaffolds with various pore sizes, they found more cells in the small 40 μm pores compared to in larger pores (Akay et al., 2004). They also found that rat cells migrated into the scaffolds faster with 100μm pores than in smaller sized pores. Based on their *in vitro* work, Akin F.A., et al (2001). concluded that human osteocytes could proliferate faster in TiO2 films on the titanium material scaffold of 0.4 and 13 μm in contrast to 49 μm size porous scaffold (Akin et al., 2001). Takahashi Y., et al (2004). applied rat mesenchymal stem cells to fiber fabric scaffold with small pores and found that cells had difficulty attaching to the material, and more spherical cells appeared (Takahashi & Tabata, 2004). They believe this to be caused by the small size of the fiber diameter (9 and 12 μm) compared to the size of rat MSCs.

Many studies also showed that variety of pore sizes affects the biological behaviors of bone cells *in vivo*. Kuboki, Y., et al. and Tsuruga, E., et al. compared rat cell proliferation on scaffolds with various pore sizes (106-200, 200-300, 300-400, 400-500, 500-600μm). The optimal results of Alkaline phosphatase activity, osteocalcin content and new bone volume were found in the group of hydroxyapatite blocks with 300-400 μm pore size (Yoshinori Kuboki et al., 2001; Tsuruga et al., 1997). The good performance of this pore size may be caused by the increased vascularization of the scaffolds. Further research noted that scaffolds with 200 μm pores showed more osseointegration compared to those with 300

μm pores. The contact surface area of the implants becomes larger as the pore size decreases, which contributes to osseointegration (Götz et al., 2004).
Another aspect of great interest regarding material pore size is the effect on bone regeneration. Kuboki, Y., et al (2001). designed scaffolds with honeycomb pores of different sizes and applied these scaffolds for BMP-2 delivery, then implanted them subcutaneously in rats(Yoshinori Kuboki et al., 2002; Yoshinori Kuboki et al., 2001). In the small hexagonal pores (90–120 μm) chondrogenesis was observed first, after which osteogenesis was initiated, whereas in the bigger tunnels (350 μm) of the scaffold osteogenesis occurred directly. A possible explanation is that the enhanced vascularization process based on the optimized size (350 μm) can ensure an adequate supply of oxygen tension and nutrients, which leads to better direct bone formation. The pore geometry of the scaffold can impact the direct osteogenesis as well, which is discussed later in this review. During their work, Kuboki, Y., et al (2002). concluded that the blocks with longer and curved pores only coated the newly forming bone on the surface as the result of poor penetration of rat cells and capillaries (Yoshinori Kuboki et al., 2002). In contrast, MSCs were able to penetrate deeper into particle-based structures.

2.2.3 Fabrication of scaffolds

Not only the design of scaffolds has its limitations. The manufacturing process imposes as many if not more, restrictions on the achievable structure of the final product. There are many different manufacturing methods available for various materials. In most cases, these methods attempt to create pores in an otherwise non-porous material.
To date, common scaffold fabrication techniques include solvent casting, particle leaching, freeze-drying, thermally induced phase separation, gas foaming, powder forming, sol-gel, and electrospinning (J. Zhang et al., 2021). Solvent casting and particle leaching involve dissolving a polymer with salt particles, followed by solvent evaporation and salt leaching to create a porous structure (Thavornyutikarn et al., 2014). However, these methods face

challenges such as toxic solvents and limited control over pore characteristics (Ghosal et al., 2018; Jahani et al., 2020). Gas foaming uses inert gases like CO2 or nitrogen to create porous biodegradable polymers with controlled pore sizes, offering advantages for tissue engineering applications (Poursamar et al., 2015).

Fused deposition modeling (FDM) is an additive manufacturing technique that involves the layer-by-layer deposition of thermoplastic materials to create three-dimensional objects. In FDM, a heated nozzle extrudes molten thermoplastic material onto a build platform, where it quickly solidifies to form a solid layer. The build platform is then lowered, and the process is repeated, layer by layer until the desired object is fully fabricated. FDM is widely used in various industries for rapid prototyping, functional part production, and creating complex geometries with high accuracy. The primary challenge associated with the FDM method is the need for pre-made fiber that possesses uniform sizes and material properties, which can be fed through the rollers and nozzle (Quero et al., 2021; Rajendran Royan et al., 2021).

3D printing, also known as additive manufacturing, is a revolutionary technique that involves the production of three-dimensional objects based on a digital model. It operates by gradually constructing successive layers of material, thereby enabling the creation of intricate designs and complex geometries that may pose challenges or limitations when using conventional manufacturing methods. The process begins with the utilization of computer-aided design (CAD) software to generate a virtual 3D model, which is then divided into thin layers. These layers are subsequently printed and stacked sequentially, utilizing a diverse array of materials such as plastics, metals, ceramics, and even biological cells. The outcome is a physical representation of the original digital model that exhibits high accuracy and precision. As the field of 3D printing continues to advance, a wide array of novel materials and machine designs are being implemented in the production of scaffolds for bone substituting (Cheng et al., 2021; S. Wang et al., 2022). These scaffolds serve as structural frameworks or support structures for various applications. This innovative approach incorporates diverse materials, ranging from traditional polymers and metals to more specialized substances like biocompatible materials and biomaterials. Despite its transformative potential, 3D printing has several drawbacks. Firstly, it can be an expensive technology, requiring substantial initial investments in printers and specialized

materials. Secondly, 3D printing suffers from limited production throughput, as the layer-by-layer process is time-consuming. The mechanical properties of 3D-printed objects may be inferior to those produced using other methods, primarily due to the layered structure (Ganguli et al., 2018; Murphy et al., 2020). Potential solutions to these challenges may be found in the innovative design of 3D printers and the development of new materials specifically tailored for 3D printing applications.

More advanced 3D printing is bio-ink printing. In bioprinting, small units of cells and biomaterials are dispensed with micrometer precision to create tissue-like structures using additive manufacturing. This technology provides accurate control over the distribution of cells, making it a promising tool for tissue engineering and regenerative medicine. Additionally, bioprinting is scalable and cost-effective, which further enhances its potential for widespread use (Duan et al., 2022; Gungor-Ozkerim et al., 2018; N. Li et al., 2021). Bioinks can be highly optimized mixtures of biomaterials for printed scaffolds, which promises a large variety of novel biomaterials for 3D printing. The practical applications of this field have been constrained by the scarcity of suitable bioinks. These bioinks must fulfil the specific criteria for bioprinting while also exhibiting the necessary bioactivity for diverse cell types (Matai et al., 2020). This disadvantage becomes even more evident when applied to cortical bone substitutions (Nie et al., 2022). Current bio-inks consist of soft materials, such as cells encapsulated in the hydrogel, that do not offer the mechanical strength required of bone scaffolds. In **Table 2.2** some scaffolds of a variety of designed methods with pictures are listed.

2.2.4 Bio-factors binding with scaffold to promote osteogenesis

Artificial scaffolds lack bio-factors which could promote osteogenesis, whereas these are present in natural grafts. Many engineers focus on bioactive molecules that play a key role in bone formation or the healing process (Safari et al., 2021). These molecules include osteogenic growth factors, hormones, cytokines and bioactive drugs, which are osteogenic and can substantially improve bone formation, regeneration and healing.

Among these growth factors, the BMP family is the most widely researched and used. BMP-2 is the most important growth factor in its family and has been authorized by the FDA. It has been applied clinically for decades, based on its safety and osteogenic effects which have been proved by many *in vitro* and *in vivo* experiments (Gillman & Jayasuriya, 2021).

BMPs which are members of the transforming growth factor-β (TGF-β) superfamily, induce ectopic chondrogenesis and progress osteogenesis via BMP receptors as well as theSmad1/5/8, MAP Kinase, and c-Jun N-terminal kinase (JNK) signal pathways (D. Chen et al., 1998; Nishimura et al., 2012; Tzameli et al., 2004). BMPs, like BMP-2, BMP-4, and BMP-7, promote osteoblast differentiation and bone regeneration. Besides bone development, they play roles in organ formation and wound healing. Clinically, BMPs are used in bone repair and spinal fusions, with BMP-2 and BMP-7 being FDA-approved. They signal through SMAD proteins to regulate cell growth and differentiation. Wang, L., et al (2019). used 3D plotters to fabricate 3d bone grafts particles and implanted them into rhesus monkey alveolar defects with BMP-2 gene vector, chitosan, and rhesus monkey bone marrow MSCs added. They found that the scaffolds with BMP-2 and MSCs could promote bone regeneration (L. Wang et al., 2019). Wei et al. combined BMP-2 with a gelatin sponge as a carrier to implant into mouse subcutaneous tissue and proved that BMP-2 can upregulate osteogenesis (Wei et al., 2017). Chen, Z., et al. coated β-tricalcium phosphate (TCP) scaffolds with magnesium to recruit macrophages, which promote osteogenesis indirectly through the secretion of BMP-2 and IL-1RA (Z. Chen et al., 2014). Lee, J., et al. (2019) believed that BMP-2 participates in many complex signalling processes and is involved in osteoimmunology, though possibly in a negative way when applied *in vivo* before fully understanding its role (J. Lee et al., 2019).

Another important growth factor for bone regeneration is Platelet-derived growth factor (PDGF), which plays a significant role in new blood vessel formation (Canalis et al., 1989). PDGF can recruit and proliferate fibroblasts, osteoblasts, tenocytes, and mesenchymal stem cells (Caplan & Correa, 2011; Lennon et al., 2018; Pham et al., 2022). These effects must work *in vivo* because the new blood vessel can only immigrate from existing capillary tissues. Zhang, Y., et al. delivered PDGF and BMP-7 with porous mesoporous-glass/silk scaffolds to treat femur defects in ovariectomised rats (Y. Zhang et al., 2012). They found

significant new bones regenerated in the defect places via the evaluation of bone volume from micro-CT. del Rosario, C., et al. (2015) treated rat calvarial defects with BMP-2 and PDGF-BB which were incorporated into thin layers of crosslinked alginate combined with beta-tricalcium phosphate scaffolds (del Rosario et al., 2015). Significant synergistic effects of osteogenesis and vascularization were observed 8-12 weeks after transplantation. PDGF has a main role in stimulating new vascular regeneration. As such, many researchers utilized PDGF incorporated with other cytokines to promote or enhance osteogenesis *in vivo*. In 2005, the FDA approved a bone graft (GEM 21S) of rh PDGF-BB with tricalcium phosphate, intended to be applied to dental defects for treatment (Gillman & Jayasuriya, 2021).

While PDGF is crucial in stimulating new vascular regeneration and enhancing osteogenesis in vivo, another key factor in bone healing is P-15, a peptide that significantly enhances cellular attachment and activity in osteogenic cells, further promoting bone formation (Qian & Bhatnagar, 1996). P-15's efficacy in promoting osteogenesis has been particularly evident in clinical applications such as iFactor, which was approved by the FDA for spinal fusion treatments. P-15 is a very small peptide sequence whose functional domain is type I collagen, responsible for cell attachment. It is known as P-15 because it is a composite of 15 amino acids (O'Brien et al., 2022). P-15 is thousands of times more active than other peptides in cells, especially in osteogenic cells when binding (Qian & Bhatnagar, 1996). Whenever the Osteogenic cell binding to P-15 activates specific molecules, the signalling pathways of the cells are stimulated to release growth factors and cytokines, thus accelerating the new bone formations. A clinic-applicated product of P-15 is iFactor, which combines inorganic scaffold via hydrogel carrier, used for fusion of anterior cervical discectomy since 2015 after its FDA-approval. Arnold et al. (2018) studied the adverse effects of 319 patients who accepted anterior cervical discectomy and fusion surgery with iFactor as allograft and found that the fusion of patients with iFactor is similar to the patients of autografts (Arnold et al., 2018). The study shows no differences between them in the adverse effects such as axial pain, postoperative radiculopathy, dysphagia and so on. However, the long-term side effects of the P-15 application need to be observed since it has been on the market for only a short time.

In addition to organic factors, bisphosphonates (BPs) are also used to treat bone defects. They are often applied directly to scaffolds for a local release (Endo et al., 2020; Ferretti et al., 1997; Wilkinson & Little, 2011). BPs have multiple functions, including regulating osteocytes and tissue (Carbone et al., 2014). Their structures are very stable analogues of pyrophosphate, which regulates bone resorption and calcification. They use P-C-P bonds to take the place of pyrophosphate's P-O-P structure to highly promote their ability of resistant to enzymatic hydrolysis (Ezra & Golomb, 2000). The bonding of different clustered structures produces different compounds with different functional effects and thus different therapeutic applications. BPs are often classified into two types, depending on whether they are nitrogen-containing or not. Nitrogen-containing BMPs generally have a stronger binding affinity compared to their nitrogen-free counterparts. They are also thought to function via different pathways. **Figure 2.1** shows the basic chemical structure and function of bisphosphates and their classifications based on with nitrogen or without nitrogen and their specific therapeutic effects (Benford et al., 1999). BPs' highly stable bidentate structure, which is formed by the connection of calcium irons and phosphate groups, shows a specific binding ability to bone hydroxyapatites. BPs are widely used clinically and have great effects in the treatment of osteoporosis and bone defects (Kajiwara et al., 2005). BPs are known to reduce osteoclast viability at a concentration of 10-4 M (Ding et al., 2022). A very well-known and widely used drug for the treatment of osteoporosis, zoledronic acid, has achieved great success (Koyama et al., 2020). However, the severe side effect of jaw osteonecrosis after long term application of Zoledronate strongly suggests that either oral or intravenous administration can cause unpredictable negative consequences (Gómez Font et al., 2008; John W. Hellstein & Marek, 2005; Marx, 2003). Many studies have combined BPs with scaffolds to locally release BPs at bone defect places where need higher working concentration to bypass osteochemonecrosis of jaw (J. W. Hellstein & Marek, 2006; Talbi et al., 2006). One common strategy of loading is to mix BPs into raw materials to fabricate composite scaffolds. S. Panzavolta, et al. mixed alendronate (ALN) and pamidronate (PAM) during the liquid phase of scaffold to sustained load drugs with osteoblasts *in vitro* (Panzavolta et al., 2009). Their study showed that scaffolds mixed with ALN and PAM facilitated cell proliferation and reduced osteoporosis via inhibiting osteoclast activities. α-TCP and β-TCP are very commonly used polymorphs of

substitutes for bone tissue based on their outstanding biodegradable and biocompatible properties (Amit Bandyopadhyay et al., 2006). BPs can very easily be bound to TCP scaffold fabricated via proper sintering method because of their natural chemical exchange. Then the TCP with BPs could be implanted into the host to fit the defect and release the chemical which could highly promote bone formation. The issue of the initial burst release of BPs from the scaffold has been immersed after many recent studies of applicating this kind of BPs-TCP scaffolds(Banerjee et al., 2010).

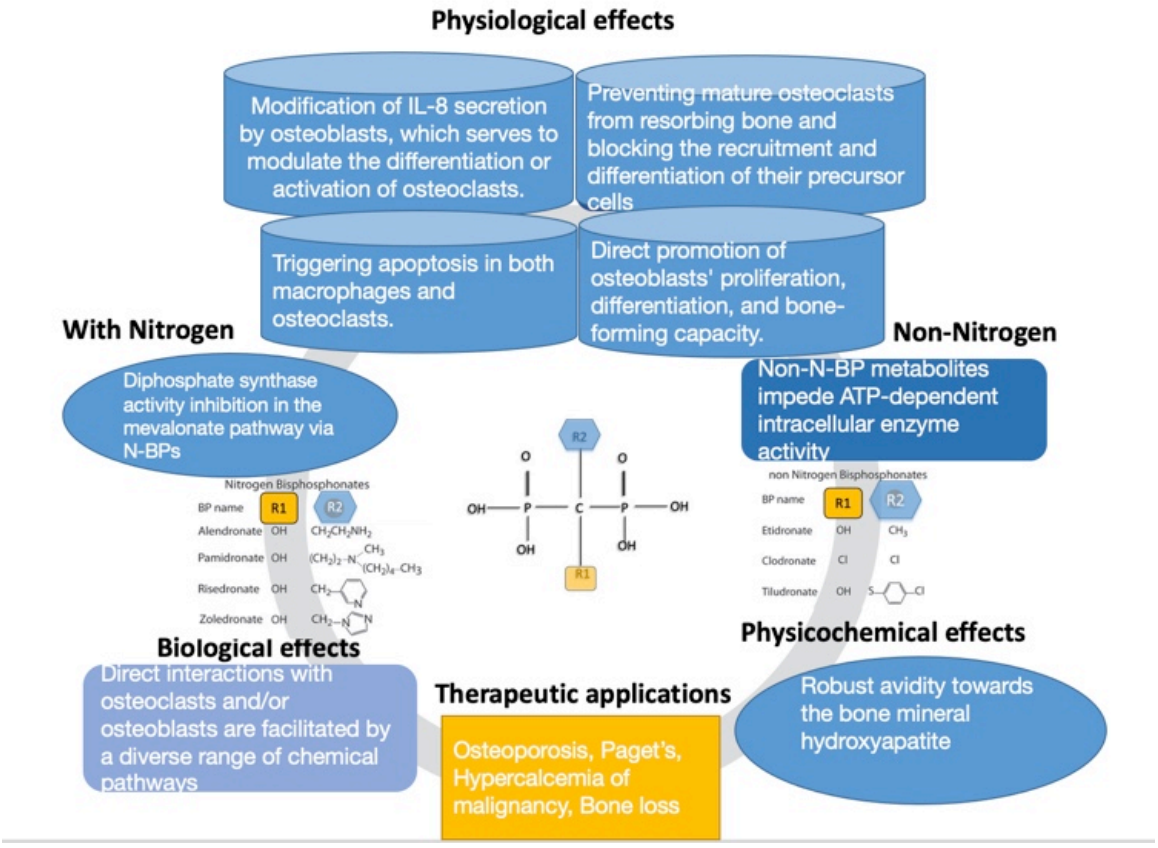

Figure 2.1 The physiological effect and binding location of BPs.
Earlier studies have indicated that the targeting and binding of BPs to HA is attributed to R1 groups, whereas the R2 side chains have a more resilient role in preventing bone resorption (Cattalini et al., 2012).

2.2.5 Perspectives of artificial bone allografts

There is a tremendous market need for bone allografts and bone autografts (Alghamdi & Jansen, 2020) for the application in severe bone defects, bone nonunion and osteoporosis (Weaver et al., 2019).

Orthopaedists always face the challenge of insufficient regeneration after operations of bone defects (Andrzejowski et al., 2020; Feng et al., 2021; Valtanen et al., 2021). Current research has more focus on composites with porous structure scaffolds and biofactors which could enhance osteogenesis to initiate osteogenesis and self-repair.

The good news is that there are many different structures and sizes of porous designs have been made in past decades. Many porous scaffolds are produced by additive manufacturing and CAD, and have great potential in the near future. However, many technical issues still need to be noticed in the field of mimicking the microstructure of natural bone tissues (Sarem et al., 2013). Any breakthrough in reducing the data calculation requirement or accelerating data processing in CT image adaptive model reconstruction would bring revolutionary changes in producing porous artificial scaffolds. Another focus of producing scaffolds is synthesizing and combining biofactors to enhance the osteogenesis ability of the scaffold. Except for the well-known biofactors such as BMPs and PDGF, the FDA also proved ifactor and BPs as clinical drugs for treatment. In the past decade, many studies have proved that BPs fabricated with multifunctional scaffolds showed great potential for osteogenesis. There are still noticeable gaps which need to be bridged to satisfy the complex requirements of BPs combined with scaffold as *in vivo* implants. One of the issues worth highlighting is to achieve the controlled release rate *in vivo* to avoid the burst release which could lead to significant impacts (Cattalini et al., 2012). A clear trend towards composite scaffolds shows that in recent years, with newly developed computer assistance techniques applied to the generation of porous bone substitute materials and more powerful growth factors combined with scaffolds, clinical treatment for bone defects and many other bone health issues could be addressed more effectively.

2.3 Mesenchymal stem cells

MSCs exhibit a broad spectrum of differentiation capabilities, having the capacity to differentiate into diverse cell types such as muscle cells, osteocytes, chondrocytes, adipocytes, and neural cells (Almalki & Agrawal, 2016). This versatile transdifferentiation potential positions MSCs as promising candidates for effective gene delivery in gene therapy applications targeting various tissues and organs.

In addition to their differentiation abilities, MSCs possess immunomodulatory advantages, characterized by low-level expression of major histocompatibility complex (MHC) class I and the absence of MHC-II, which help in mitigating immune responses following allograft treatments (Oh et al., 2022).

Moreover, MSCs exhibit inherent homing capabilities, enabling them to migrate towards sites of inflammation or injury in a process that is likely mediated by specific signalling cues (Ullah et al., 2019). This intrinsic ability can be utilized for precise and targeted gene delivery to specific locations, offering a strategic advantage in therapeutic applications.

Due to these inherent characteristics of MSCs and their differentiation potential have garnered widespread attention in osteogenesis research. Modifying MSCs to express or overexpress osteogenic-related genes and proteins can overcome the current limitations in bone research (Tjempakasari et al., 2021). For example, allografts have a limited source, and existing bone graft substitutes lack the ability for osteogenesis. Even the extracellular matrix of MSCs itself can facilitate the effective osteogenic differentiation of surrounding cells and the recruitment of osteogenic cells.

MSCs can be readily extracted from various sources, including muscle tissues, bone marrow, adipose tissue, and the umbilical cord. Through *in vitro* or *ex vivo* cultivation, these cells can be expanded on a substantial scale while preserving their stem cell characteristics. The clinical deployment of MSCs for therapeutic purposes offers several modalities, including localized transplantation, systemic delivery, or integration with tissue engineering strategies (Volarevic et al., 2018).

2.4 Decellularisation

Presently, there has been noteworthy progress in the advancement of decellularisation technology (Phothichailert et al., 2024). The extracellular matrix with scaffold, derived through the process of decellularisation, offers various discernible advantages compared to artificially manufactured scaffolds. These advantages include the provision of a more inherently supportive microenvironment for cellular proliferation and migration. Various methodologies have been devised to accomplish the decellularisation of tissue scaffolds, encompassing broad categorizations into chemical, biological, and physical approaches. Each technique is apt for eliminating distinct types of cells and tissues under different conditions.

2.4.1 Decellularisation through Physical Means

As advancements in decellularisation technology have progressed, the focus on physical decellularisation methods has gained prominence. These methods, involving diverse physical approaches such as variations in temperature, pressure, and electric shock dissociation, contribute to the preservation of the extracellular matrix. The term physical decellularisation pertains to the utilization of diverse physical methodologies for the elimination of cells, resulting in the preservation of the extracellular matrix. These methodologies encompass variations in temperature, pressure, and electric shock dissociation. Among these, the most commonly employed methods are freeze-thaw cycles (Arumugam et al., 2024).

Through the rapid freezing of tissue, the induction of numerous ice crystals within cells occurs. The augmented volume of these ice crystals, coupled with their sharp geometrical angles, has the potential to disrupt cellular membranes, consequently inducing cell lysis. Employing multiple iterations of freeze-thaw cycles provides effeciency in cell destruction, and when complemented with thorough washing, facilitates a homogenous decellularisation process. In addition, immersion and agitation can also effectively facilitate decellularisation. This method is often employed for relatively thin tissues, such as the small intestine and bladder. The duration of immersion and the intensity of agitation may need to be adjusted based on variations in tissue type and thickness. Multiple experimental adjustments are often required to achieve the optimal protocol.

Supercritical fluid (Lebedev et al., 2015), due to its distinctive pressure and temperature conditions, endows decellularisation agents with exceptional penetrating capability, enabling effortless dissociation and removal of cellular tissue. Among its representatives, supercritical carbon dioxide not only efficiently facilitates the decellularisation of diverse tissues but also excellently preserves the extracellular matrix (ECM) structure. Serving as an effective decalcifying agent, supercritical fluid is also employed in the sterilization processing of decellularised ECM (dECM).

2.4.2 Biological enzymes for decellularisation

Various enzymatic agents with biological activity can be employed in the decellularisation process. These include lipases, thermophilic proteases, β-glucosidases, nucleases, and pancreatic proteases. For instance, pancreatic protease can cleave the intercellular protein connections, facilitating the dissociation of cells from the scaffold. The reason for choosing biological enzymes for decellularisation is their ability to effectively remove cellular components from tissue matrices while preserving the native architecture and bioactive molecules (Blaudez et al., 2020). Biological enzymes, such as nucleases and proteases, specifically target DNA, RNA, and proteins, leading to thorough cell removal without damaging the extracellular matrix (ECM). This process ensures minimal disruption to the structural and functional integrity of the tissue, making it suitable for various biomedical applications, including tissue engineering and regenerative medicine. Additionally, biological enzymes offer a safer and more controlled method compared to chemical agents, reducing the risk of residual toxicity and immunogenicity in the decellularized ECM. One disadvantage of using biological enzymes for decellularisation is their potential to degrade or alter the composition of the extracellular matrix (ECM) components. Additionally, the enzymatic process may require longer incubation times and multiple enzyme treatments to achieve thorough decellularisation, which can prolong the overall process and increase the cost.

2.4.3 Chemical methods for decellularisation

Specific chemical agents or combinations of chemical agents are commonly employed for decellularisation. The choice of particular chemical agents is often tailored to the characteristics, thickness, and distinct extracellular matrix of the tissue or organ under consideration (Grauss et al., 2005). Currently, available chemical agents for decellularisation include acidic agents, alkaline agents, ion detergents, non-ionic

detergents, and amphoteric detergents. Chemical agents provide numerous advantages for decellularisation. Firstly, they exhibit versatility by effectively removing cellular components from various tissues and organs, rendering them suitable for a wide range of biological materials. Additionally, chemical methods ensure consistency, yielding reproducible results and enabling the establishment of standardised decellularisation protocols. Moreover, these agents offer scalability, as they are cost-effective and readily accessible in large quantities, thereby facilitating efficient large-scale decellularisation processes. The chemical method of decellularisation presents several drawbacks. These include the risk of residual toxicity from chemical agents, incomplete removal of cellular components, potential structural damage to ECM, and the complexity of multi-step protocols with long incubation periods (León-Félix et al., 2024).

2.5 Process of Bone Healing

The tissue morphology of bone repair undergoes the following processes: Impaired blood supply at the site of bone defect leads to the formation of a hematoma in the vicinity of the fracture (Marsell & Einhorn, 2011). Progenitor cells within the periosteum are recruited and differentiate into osteoblasts, aiding in intramembranous ossification in regions where intact blood supply persists (Berendsen & Olsen, 2015); alternatively, they may differentiate into chondrocytes, assisting in endochondral ossification in hypoxic regions near the fracture. As robust bone matrix mineralization occurs at the distal end of the fracture where the blood supply is strong, intramembranous ossification continues. With the support of forming cartilaginous tissue, an expanding cartilaginous callus is formed as more chondrocytes contribute, and simultaneous endochondral ossification takes place. The cartilaginous tissue continues to mature, ultimately forming a bony callus enveloping the closest portion of the fracture.

The process of bone formation can be delineated into two primary modalities. The first involves the direct ossification pathway, wherein mesenchymal stem cells initially differentiate into translucent cartilage, which undergoes continuous growth and progressively undergoes mineralization to transform into bone. This mode of bone

formation is prevalent in both humans and the majority of mammals. The second modality entails the direct ossification of mesenchymal stem cells, commonly referred to as intramembranous ossification (Batoon et al., 2019). However, this method contributes to the formation of a limited proportion of bones. In addition to the natural embryonic development of bones, our emphasis is predominantly directed towards the intricacies of new bone formation within the context of bone defect repair and the ensuing bone healing process.

Presently, the prevailing consensus among scholars asserts the occurrence of both scenarios during the process of fracture repair (Berendsen & Olsen, 2015). Impaired blood supply at the site of bone defect leads to the formation of a hematoma, recruiting precursor cells from the local periosteum that differentiate into osteoblasts, thereby facilitating intramembranous ossification in areas where the blood supply remains intact. Concurrently, within hypoxic regions, differentiation of these cells into chondrocytes is promoted, aiding in endochondral ossification within the cartilaginous framework of the fracture site. The osteogenesis observed following the implantation of nodules in our experiment is also considered to encompass both forms of ossification, the only distinction lying in the varying proportions of their contribution.

2.6 Undecalcified Tissue Section

Since Donath introduced the hard tissue section technique in 1982, it has revolutionized conventional methods for processing teeth and jawbone tissues, eliminating the prerequisite decalcification step for sectioning teeth and bone tissues with attached soft tissues(Donath & Breuner, 1982). This advancement allows for the preparation of thin slices without decalcification, facilitating histological staining examinations.
The hard tissue section technique was designed for the histological assessment of jawbones containing implants (ceramic or metal) in teeth or bones. The method involves embedding undecalcified bone specimens in acrylic resin and sectioning them into 100 to 150 µm using a sawing process. Subsequently, specialized machinery automatically grinds

the sections to a thickness of 5-10 µm. These sections can then be stained using various histological stains to highlight different tissue components, providing detailed insights into the tissue's structure and composition.

Undecalcified tissue sectioning is particularly advantageous when studying conditions like osteoporosis, bone tumours, and other diseases affecting the mineralized tissues. It allows researchers and pathologists to observe the spatial distribution of mineralized and unmineralized tissues, providing a more accurate representation of the tissue's natural state compared to decalcified sections (Bemenderfer et al., 2021).

The application of the hard tissue sectioning technique in this study has made histological research on previously deemed non-sectionable hard tissue specimens feasible. These specimens include bone with metal or ceramic implants, teeth with fillings, crowns, and bridges, as well as thick bone cortices (Gore & Abbott, 1964). By employing this sectioning technique, hard tissue specimens can be directly sliced into thin sections of 5-15 µm for histological observation. The hard tissue sectioning technique preserves the integrity of tissue interfaces, including those of implants, and the surrounding soft tissues.

Another characteristic of the hard tissue sectioning technique is its ability to measure and analyze metal implant materials (Ikarashi et al., 2023). This technique is routinely used to assess the bone integration of bone implants within the jawbone. The quantity and characteristics of the bone in direct contact with the implant can be determined using various morphometric measurements. Additionally, factors such as the biocompatibility of materials, structural morphology, and tissue changes before and after implant loading can be satisfactorily analyzed at the cellular level.

The application of the hard tissue sectioning technique facilitates the evaluation of the integration between HA/CC and the bone matrix. It allows for the analysis of the local positioning, activity, particle size, shape, and other physical factors of HA/CC. Furthermore, the biocompatibility of bone graft materials like HA with the bone can be assessed. Conventional histological sections, requiring decalcification, cannot differentiate whether

bone graft materials are lost due to physiological absorption or simple decalcification processes.

2.7 Transformation

The process by which bacterial cells uptake non-self-genetic material from their environment is known as transformation (Lorenz & Wackernagel, 1994). In natural environments, this genetic material can originate from adjacent lysed bacteria, including plasmid DNA or DNA fragments released into the surrounding environment. Certain factors can promote natural transformation in different bacteria, such as the presence of specific substances or particular growth phases of the cells (Hofreuter et al., 2000), which may accelerate natural transformation. While some bacteria naturally uptake DNA in the environment, studies have shown that this process can be replicated in the laboratory through chemical manipulation of specific bacteria to facilitate DNA uptake. One common method involves using calcium chloride to permeabilize the bacterial cell membrane, allowing the bacteria to easily uptake the desired plasmid. Researchers also utilize electroporation to increase cell membrane permeability, thereby enhancing transformation efficiency (Kumar et al., 2019).

2.8 Transduction

Transduction refers to the introduction of exogenous genetic material, DNA or RNA, into bacterial or eukaryotic cells via viral particles or viral vectors (Satoh & Manel, 2013). Scientists have also observed the process of transduction in bacteriophage-infected bacterial cells. Bacteriophages attach to the bacterial cell membrane and inject their genetic material into the cell. Once inside, some bacteriophages undergo lysis, replicating themselves to produce numerous viral particles, leading to cell lysis and the release of more viral particles that can infect other bacteria. Another portion of bacteriophage genetic material integrates into the host genome at specific integration sites. Integrated bacteriophages remain dormant until triggered to enter the lytic cycle (Aksyuk & Rossmann, 2011).

In both processes, bacterial DNA is inadvertently packaged into new bacteriophages, facilitating the transfer of this DNA to another cell, known as transduction. Transduction has been commonly utilized by researchers as a tool to introduce different DNA sequences of interest into bacterial cells or host genomes. Phage vectors, which simultaneously possess bacteriophage and plasmid characteristics, are often used for transduction. These vectors are packaged into non-replicating bacteriophage particles before transduction.

Researchers frequently employ lentivirus and adeno-associated viruses (AAV) to introduce exogenous DNA of interest into eukaryotic cells, such as mammalian cell lines (Verdera et al., 2020). Both lentivirus and AAVs can modify both transient and stable cell lines. Stable cell lines integrate the exogenous DNA into the cell genome, which is then passed on continuously through cell division (Perry & Rayat, 2021).

2.9 Transfection

In the laboratory, transfection refers to the deliberate introduction of exogenous DNA into eukaryotic cells using various non-viral methods, including chemical and physical approaches . Among these methods, transfection is effective for eukaryotic cells. In chemical methods, substances like calcium phosphate and diethylaminoethyl (DEAE)-dextran neutralize DNA molecules, imparting a positive charge that allows them to cross the cell membrane of eukaryotic cells for transfection (Selden, 2001). Physical methods include electroporation and microinjection. Electroporation involves momentarily creating pores in the cell membrane by applying an electric pulse, facilitating the direct introduction of surrounding DNA into the cell. Microinjection, on the other hand, entails using a fine needle to inject genes of interest into individual cells (Suarez & McElwain, 2010).

2.10 Conclusion

Bone tissue engineering is evolving with advanced scaffold designs, bio-factors like growth factors enhancing osteogenesis, and promising yet unproven allografts. Mesenchymal stem cells are key for bone regeneration, while decellularization techniques effectively prepare

scaffolds by removing cells but retaining essential structures. Bone healing assessment is enhanced by tools like Micro-CT and specific histological stains. Genetic methods like transformation, transduction, and transfection offer potential for further advances but face challenges in efficiency. Overall, combining materials, cells, and genetic tools is crucial for future bone regeneration strategies.

Chapter 3: Material and Methods

3.1 Materials

3.1.1 Chemical and reagents

Nocardia corallina I (Nco I) (NEW ENGLAND Biolads, UK, cat No: R3193)

Bacillus globigii II (BglII) (NEW ENGLAND Biolads, UK, cat No: R0144S)

DNA Transfection Reagents (jetOPEIMUS® , Polyplus®, UK, cat No: 101000025/0.75 ML)

MicroPulser (BIO-RAD, UK)

Lentivirus particles:

pRSV-rev (Addgene, UK, cat No: 12253)

pCMV-VSV-G (Addgene, UK, cat No: 8454)

pMDLg/pRRE (Addgene, UK, cat No: 12251)

Orbital incubator (Stuart® SI500, UK)

GenElute™ Plasmid Miniprep Kit (SIGMA life science, UK, cat No: PLN350-1KT)

GenElute™ Endotoxin-free Plasmid Midiprep Kit (Sigma-Aldrich, UK, cat No: PLED35-1KT)

Human BMP-2 Elisa test Kit (DuoSet® R&D SYSTEM, USA, cat No: DY355)

Human BMP-7 Elisa test Kit (DuoSet® R&D SYSTEM, USA, cat No: DY354)

Flow cytometer (NOVOCyte, ACCELA, US)

0.2% Iodophor Sanitizer (Jiangxi Caoshanhu Disinfection Supplies Co. Ltd)

Sterile phosphate-buffered saline (PBS): Dulbecco's PBS, without calcium or magnesium chloride, PH7.4 (Sigma-Aldrich， U.K., CAT No: D5652-500ml)

Washing buffer: 1% TritonTM X-100 in sterile PBS.

1X Trypsin-ethylenediaminetetraacetic acid (EDTA): Trypsin-EDTA (Sigma-Aldrich, U.K.; Cat No: T4299-100ml)

Blocking buffer: 0.1% TritonTM X-100 (Sigma-Aldrich, U.K.; Cat No. X100-1L) 0.5% bovine serum albumin (BSA, Sigma-Aldrich, U.K.; Cat No. A7030-500g) in sterile PBS.

Radioimmunoprecipitation assay (RIPA) buffer: 150 millimolar (mM) sodium chloride (NaCl) (Thermo Fisher Scientific, U.S.A.; cat No: S/3160/65), 1% TritonTM X-100, 0.5% sodium deoxycholate (Sigma-Aldrich, U.K.; cat No: D6750-100G), 0.1% sodium dodecyl sulphate (SDS) (PanReac AppliChem, U.S.A.; cat No: A7449/0500) 10 mM Tris HCL, PH 8.0, 10 mM EDTA (Thermo Fisher Scientific, U.S.A.; cat No: 10213570)

PBS-Tween 20: Sterile PBS with 0.02% Tween 20 (Sigma-Aldrich, U.K.; cat. No.: P7949-500ml)

All chemicals were from Sigma-Aldrich (UK) unless specified otherwise.

3.1.2 Double distilled water (ddH_2O)

The water employed in this study was ddH_2O, with a purity level of 18.2 MΩ.cm (million ohms). It was acquired using the Milli-Q® Synthesis System (Millipore, Nottingham, UK).

3.1.3 Umbilical Cord Tissue Samples

The human umbilical cords were obtained from Singleton Hospital. They were collected only after obtaining fully informed consent from the anonymised donors, following the guidelines of the West Wales Research Ethics Committee (REC11/WA/0040).

3.1.4 Cell Lines

3.1.4.1 MSC-TERT

The MSC-TERT cell line was obtained from ATCC® (Virginia, U.S.A.), and the MSC-TERT cell line was used in the cell treatment and transfection studies.

3.1.4.2 HEK293T

The transfection and treatment studies utilised Human Embryonic Kidney (HEK) 293T cells. The 293T cell lines were acquired from ATCC (USA).

3.1.5 Plasmids

3.1.5.1 The plasmids from Addgene

The plasmids containing BMP-2, BMP-7, and BMP-2/7 were obtained from Addgene (UK). The plasmid maps are displayed in **Figure 3.1**.

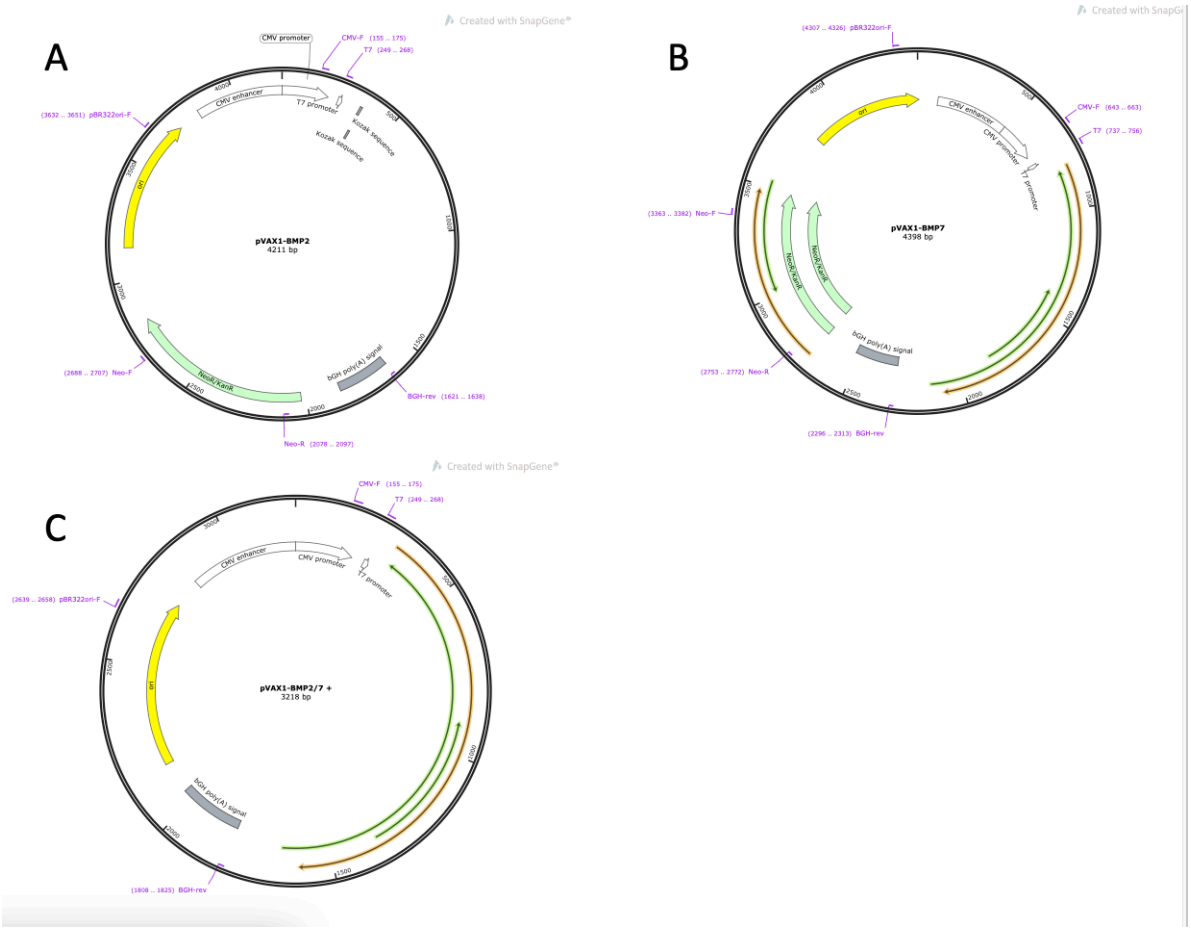

Figure 3.1. The plasmid map of BMP-expression vectors.
The plasmid map of BMP genes containing pVAX1 vector and the restriction enzyme sites of (A) BMP-2, (B) BMP-7 and (C) BMP-2/7.

3.1.5.2 The plasmids from Vector Builder

We obtained the plasmids containing BMP-2, BMP-7, and BMP-2/7 from Vector Builder (U.S.A). The plasmid maps are displayed below in **Figure 3.2**.

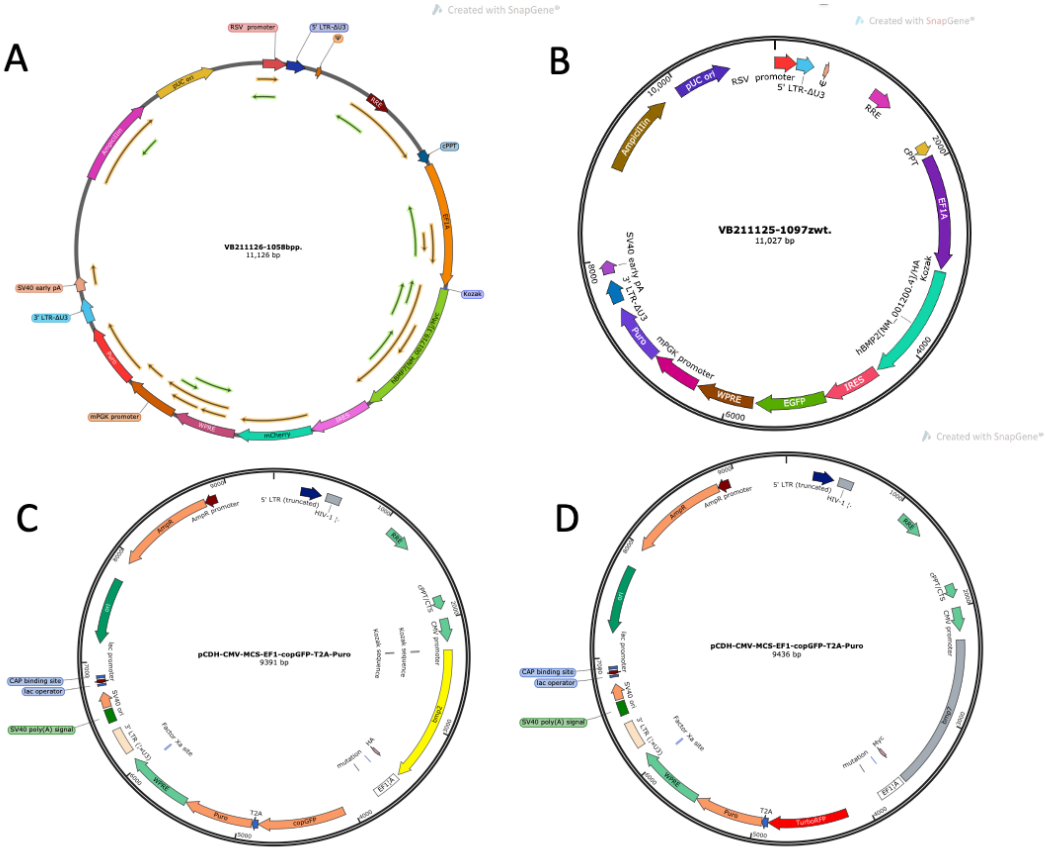

Figure 3.2. The plasmid map of BMP-expressing lentiviral vectors.
The plasmids map of BMP-expressing genes with the pCDH vector and the restriction enzyme sites of (**A**) VB-BMP-7-mCherry, (**B**) VB-BMP-2-EGFP, (**C**) pCDH-BMP-2-GFP and (**D**) pCDH-BMP-7-RFP from Vector Builder (USA).

3.1.6 Gene Sequences

3.1.6.1 Human BMP-2 (Accession: NM_001200 [https://www.ncbi.nlm.nih.gov/])

AT GGTGGCCGGG ACCCGCTGTC TTCTAGCGTT GCTGCTTCCCCAGGTCCTCC TGGGCGGCGC GGCTGGCCTC GTTCCGGAGC TGGGCCGCAG GAAGTTCGCG GCGGCGTCGT CGGGCCGCCCCTCATCCCAG CCCTCTGACG AGGTCCTGAG CGAGTTCGAG TTGCGGCTGC TCAGCATGTT CGGCCTGAAA CAGAGACCCACCCCCAGCAG GGACGCCGTG GTGCCCCCCT ACATGCTAGA CCTGTATCGC AGGCACTCAG GTCAGCCGGG CTCACCCGCCCCAGACCACC GGTTGGAGAG GGCAGCCAGC CGAGCCAACA CTGTGCGCAG CTTCCACCAT GAAGAATCTT TGGAAGAACTACCAGAAACG AGTGGGAAAA CAACCCGGAG ATTCTTCTTT AATTTAAGTT CTATCCCCAC GGAGGAGTTT ATCACCTCAGCAGAGCTTCA GGTTTTCCGA GAACAGATGC AAGATGCTTT AGGAAACAAT AGCAGTTTCC ATCACCGAAT TAATATTTATGAAATCATAA AACCTGCAAC AGCCAACTCG AAATTCCCCG TGACCAGACT TTTGGACACC AGGTTGGTGA ATCAGAATGCAAGCAGGTGG GAAAGTTTTG ATGTCACCCC CGCTGTGATG CGGTGGACTG CACAGGGACA CGCCAACCAT GGATTCGTGGTGGAAGTGGC CCACTTGGAG GAGAAACAAG GTGTCTCCAA GAGACATGTT AGGATAAGCA GGTCTTTGCA CCAAGATGAACACAGCTGGT CACAGATAAG GCCATTGCTA GTAACTTTTG GCCATGATGG AAAAGGGCAT CCTCTCCACA AAAGAGAAAAACGTCAAGCC AAACACAAAC AGCGGAAACG CCTTAAGTCC AGCTGTAAGA GACACCCTTT GTACGTGGAC TTCAGTGACGTGGGGTGGAA TGACTGGATT GTGGCTCCCC CGGGGTATCA CGCCTTTTAC TGCCACGGAG AATGCCCTTT TCCTCTGGCTGATCATCTGA ACTCCACTAA TCATGCCATT GTTCAGACGT TGGTCAACTC TGTTAACTCT AAGATTCCTA AGGCATGCTGTGTCCCGACA GAACTCAGTG CTATCTCGAT GCTGTACCTT GACGAGAATG AAAAGGTTGT ATTAAAGAAC TATCAGGACATGGTTGTGGA GGGTTGTGGG TGTCGCTACC CATACGATGT TCCAGATTAC GCTTAG

3.1.6.2 Human BMP-7

AT GCACGTGCGC TCACTGCGAG CTGCGGCGCC GCACAGCTTCGTGGCGCTCT GGGCACCCCT GTTCCTGCTG
CGCTCCGCCC TGGCCGACTT CAGCCTGGAC AACGAGGTGC ACTCGAGCTTCATCCACCGG CGCCTCCGCA GCCAGGAGCG
GCGGGAGATG CAGCGCGAGA TCCTCTCCAT TTTGGGCTTG CCCCACCGCCCGCGCCCGCA CCTCCAGGGC AAGCACAACT
CGGCACCCAT GTTCATGCTG GACCTGTACA ACGCCATGGC GGTGGAGGAGGGCGGCGGGC CCGGCGGCCA GGGCTTCTCC
TACCCCTACA AGGCCGTCTT CAGTACCCAG GGCCCCCCTC TGGCCAGCCTGCAAGATAGC CATTTCCTCA CCGACGCCGA
CATGGTCATG AGCTTCGTCA ACCTCGTGGA ACATGACAAG GAATTCTTCCACCCACGCTA CCACCATCGA GAGTTCCGGT
TTGATCTTTC CAAGATCCCA GAAGGGGAAG CTGTCACGGC AGCCGAATTCCGGATCTACA AGGACTACAT CCGGGAACGC
TTCGACAATG AGACGTTCCG GATCAGCGTT TATCAGGTGC TCCAGGAGCACTTGGGCAGG GAATCGGATC TCTTCCTGCT
CGACAGCCGT ACCCTCTGGG CCTCGGAGGA GGGCTGGCTG GTGTTTGACATCACAGCCAC CAGCAACCAC TGGGTGGTCA
ATCCGCGGCA CAACCTGGGC CTGCAGCTCT CGGTGGAGAC GCTGGATGGGCAGAGCATCA ACCCCAAGTT GGCGGGCCTG
ATTGGGCGGC ACGGGCCCCA GAACAAGCAG CCCTTCATGG TGGCTTTCTTCAAGGCCACG GAGGTCCACT TCCGCAGCAT
CCGGTCCACG GGGAGCAAACAGCGCAGCCAGAACCGCTCCAAGACGCCCAAGAACCAGGA AGCCCTGCGG
ATGGCCAACG TGGCAGAGAA CAGCAGCAGC GACCAGAGGC AGGCCTGTAA GAAGCACGAGCTGTATGTCA
GCTTCCGAGA CCTGGGCTGG CAGGACTGGA TCATCGCGCC TGAAGGCTAC GCCGCCTACT ACTGTGAGGGGGAGTGTGCC
TTCCCTCTGA ACTCCTACAT GAACGCCACC AACCACGCCA TCGTGCAGAC GCTGGTCCAC TTCATCAACCCGGAAACGGT
GCCCAAGCCC TGCTGTGCGC CCACGCAGCT CAATGCCATC TCCGTCCTCT ACTTCGATGA CAGCTCCAACGTCATCCTGA
AGAAATACAG AAACATGGTG GTCCGGGCCT GTGGCTGCCA CGAACAAAAA CTCATCTCAG AAGAGGATCTGTAG

3.1.7 Primers

We designed and obtained primers for BMP-2, BMP-7, Runx2, Osteocalcin, and Osterix from Sigma-Aldrich (UK). The BMP-2 and BMP-7 cloning primer sequences are shown in **Tables 3.1** and **3.2, respectively,** and the qPCR primers are outlined in **Table 3.3**.

Table 3.1. Human BMP-2 Forward and Reverse Primers.

Sequence (5'->3')		Template strand	Length	Start	Stop	Tm	GC%	Self complementarity	Self 3' complementarity
Forward primer	TGTATCGCA GGCACTCAG GTCA	Plus	22	1442	1463	63.69	54.55	3.00	1.00
Reverse primer	CGGGTTGTTT TCCCACTCGT	Minus	20	1586	1567	60.82	55.00	3.00	2.00

Table 3.2. Human BMP-7 Forward and Reverse Primers.

Sequence (5'->3')		Template strand	Length	Start	Stop	Tm	GC%	Self5' complementarity	Self 3' complementarity
Forward primer	TTCGTCAA CCTCGTGG AACA	Plus	20	925	944	59.54	50.00	4.00	1.00
Reverse primer	ACGTCTCA TTGTCGAA GCGT	Minus	20	1087	1068	60.04	50.00	4.00	2.00

Table 3.3. qPCR Forward and Reverse Primers Used in qPCR.

Gene (bp)	Forward primer	Reverse primer	Product size
Runx2.	5'-GACAGCCCCAACTTCCTGT-3'	5'-CCGGAGCTCAGCAGAATAAT-3'.	159
Osterix.	5'-TGCTTGAGGAGGAAGTTCAC-3'	5'-CTGCTTTGCCCAGAGTTGTT-3'.	114
Osteocalcin	5'-CTCACACTCCTCGCCCTATT-3'.	5'-TCAGCCAACTCGTCACAGTC-3'.	245

3.2 Methods

3.2.1 Umbilical Cord Tissue Dissection

Human umbilical cord (UC) tissue dissection was conducted under the approval of the Southwest Wales Research Ethics Committee donors(West Wales Research Ethics Committee REC11/WA/0040). The tissue was dealt with in a 150mm petri dish in a class 2 tissue culture hood (GS BIOTECH LIMITED - 170LGOLD/HT (Wolf Laboratories Ltd., U.K). The UC samples were cleansed with fresh DMEM F12 media (Gibco^{TM}; ThermoFisher, cat. No: 11320033) to eliminate blood clots and maintain moisture. Utilising sterilised forceps and a scalpel, the UC was longitudinally dissected, revealing Wharton's jelly and blood vessels. All three blood vessels were slowly extracted using sterilised surgical tools and transferred to a separate petri dish for disposal. The remaining tissue was washed again with fresh DMEM F12 media to ensure complete blood removal and then sliced into 1-2mm fragments using a scalpel. These tissue pieces were placed into a 25 cm^2 tissue culture flask (CELLSTARTM; Greiner Bio-One, UK) with even distribution across the surface area. The tissue culture flasks were incubated at 37°C with 5% CO_2 for 5 minutes to facilitate tissue attachment to the plastic base. Following this, 2 ml of fetal bovine serum (FBS [Sigma-Aldrich, U.K.; cat. No. F7524-500mL]) was added to the flasks to avoid disturbing the adhered tissue. The tissue culture flasks were returned to the incubator. Approximately 24 hours later, 2 ml of FBS was replaced with 3 ml of culture media (Dulbecco's modified eagle medium [DMEM] supplemented with 10% FBS and 1% penicillin-streptomycin [PS]). The tissue culture was monitored for the emergence of new mesenchymal stromal cell outgrowths by light microscopy. The tissue culture media was replaced every 3-4 days.

3.2.2 Mesenchymal Stem Cells Culture

Building on the successful isolation of mesenchymal stromal cells from the UC tissue, the subsequent steps focused on MSC culture and maintenance.

3.2.2.1 Cell Preservation

Upon reaching 70-80% confluency, mesenchymal stem cells (MSCs) were passaged. Briefly, the culture medium was removed from the cells, and the cells were washed with 3 ml Phosphate-Buffered Saline (PBS). MSCs were detached by incubating in 2ml trypsin (Sigma-

Aldrich, U.K.; Cat No. T4299-100ml) for 2 minutes. After the incubation, the digestion reaction was halted by 8 ml of culture medium with serum. The cell count was measured by mixing 10 µl of cell suspension with 10 µl of trypan blue (Sigma-Aldrich, UK, cat. No: T8154-100mL) and transferring 10 µl of resuspended cells onto the Countess™ cell counting chamber slide (Invitrogen", ThermoFisher Scientific, U.S.A.) and subjected to Countess Automated Cell Counter (Invitrogen, ThermoFisher Scientific, U.S.A.). Then 1 ml of cell suspension which contained approximately 2 x 10^5 cells (10% confluency) was seeded into a new 10 cm culture dish, supplemented with 10 ml of fresh culture medium. The cells were incubated at 37C° and 5% CO_2 for cultivation. The culture medium was refreshed every 3-4 days.

3.2.2.2 Reviving of Frozen Cells

MSC-TERT (ATCC® Virginia, U.S.A) cells were revived from liquid nitrogen by thawing. A 1 ml aliquot of cells was resuspended in 9 ml cell culture media (Dulbecco's modified eagle medium [DMEM] supplemented with 10% FBS and 1% penicillin-streptomycin [PS]) (Dulbecco's modified eagle medium [DMEM] supplemented with 10% FBS and 1% penicillin-streptomycin [PS]) by vortexing. The cells were then centrifuged at 300 xg at 20°C for 6 minutes. The supernatant was removed, and 10 ml of fresh culture medium was added to the cells. The cells were then resuspended by vortexing. Subsequently, the MSC-Tert cells were seeded into 10 cm culture dishes and incubated at 37°C and 5% CO_2 in a 170LGOLD/HT tissue culture incubator (Wolf Laboratories Ltd., U.K).

3.2.2.3 Cell Viability

Following the successful revival of the MSC-TERT cells, an experimental setup was established to assess their growth dynamics using a 96-well plate (Greiner Bio-One, Austria; cat. No: 675090) to investigate and graphically represent the growth dynamics of MSC-TERT cells. Varying cell concentrations of 500, 1000, 2000, 4000, 8000, 16000, and 32000 cells per well were introduced. This configuration included duplicate wells for each cell density. The cell culture was maintained at a controlled environment of 5% CO_2 and

37°C in the culture medium (DMEM medium [Sigma-Aldrich, UK] supplemented with 10% FBS and 1% PS). The culture medium was renewed every 72 hours. Daily during the culture period, cells from different seeding densities were subjected to Alamar Blue assays (Invitrogen®, UK, cat No: DAL1100). At specific time points (every 24 hours up to 144 hours), the cell culture media of both groups were replaced with a culture medium containing 10 µl 10% Alamar Blue. Subsequently, the growth curve for MSC-TERT cells was constructed based on the obtained assay results.

3.2.2.4 Cryopreservation

Once optimal growth was observed**,** the MSC-TERT cells were prepared for cryopreservation upon reaching 70-80% confluence. Briefly, the culture medium was removed and the cells were washed with PBS. Subsequently, the cells were detached from the culture flask by the addition of 2ml of 1% trypsin (in PBS), followed by a 2-minute incubation period. Once it was confirmed that the cells had detached from the flask, the reaction was neutralised by adding 8ml of culture medium. The flask walls were rinsed to ensure all cells were harvested. Cell counting was performed using a Countess™ Automated Cell Counter as described in **Section 3.2.2.1**. Following the cell count, the cells were then centrifugated at 1,200 rpm for 6 minutes. The supernatant was discarded, leaving the cell pellet. The cells were resuspended in freezing medium (25% FBS [Sigma-Aldrich, U.K.; cat. No. F7524-500mL] and 10% dimethyl sulfoxide [DMSO] in FSM). The cell suspension in the freezing medium was transferred to cryovials (Greiner bio-one, UK) and temporarily stored in a Mr Frosty™ Freezing container filled with isopropanol at 4°C for 4 hours. Following this, the cryovials were placed in a -80°C freezer overnight before being transferred to long-term storage in liquid nitrogen.

Following successful isolation and cultivation of MSCs from the umbilical cord tissue, the next step was to prepare a suitable scaffold for cell seeding and tissue engineering applications.

3.2.3 Scaffold Preparation

Hydroxyapatite and calcium carbonate (HA/CC) scaffold material produced and provided by Dr Zhidao Xia's laboratory of Centre for NanoHealth, Swansea University, UK. HA/CC scaffold material underwent a process of grinding with mortar and pestle. These nano-particles were subsequently sorted by employing a multi-layered sieve mechanism to obtain particles within the 200-300 µm size range. The resultant micro-scale particles were aseptically transferred into glass vials and autoclaved. Following sterilisation, the treated particles were immersed in a culture medium (Sigma-Aldrich, UK, cat No: D6429-500ML) under strict aseptic conditions for 24 hours in preparation for their further experiments.

3.2.4 Alamar Blue Assay

After a 24-hour incubation of the scaffold with culture media, 20-30 particles of the scaffold material were introduced into a 96-well plate containing previously cultured MSCs. In the control group, no particles were added to the cell wells. The cells and particles were cultured together within an incubator at 37°C and 5% CO_2. The culture medium was refreshed every three days. At specific time points (every 24 hours up to 144 hours), the cell culture media of both groups were replaced with a culture medium containing 10 µl 10% Alamar Blue (Invitrogen®, UK, cat No: 799771). The plates were then returned to the incubator and cultured for 4 hours at 37°C and 5% CO_2. Upon observing a change in the colour of the reaction solution within the wells, the culture medium was transferred into the corresponding wells of a 96-well plate. The absorbance wavelength of 570 nm was read using a plate reader (BMG LABTECH, Germany), and fluorescence readings were obtained at each time point. The obtained absorbance values were normalised to the control and plotted to measure the viability of the cells.

3.2.5 CCK-8 Assay

Following a 24-hour incubation of scaffold with culture media, 20-30 microspheres that had been soaked were introduced into a 96-well plate containing previously cultured MSCs.

The control group's cell wells remained devoid of microspheres. Scaffold particles and cells were co-cultured at 37°C and 5% CO_2 in a cell culture incubator. On the second, fourth, and sixth days of incubation, the culture was terminated, and both sets of cell culture media were replaced with media containing 10 µl 10% CCK-8 reagent (CCK-8 test kit [Sigma-Aldrich, UK; cat No: B34304-25 mL]) and incubated for further 4 hours. The colour change was observed following the reaction. Subsequently, the CCK-8 reaction solution was collected from the 96-well plate, and the optical density (OD) at 450 nm values for each group at each time point were determined using a plate reader FLUOstar Omega (BMG LABTECH, Germany). CCK-8 test curves were generated based on the OD values.

3.2.6 Scanning Electron Microscopy

Following the culture of HUMSCs with HA/CC for 10 days, the cells were analysed by scanning electron microscopy (SEM). Briefly, the cultured HUMSCs were fixed with 500 µl of a 2.5% glutaraldehyde solution in PBS for 10 minutes. Following this fixation phase, the samples underwent three washes with PBS to eliminate any residual glutaraldehyde. Subsequently, a gradual dehydration process was carried out by introducing escalating concentrations of ethanol. The samples were immersed in ethanol solutions of 30%, 50%, 70%, 90%, and twice in 100%, each for 15 minutes. The initial step in cell infiltration involved the application of 50% hexamethyldisilane in PBS for 20 minutes, followed by an additional 20 minutes with 100% hexamethyldisilane. Lastly, fresh 100% hexamethyldisilane was introduced to the samples, and the plate was left in a fume cupboard overnight to allow for drying.

3.2.7 Osteogenic differentiation

Three sets of 24-well plates were established and categorised into three groups: In Group 1, MSC cells were cultured using a standard growth medium (Dulbecco's modified eagle medium [DMEM] supplemented with 10% FBS and 1% penicillin-streptomycin [PS]) medium (Sigma-Aldrich, UK, cat No: D6429-500ML). In Group 2, MSC cells were cultured in an osteogenic differentiation medium (DMEM F12 supplemented with 10% FBS, 1% PS, and

10% commercial StemPro osteogenic supplement (ThermoFisher Scientific, UK)). In Group 3, MSCs cells were cultured in osteogenic differentiation medium supplemented with 100ng/ml BMP-2 (CellGuidance, UK, cat No: GFH53-100). The cells were maintained 37°C and 5% CO_2 in the incubator. The culture medium was replaced every 3-4 days. Cell cultures in each group were terminated at specific time points, 1, 7, 14, 21, and 28 days. Some cells were harvested for quantitative PCR (qPCR) analysis, while others were preserved for subsequent staining analysis.

3.2.8 ALP Staining

At the time points of 1, 7, 14, 21, and 28 days following the initiation of HUMSC differentiation, the cellular samples were prepared for fixation and subsequent staining. The cells within each designated group were gently rinsed with PBS. The working solution of 5-bromo-4-chloro-3-indolyl-1-phosphate (BCIP) (Sigma-Aldrich, UK, cat No: B6149-100MG) and nitroblue tetrazolium (NBT) (Sigma-Aldrich, UK, cat No: N6876-100MG) (BCIP/NBT solution) was prepared with 100 µL 2%BCIP mixed with 330 µL of 1% NBT in 10 mL AP buffer. Subsequently, 200 µL of the appropriate BCIP/NBT working solution was applied to uniformly cover the cellular monolayer. The staining process was carried out within a dimly lit environment at room temperature, spanning 30 minutes. The enzymatic reaction was stopped by introducing 20 mM ethylenediaminetetraacetic acid (EDTA). Visual examination and image acquisition of the stained cells were conducted using a light microscope (Carl ZEISS NTS Ltd, Germany).

3.2.9 Oil Red Stain

Following the completion of adipogenic differentiation, the HUMSC cells seeded in a 6-well plate were subjected to a delicate washing procedure with 2.4 ml PBS. Subsequently, fixation of the cells was carried out by introducing 2.4 ml of 4% paraformaldehyde (PFA) solution at room temperature for 15 minutes. A stock solution of Oil Red O (Sigma-Aldrich, UK, cat No: O0625-25G), which was at a concentration of 0.5% in isopropanol, was

appropriately diluted in ddH_2O at a ratio of 6:4. The cells were subsequently subjected to PBS washing, followed by a brief rinsing step involving 2.4 ml 60% isopropanol. The adipocytes were subjected to staining by applying of 1 ml of the Oil Red O working solution, maintained at room temperature for 30 minutes. After the staining process, the cells underwent four consecutive washes using ddH_2O. Finally, the cells were observed utilising phase-contrast microscopy at a magnification of x10, and images were acquired.

3.2.10 Alizarin Red Stain

After a 28-days of inducing cellular differentiation in the culture of HUMSC cells, the culture medium was removed, and the cells were gently rinsed with PBS. Subsequently, 250 µl of Alizarin Red Staining solution (Millipore, UK, cat No: 2003999) was introduced into each well, followed by a 30-minute incubation period at room temperature in the absence of light. Following this incubation, the Alizarin Red Stain solution was aspirated and replaced with 250 µl of PBS to cover the cell surface. The Alizarin Red staining was then examined under optical microscopy, and photos of the cells were taken.

3.2.11 qPCR

3.2.11.1 RNA and Protein Extraction

MSCs were lysed by TRI Reagent (Sigma-Aldrich, UK) to extract RNA and protein. Following cell differentiation, the culture medium was removed and cells were rinsed with PBS. Subsequently, for a 24-well plate 50 µl TRI Reagent was introduced into the wells and cell detachment was facilitated using a 1 mL syringe plunger. The harvested cells were homogenised using 25G AGANI™ needle (Terumo, China), and incubated at room temperature for 5 minutes. Following this, 10 ml chloroform (Sigma-Aldrich, UK, cat No: C2432BCA) was added to homogenised and lysed cells. The cell lysate was inverted ten times and then incubated for 15 minutes at 4°C. The lysed cells were then centrifuged (Centrifuge 5180 R, Eppendorf, Germany) at 12,000 xg for 15 minutes at 4°C. Post-centrifugation, the mixture separated into three phases: RNA, DNA and Proteins. The upper RNA-containing phase was carefully transferred to new Microfuge tubes and combined

with 25 µl isopropanol. After ten inversions, the mixture was incubated for 10 minutes at room temperature, followed by centrifugation at 12,000 xg at 4°C for 5 minutes. The supernatant was discarded, and 75% ethanol was added, followed by centrifugation at 7,500 xg for 5 minutes at 4°C. The ethanol was removed, and the washed RNA pellet was air-dried for 10 minutes. The resulting RNA pellet was then reconstituted and thoroughly mixed in nuclease-free water. Subsequently, the concentration and quality of the isolated RNA were assessed using a Nanodrop spectrophotometer (NANODROP ONE, Thermo Scientific, UK) before being stored at -80°C for future use. In the protein isolation process, the lower protein-rich phase was transferred into new Microfuge tubes and 0.3M guanidine hydrochloride in 95% ethanol was added. The contents were thoroughly mixed using a vortex, allowed to stand for 15 minutes at room temperature, and then subjected to centrifugation at 7,500 × g for 5 minutes at 4°C. The cell lysate pellet was washed three times. Following the last wash, the supernatant was discarded, and 100% ethanol was added. The protein pellets were centrifuged at 7,500 × g for 5 minutes at 4°C, and the resulting supernatant was removed to facilitate air-drying of the protein pellet for 10 minutes. The protein pellet was then dissolved and resuspended in a solution consisting of 5% SDS (sodium dodecyl sulfate) and agitated until the pellet was dissolved entirely. Following the protein extraction, ¼ of the volume of 5X SDS-PAGE sample buffer (comprising 5% [w/v] SDS, 125mM Tris HCl [pH 6.8], 50% [v/v] glycerol, 0.005% [w/v] bromophenol blue, and 10% 2-mercaptoethanol) was added to the remaining protein sample. The mixture was then denatured at 95°C for 5 minutes and subsequently stored in a -20°C.

3.2.11.2 Bicinchoninic Acid Assay (BCA)

The protein concentration in cell lysates of transfected MSC and HEK293T cells was quantified using the BCA assay. Bovine serum albumin (BSA) protein standards ranging from 0 to 1 mg/ml were employed to create a standard curve. The cell lysates were diluted 1:5 in ddH2O and loaded into duplicates in wells of a 96-well plate (Greiner Bio-One, Germany). A working solution containing Reagent B (4% Copper II sulphate pentahydrate) and Reagent A (BCA reagent) from the Pierce™ BCA Protein assay kit (ThermoFisher, USA)

was prepared in a 1:50 ratio. Subsequently, 80 µL of the working BCA solution was added to the standards and unknown diluted cell lysates, and the mixture was incubated at 37°C for 30 minutes. The plate was then read at 490 nm using a FLUOstar Omega plate reader (BMG Labtech). A standard curve with gradients exceeding 0.99 was generated, and unknown samples were extrapolated accordingly. Finally, the protein concentration was normalized to the dilution factor, yielding the final total protein concentration.

3.2.11.3 cDNA Synthesis

Following the instructions outlined in the manual accompanying the High-Capacity cDNA Reverse Transcription kit from Applied Biosystems (4374966), 2 µg of RNA was converted to cDNA. Briefly, a mixture was prepared, comprising 3.2 µl nuclease-free water, 2 µl 10X Reverse Transcription (RT) buffer, 0.8 µl 25X deoxyribonucleotide triphosphate (dNTP) mix (100 nM), 2 µl 10X RT Random Primers, 1 µl Multiscribe Reverse Transcriptase (MRT), and 1 µl RNase inhibitor. The reaction mixture was incubated in a Thermal cycler (T100^{TM} BIO-RAD, UK), as outlined in **Table 3.4**. The concentration and purification of the cDNA were tested using a Nanodrop spectrophotometer (NANODROP ONE, Thermo Scientific, UK). The cDNA was stored at -20°C for later use.

Table 3.4. cDNA Synthesis Incubations.

Step	Temperature	Time (min)
1	42°C	10
2	25°C	10
3	37°C	125
4	85°C	5
5	4°C	∞

3.2.11.4 qPCR Composition

We quantified the expression levels of BMP-2, BMP-7, RUNX2, and Osteocalcin in MSC-TERT cells using quantitative PCR (qPCR). The forward and reverse primers were diluted at

a ratio of 1:20 using Nuclease-Free Water (Merck, China, CAT No: 7732-18-5) (**Table 3.4**). Also, the cDNA samples were diluted at 1:20 in Nuclease-Free Water. The master mix was prepared by combining 1 µl of diluted sample, 1 µl of Nuclease-Free Water, and 5 µl of SYBR Green(SYBR™ Green PCR Master Mix, CAT No:4309155) per well for subsequent usage. The forward and reverse diluted primers were mixed at a 1:1 ratio. In each well of the plate, 8 µl of the master mix and 2 µl of the primer mixture were loaded at 4°C. The reaction was run using the CFX Connect™ PCR (BIO-RAD, UK) as outlined in **Table 3.6,** and the plate was configured for real-time reaction monitoring.

Table 3.5. RT-PCR Forward and Reverse Primers.

Primer Name	**Sequence**
BMP-2	FORWARD: 5'- TGTATCGCAGGCACTCAGGTCA – 3' REVERSE: 5' – CGGGTTGTTTTCCCACTCGT – 3'
BMP-7	FORWARD: 5' – TTCGTCAACCTCGTGGAACA – 3' REVERSE: 5' – ACGTCTCATTGTCGAAGCGT – 3'
Runx2	FORWARD: 5' – GACAGCCCCAACTTCCTGT – 3' REVERSE: 5' – CCGGAGCTCAGCAGAATAAT – 3'
Osteocalcin	FORWARD: 5' – CTCACACTCCTCGCCCTATT – 3' REVERSE: 5' – TCAGCCAACTCGTCACAGTC – 3'
GAPDH	FORWARD: 5' – CTCATGACCACAGTCGATGCC – 3' REVERSE: 5' – GGGATGACCTTGCCCACAG – 3'

Table 3.6. qPCR Running Conditions.

Step		Temperature	Time
Initial denaturation	Amplification	95°C	5 minutes
Denaturation	cyclesX39	95°C	15 seconds
Annealing		60°C	15 seconds
Extension		72°C	1 minute
Melt curve		95°C	15 seconds
		58°C	1 minute

	95°C	15 seconds

We used the cycle threshold (CT) values obtained from the qPCR machine to analyse qPCR data. The CT value represents the cycle number at which the fluorescence signal of the PCR reaction crosses a threshold level, indicating the initial amount of target RNA present in the sample. The comparative CT method (2^-ΔΔCT) was used to calculate relative gene expression levels by comparing the CT values of the gene of interest (GOI) to those of the reference gene, Glyceraldehyde-3-phosphate dehydrogenase (GAPDH). GAPDH was selected as the reference gene due to its stable expression across various cell types and experimental conditions, making it suitable for normalization.

3.2.11.5 Flow cytometry

Transfection efficiency and intracellular protein expression were assessed by quantifying the expression of green fluorescent protein (GFP) or mCherry protein within MSC cells transduced with plasmids. Following transduce of MSC cells with GFP or mCherry expressing plasmids in a 6-cm plate, the cells were suspended in cell medium by pipetting up and down. The cells were then collected by centrifugation at 300 rcf for 5 minutes. Subsequently, the cells were washed twice with ice-cold PBS before being detected based on the GFP or mCherry tag fluorescence. Following PBS washes, the cells were resuspended in 100 µL FACS buffer (0.2% BSA in PBS) and transferred to a transparent 96-well U-shaped plate (Greiner Bio-One, UK, cat No: 655866) for analysis using the ACEA NovoCyte Flow Cytometer (Agilent, USA). Analysis was performed on either 100,000 cells or 90 µL of resuspended cells in the medium, with mCherry fluorescence measured at excitation 587 nm and emission 610 nm, and GFP fluorescence measured at excitation 488 nm and emission 507 nm. Flow cytometry data was analyzed using FlowJo™ software (Ashland, Oregon, USA), employing a gating strategy to identify transfected HUMSCs, including gating healthy cells within the total population and singlets within healthy cells. Unstained cells were used as a control to detect the shift in fluorescence caused by protein-expressing cells. The data analysis allowed for the quantifying of transfection

efficiency, expressed as the percentage of fluorophore-positive cells relative to the total number of cells in the sample.

3.2.12 Purification of Plasmid DNA

3.2.12.1 Transformation

To obtain a sufficient quantity of plasmids, transformations were carried out using products purchased from Addgene. A 50-100 µL aliquot of XL1-Blue ultracompetent *Escherichia coli* (*E. coli*) bacterial culture was thawed on ice. Subsequently, 1 µg of pvax1-BMP-2 plasmid DNA (Addgene, UK) was introduced to the *E. coli* cells, and the mixture was incubated on ice for 30 minutes. Following this, the *E. coli* cell and plasmid DNA mixture underwent a heat shock treatment at 42°C for 45 seconds in a Grant GD100 water bath (Cambridgeshire, UK) and was then promptly cooled on ice for 2 minutes. A volume of 0.5-1 ml of Luria-Bertani (LB) medium (SIGMA Life Science, UK, cat No: L3022-1KG) was added to the transformed cells, and the culture was further inoculated at 37°C with constant orbital agitation (Stuart® SI500, UK) at 250 rpm. The transformed cells were subsequently centrifugated at 15,000 xg for 1 minute. Approximately 0.4-0.9 ml of the supernatant medium was decanted, and the cell pellet was resuspended in the remaining 100 µl of the medium. A 100 µl aliquot of the transformed cells was evenly spread onto an LB agar plate containing the kanamycin antibiotic for selection. These plates were then inverted and incubated overnight at 37°C in an incubator (Genlab, UK). Following incubation, the plates were sealed with parafilm and stored inverted at 4°C.

3.2.12.2 Mini-prep

To isolate and assess the purity of plasmid DNA, the GenElute™ Plasmid Miniprep Kit was employed for the extraction of plasmids from *E.coli* that had been previously transformed. Initially, *E. coli* cultures were harvested following a 24-hour incubation period and subsequently subjected to centrifugation at 3220 relative centrifugal force (rcf) and room temperature for 10 minutes, resulting in the formation of cell pellets. These pellets were then reconstituted in 250 µL of Buffer P1, as provided by the kit, containing RNase A. 250 µL of Buffer P2 was added to resuspend pellets, followed by immediate inversion 5 times to

initiate lysis. The mixture was allowed to stand for 5 minutes to facilitate the lysis reaction. Subsequently, 350 µL of neutralization buffer N3 was introduced to halt the lysis process, and the tubes were inverted 5 times to ensure thorough mixing. The lysed cells were centrifuged for 10 minutes at 15,000 rcf, after which the resulting supernatant was transferred to spin columns and centrifuged for 1 minute at 15,000 rcf. The flow-through was discarded, and 750 µL of Buffer PE was applied, followed by another round of centrifugation for 1 minute at 15,000 rcf. After discarding the flow-through, the columns were once again subjected to centrifugation at 15,000 rcf to eliminate any residual wash buffer. Finally, the columns were transferred to fresh Microfuge tubes, and 100 µL of EB Buffer was added and allowed to stand for 1 minute. The columns were then centrifuged at 15,000 rcf and room temperature for 1 minute to collect the plasmids, which were subsequently transferred to new Microfuge tubes. The quality and concentration of the plasmids were assessed using a nanodrop spectrophotometer (NANODROP ONE, Thermo Scientific, UK), and the purified plasmids were stored at -20°C for future applications.

3.2.12.3 Midi-prep

1 Plasmid Recovery

The plasmids were recovered following transformation using the Endotoxin-free Plasmid Midiprep Kit (Sigma-Aldrich, UK, cat No: PLED35-1KT).

2 Cell Harvesting

E. coli cultures were removed from the incubator (INFORS AG CH-4103, UK). The 40 ml of E. coli culture in each flask was then centrifuged at 3220 rcf and room temperature for 10 minutes. The supernatant was discarded, leaving behind cell pellets.

3 Cell Resuspension

Each cell pellet was resuspended in 1.2 ml of resuspension solution provided by the kit. Vigorous vortexing was performed for 5-10 minutes until the cells formed a homogeneous suspension. The 1.2 ml homogeneous suspensions were divided into two separate 2 ml microfuge tubes.

4 Cell Lysis

Each microfuge tube was supplemented with 0.6 ml of lysis solution from the kit. These mixtures were gently inverted 6-8 times and left to stand for 2-3 minutes to allow cell lysis.

5 Neutralization

After lysis, 0.4 ml of neutralizing solution was added to each microfuge tube, and they were gently inverted several times. The tubes were then centrifuged at 4°C and 15,000 rcf for 15 minutes.

6 Endotoxin Removal

The cleared lysate was transferred into 15 ml centrifuge tubes. To the lysate, 300 µl of Endotoxin Removal Solution was added, followed by inversion for 1 minute, chilling on ice for 5 minutes with intermittent mixing, and incubation in a 37°C water bath for 5 minutes until the liquid became cloudy. The tubes were centrifuged at 4000 rpm and room temperature for 5 minutes, and the upper phase containing plasmid DNA was transferred into new 15 ml centrifuge tubes. This process was repeated to ensure endotoxin removal.

7 DNA Binding

To the endotoxin-free lysates, 0.8 ml of DNA Binding Solution was added and thoroughly mixed by vortexing.

Column Preparation

Columns were prepared by placing them into collection tubes and adding 3 ml of Column Preparation Solution to each column. The columns were centrifuged at 4000 rpm and room temperature for 2 minutes, and the flow-through was discarded.

8 DNA Binding to Columns

The lysates mixed with the Binding Solution were loaded into the prepared columns and centrifuged at 4000 rpm and room temperature for 2 minutes. The flow-through was discarded after centrifugation.

9 Column Washing

The columns were washed by adding 3 ml of Washing Solution and centrifuging at 4000 rpm, room temperature, for 5 minutes.

10 DNA Elution

To elute the DNA plasmids, 0.5 ml of Endotoxin-free water was added to the washed columns in new clean collection tubes. Centrifugation was carried out at 4000 rpm, room temperature, for 5 minutes, resulting in the collection of DNA plasmids in the flow-through eluates.

11 Plasmid Concentration Measurement and Storage

The concentration of the plasmids was measured using a nanodrop, and they were stored at -20°C for future use.

3.2.12.4 Restrict Digestion of Plasmid DNA

Following the mini- or midi-preps of the plasmids of interest, the plasmids were authenticated by restriction enzyme digestions. Briefly, 1 µg of plasmid DNA, 0.5 µl of the Nco I (NEW ENGLAND Biolads, UK, cat No: R3193),1 µl of H restriction enzyme buffer, and topped up to 10 µl with ddH_2O. The mixtures were then incubated at 37°C in a water bath for 4 hours to ensure complete digestion. The digested plasmids were analysed using agarose gel electrophoresis, as described in **Section 3.2.12.5.**

3.2.12.5 Agarose gel electrophoresis

Following the completion of restriction digestion, an assessment of the plasmid products obtained from the minipreparation was performed using agarose gel electrophoresis. To prepare a 1% agarose gel, 1 g of agarose tablets was combined with 100 ml of Tris-acetate ethylenediaminetetraacetic acid ([EDTA] TAE) buffer (40 mM Tris-acetate and 1 mM EDTA [pH 8.3]). The mixture was gently swirled and allowed to stand at room temperature for 10 minutes to allow the tablets to dissolve to release agarose, after which it was heated in a microwave for 5 minutes until the agarose was completely melted. Subsequently, 10 µl of SafeView (NBS Biologicals, Cambridgeshire, UK) with a concentration of 1 µg per ml was

introduced to the solution. After cooling for 2 minutes, the mixture was poured into a casting tray equipped with a comb to create wells. The agarose gel was then left at room temperature to solidify. Once the gel had solidified, the electrophoresis tank was filled with TAE buffer until the gel was submerged, and the comb was carefully removed. A 5 µl sample of digested plasmids was combined with 1/5th volume of 6x DNA loading dye (0.25% bromophenol blue, 30% glycerol). 5 µl of the sample and 5 µl marker (1 kb Ladder Plus [NBS Biologicals, UK) were loaded. The gel was run at 250V for 5 minutes during the initial phase. Subsequently, the voltage was reduced to 100V, and the electrophoresis continued for an additional 40 minutes. Finally, the gel was visualised under UV light using the ChemiDoc™ XRS imaging machine (BioRad, UK).

3.2.13 Transfection

3.2.13.1 Chemical method

Human embryonic Kidney (HEK)293T cells and MSCs were transfected using DNA Transfection Reagents (jetOPTIMUS®, Polyplus®, UK, cat No: 101000025/0.75 ML). Initially, 2 µg of plasmid DNA was combined with 200 µl of jetOPTIMUS® . The mixture was then briefly vortexed and centrifuged. Subsequently, 3 µl of JetOPTIMUS® Reagent was added to the diluted plasmid DNA, followed by another brief vortexing and centrifugation. The mixture was incubated for 10 minutes and then transferred to the cells in culture plates dropwise. The transfected cells were incubated at 37°C with 5% CO2 for 24 hours. The following day, the cells were examined under a microscope or a fluorescence microscope for evaluation (Zeiss, Germany).

3.2.13.2 Neon ™ Electroporation

Plasmids were prepared at a concentration of 5 µg per microliter in TE buffer (as supplied by the kit). Simultaneously, a control plasmid containing GFP was also prepared at the same concentration. On the day of transfection, cells were harvested when they reached 80% confluence. Following cell counting, they were suspended in PBS to achieve a final density of 1.0 x 10^^{7} cells per ml. A 24-well plate was used, with each well containing 0.5 ml of DMEM supplemented with 5% FBS but devoid of PS. The plate was preheated in an

incubator set at 37°C with 5% CO2. An electrolytic buffer, provided by the kit, was introduced into the Neon™ tube. Subsequently, 5 µg of plasmid were transferred to a sterile Eppendorf tube. Cells were then added to the Eppendorf tube containing plasmids and gently mixed. A new Neon™ tip was affixed to the Neon™ pipette, as per the manual's guidance. The tip was immersed into the mixture of plasmids and cells, drawing up 10 µl of the mixture. Following this, the entire pipette, with cells and plasmids, was inserted into the Neon™ tube, placed in the Neon™ Pipette station. The appropriate voltage and pulse duration were set, and upon pressing the start button, an electric pulse was delivered. After the display indicated "complete," the Neon™ Pipette was promptly removed, and the cell mixture was transferred into the previously prepared 24-well plate. The plate was gently shaken to ensure even cell seeding. Subsequently, the cells were incubated at 37°C with 5% CO2 overnight. The following day, the medium was replaced with regular DMEM supplemented with 5% FBS and 1% PS. Cell transfection was observed via a fluorescence microscope (Zeiss, Germany). Plasmids of interest were diluted to a 5 µg/µl concentration in TE buffer. Simultaneously, a control plasmid containing GFP was also diluted up to 5 µg/µl. On the day of transfection, MSC cells were harvested when they reached 80% confluency. Following the cell counting, the MSC cells were diluted in PBS to achieve a final density of 1.0 x 10^^{7} cells/ml. A 24-well with 0.5 ml of DMEM supplemented with 5% FBS but devoid of PS was preheated in an incubator at 37°C with 5% CO_2. An electrolytic buffer (ThermoFisher, Neon™, UK, cat No: MPK10096) was introduced into the Neon™ tube. Subsequently, 5 µg of the plasmid of interest was transferred to a sterile eppendorf tube, and the MSC cells were added to the plasmid-containing tube and gently mixed. A new Neon™ tip was affixed to the Neon™ pipette, as per the manual's guidance. The tip was immersed into the mixture of plasmids and MSC cells, drawing up 10 µL of the mixture. Following this, the entire pipette, with MSC cells and plasmids, was inserted into the Neon™ tube and placed in the Neon™ Pipette station. The 990 voltage and 1 time 40 ms pulse duration were set, and the mixture of cells and plasmid was subjected to electrical pulses. Once the electrical transfection was complete, the Neon™ Pipette was promptly removed, and the cell mixture was transferred into the previously prepared 24-well plate. The plate was gently swirled to ensure even cell seeding. Subsequently, the cells were incubated at 37°C with 5% CO_2 overnight. The following day, the medium was replaced

with regular DMEM supplemented with 5% FBS and 1% PS. Cell transfection was observed via a fluorescence microscope (Zeiss, Germany).

3.2.14 Transduce

For the transfection studies, HEK-293T cells were seeded at 40% in 10 cm culture plates and incubated at 37°C with 5% CO2 overnight. Once the cells had reached 80% confluency the next day, they were deemed suitable for the assembly of viral particles. HEK293T cells were then subjected to two washes with PBS, and their culture medium was replaced with DMEM, which was devoid of antibiotics. Subsequently, 600 µL of OPTI-MEM buffer (Gibco™, UK, cat No: 31985062) and plasmid DNA were added together, as shown in Table 3.6. The contents were homogenized either by gentle swirling or by careful agitation of the tube. The amount of PEI to DNA was a 3:1 ratio. The mixture was then incubated for 5 minutes. Following this, 54 µl PEI was added to each tube and the resultant mixture was incubated for 20 minutes at room temperature. Subsequently, the DNA:PEI mixture was added dropwise to the cells in the culture plate, with caution to avoid contact with the plate's walls. The contents were gently swirled to ensure even dispersion, and the cells were further incubated at 37 °C with 5% CO2 for a duration of 16 hours. The culture medium was then replaced with a standard growth medium (DMEM), and the medium containing viral particles was transferred to a waste container treated with Virkon. The cells were once again incubated at 37 °C with 5% CO2 for an additional 48 hours. After this 48-hour period, the medium containing viral envelope particles was harvested from the cells and transferred to a polypropylene storage tube. The medium was subsequently filtered through a 0.45 µm filter to remove any cellular debris. The collected medium was employed for lentivirus particle titration and transfection of target cells, while any remaining particles were stored at -80°C freezer. When mesenchymal stem cells (MSCs) reached a 50-60% confluence, polybrene (Santa Cruz Biotechnology, cat No: sc-134220) was added at a dilution ratio of 1:1000 to the lentivirus particle medium, which was then transferred to the MSCs. The cells were incubated at 37 °C with 5% CO2 for 4 hours before being replenished with DMEM medium. After 24 hours of incubation, the cells were examined using a confocal microscope (ZEISS LSM 980 Airyscan 2, Germany).

Table 3.7. Transduce Reagents Amounts.

Dish size (m)	Surface area (cm2)	HEK293 Cell density	DMEM/ 10%FBS no ABs (mL)	Opti-mem in tube (µl)	PEI (µl)	pRSV-rev (µg)	VSV-G (µg)	pMDLg/ pRRE (µg)	pLKO (µg)	DNA plasmid (µg)
100	55	3 x10^6	10	600	54	1.8	2.7	4.5	9.0	18

3.2.15 Enzyme-linked immunosorbent assay (ELISA)

The levels of BMP-2 in the cell lysates and media of transfected MSC-TERT and HEK293T cells were quantified using DuoSet R&D SYSTEM, USA, cat No: DY355. 100 µL of BMP-2 capture antibody in an assay diluent (PBS) was coated overnight on a 96-well half-area plate. Next day, the capture antibody was removed and the plate was washed three times using wash buffer (0.01% TBS with Tween-20 [TBST]). The plate was then blocked with 300 µL of reagent diluent (1% Bovine Serum Albumin (BSA)) at room temperature for 1 hour. Following this, 100 µL of either the sample or standards (46.9 –3000 pg/mL) in reagent diluent (top standard: 8 µL in 491 µL reagent dilute = 3000 pg/mL) was added to each well. The plate was covered with a lid and incubated for 2 hours at room temperature. After the incubation period, the plate was washed three times. Next, 100 µL of 0.25 µg detection antibody was incubated for 2 hours at room temperature. The plate was then washed three times with wash buffer. A 100 µL of the working dilution of Streptavidin-HRP was added to each well and incubated for 20 minutes at room temperature in the dark. After this incubation, the plate was washed three times. Following the washing steps, 100 µL of Ultra 3,3′,5,5′-Tetramethylbenzidine (TMB) substrate solution was added and incubated on a shaker at room temperature for 20 minutes in the dark. 50 µL of Stop Solution (0.18 M H2SO4 solution) was then added to each well, and the plate was gently tapped to ensure thorough mixing. Subsequently, the colour change was recorded by measuring the optical density (OD) at 450 nm using a microplate reader (FLUOstar Omega, BMG LABTECH,

Germany). The standard curve was generated, and the unknown samples were interpolated. The final concentrations of the samples were corrected by the dilution factor.

3.2.16 Cells Selection for Stable Cell Line

Various concentrations of puromycin can induce cell death across a range of cell types (Caputo et al., 2021). As a result, it was imperative to establish the minimum concentrations required to eliminate all cells for the establishment of stable cell lines. To accomplish this, both MSCs and HEK-293T cells were separately cultured in 24-well plates until they reached an 80% confluence. Subsequently, a series of gradient concentrations of puromycin (0 mg/ml, 0.25mg/ml, 0.5mg/ml, 0.75mg/ml, 1mg/ml, 1.25mg/ml, 1.5mg/ml, 2.0mg/ml 2.25mg/ml,2.5mg/ml) were introduced into the wells containing the cell cultures. These cells were then incubated for 1-2 weeks to ascertain the concentration that resulted in the minimum cell line viability. Throughout this period, the culture media containing different concentrations of puromycin were refreshed every 3 days to sustain the drug's effect on the cells. Daily observations were conducted to monitor the cells in the plates and construct a puromycin dose-response curve for both MSCs and HEK-293T cells.

3.2.17 Confocal Microscopy

Confocal microscopy was employed for the assess of transduced MSCs and transfected HEK-293T cells for expression of flouresence protein which were cultivated on 13 mm coverslips. The cells were cultured on these coverslips in the presence of medium obtained from the transfection and selection processes. Subsequently, the slides were meticulously examined and imaged using a confocal microscope equipped (ZEISS LSM 980 Airyscan 2, Germany) with a 20x objective lens. Emission wavelengths were specifically set at 405 nm for DAPI, 488 nm for GFP, and 647 nm for RFP or Cherry, respectively. Nuclear staining was assessed by DAPI (405 nm).

3.2.18 Histology of Undecalcificated Samples

The left limb of mouse from each group at a particular time-point (D7, D14, D28) was embedded in poly (methyl methacrylate) (PMMA) following serial dehydration. The embedded samples were cut into 10 μm sections using a microtome (EXAKT 300 CP Band System, Norderstedt, Germany), and undecalcified sections were stained using Toluidine Blue and Masson-Goldner's trichrome. These processes were outsourced from AICA Sci-tech Ltd. (Beijing, China). The histology sections were then imaged using a light microscope (Zeiss; Carl Zeiss Microscopy GmbH, Jena, Germany). The overall gross appearance of the specimens was imaged using a TM-DM10 imaging system (TOMLOV, Los Angeles, CA, USA).

3.2.19 Statistical Analysis

Statistical analyses were conducted using IBM SPSS Statistics software (IBM Corp., Armonk, NY, USA) and GraphPad Prism (GraphPad Software Inc., San Diego, CA, USA). Results are expressed as mean ± standard deviation (SD). A t-test was used for comparing two groups, while a 2-way analysis of variance (ANOVA) was utilised for comparisons involving multiple groups. Statistical significance was defined as $p<0.05$, where ns was non-significant, * $p<0.05$, ** $p<0.01$, *** $p<0.001$, and **** $p<0.0001$.

Chapter 4: Culturing of Mesenchymal Stem cells and Preparation of Artificial Allograft

4.1 Introduction

The production of bone grafts is a well-researched aspect within the field of regenerative medicine. Raw materials can be enhanced with medicines or growth factors to enhance their osteogenic capacity and improve patient outcomes. This chapter in the thesis explores the production of artificial allografts made by the culture of HA/CC scaffolds and MSCs, providing an entry point into the further enhancement of the scaffold's osteogenic capability.

4.1.1 Isolation and Culture of MSCs

The first step into the co-culture of scaffold and cells is the isolation of cells from the umbilical cord. Human umbilical cord-derived MSCs are a rich source of multipotent cells with immense regenerative potential (Dominici et al., 2006). Unlike other sources, such as bone marrow, obtaining MSCs from the umbilical cord is a non-invasive procedure and offers a unique population of cells primed for therapeutic applications. These cells, often referred to as HUMSCs, possess the ability to differentiate into various cell lineages, making them a valuable asset in tissue engineering endeavours. The initial phase of our exploration delves into the meticulous process of isolating MSCs from the umbilical cord. This involves a series of precise techniques to extract and cultivate these cells, ensuring their viability and potency. The umbilical cord, a previously overlooked biological treasure trove, is now recognized for harbouring MSCs with immense potential for tissue repair and regeneration. The isolation process bears importance, as which exact tissues they are isolated from and/or mixed can greatly affect the HUMSCs' differentiation potential (Ahmed et al., 2019; Hasegawa et al., 2010; Lode et al., 2008; Malladi et al., 2006; Wilson et al., 2002). With the successfully isolated HUMSCs, the next crucial step involves their cultivation. In the controlled environment of a cell culture, these cells undergo a series of passages and expansions, amplifying their numbers while maintaining their stem cell characteristics. This cultivation process not only ensures an abundant supply of cells for subsequent experiments but also allows us to observe their growth dynamics over time.

4.1.2 Scaffold Biocompatibility Assessment

The integration of synthetic scaffolds with HUMSCs marks a pivotal juncture in our exploration (Fu et al., 2013). Biocompatibility, a term that encapsulates the harmony between cells and materials, is scrutinised through rigorous assessments. Alamar Blue and cell counting kit (CCK)-8 tests stand as sentinels, gauging the metabolic activity and viability of cells when cultured with scaffolds. These tests are not just assays; they are windows into the symbiotic relationship between cells and the engineered environment, guiding us toward scaffolds that foster optimal cellular responses.

4.1.3 MSC Differentiation

In the intricate landscape of regenerative medicine, understanding the trajectory of MSCs goes beyond their fundamental aspects of growth and biocompatibility. MSCs, known for their remarkable versatility, embark on a cellular journey characterised by fate determination, wherein they exhibit their remarkable potential for differentiation into distinct lineages. HUMSCs possess the unique ability to undergo differentiation along adipogenic and osteogenic pathways (James, 2013). Adipogenic differentiation signifies the cells' capability to metamorphose into adipocytes, specialised cells responsible for fat storage. On the other hand, osteogenic differentiation marks the cells' commitment to the osteoblastic lineage, emphasising their role in bone formation and mineralisation.

These differentiation pathways represent a dynamic cellular orchestra, where HUMSCs showcase their adaptive prowess and capacity to specialize in response to environmental cues. The cellular fate determination process is not merely a biological phenomenon; it is a finely tuned response to the microenvironment, where signals dictate whether the cells will assume a fat-storing (adipogenic) or bone-forming (osteocytic) identity. This intricate dance of fate determination holds profound implications for tissue engineering and regenerative medicine, as it opens avenues for manipulating and directing cellular

behaviour for therapeutic purposes (Safari et al., 2021). As the HUMSCs navigate these divergent pathways, the cellular orchestra unfolds, revealing the plasticity and responsiveness of these cells to the cues present in their surroundings. The ability to seamlessly transition between adipogenic and osteogenic lineages underscores the regenerative potential of MSCs, positioning them as key players in the quest for developing advanced tissue engineering strategies.

4.1.4 Analysis of Osteogenic Genes Expression Level

As the HUMSCs undergo osteogenic differentiation, our focus sharpens on key markers indicative of this transformative process. RUNX2 and Osteocalcin, pivotal players in osteogenesis, become the focal points of analysis (Dong et al., 2016; Neve et al., 2013). Quantifying expression levels offers a molecular perspective for evaluating the success and efficiency of osteogenic differentiation.
Overall, this part of the stuy aimed to isolate and culture/expand HUMSCs and observe their growth characteristics and compatibility with scaffold particles in co-culture, providing technical and material support for research studies in subsequent results chapters. Simultaneously, efforts were made to detect and analyze whether MSCs sourced from the umbilical cord effectively retain their osteogenic differentiation potential. (Safari et al., 2021).

4.1.5 Aim and Objective

The aim of this study is to culture MSCs, fabricate scaffolds for later use, and verify the osteogenic differentiation potential of MSCs.

The objectives of this section of the study are as follows:

1. To successfully isolate and culture MSCs and observe their growth characteristics.

2. To assess the biocompatibility of the scaffold and observe the microscopic biological interactions between MSCs and the scaffold.

3. To determine the osteogenic differentiation potential of MSCs through culturing in various differentiation media and analysing multiple biomarkers of differentiation.

4.2 Methods

4.2.1 Isolation of MSCs from Umbilical Cord (HUMSCs)

Umbilical cord tissue was aseptically dissected, cleaned, and blood vessels removed to isolate Wharton's jelly. Fragments were placed in culture flasks with medium (DMEM, FBS, penicillin-streptomycin) and incubated at 37°C. MSC outgrowth was monitored, with medium changed every 3-4 days(see **Section 3.2.1**).

4.2.2 MSCs growth curve producing

To investigate the growth dynamics of immortalized MSCs isolated from human bone marrow (MSC-TERT cells), varying cell numbers (500, 1000, 2000, 4000, 8000, 16000, or 32000 cells per well) were introduced in 100µl of DMEM cell culture medium across different wells of a 96-well plate. This configuration included duplicate wells for each cell density. The cell culture was maintained at a controlled environment of 5% CO_2 and 37°C in an incubator, utilising DMEM medium supplemented with 10% FBS and 1% PS. The culture medium was replaced with a fresh medium every 72 hours. During the culture period, cells from different seeding densities were subjected daily to the Alamar Blue assay. Subsequently, the growth curve for MSC-TERT cells was constructed based on the obtained assay results.

4.2.3 Biocompatibility Assay

1 Scaffold preparation

The hydroxyapatite (HA)/calcium carbonate ($CaCO_3$) (HA/CC) scaffold material underwent a process of grinding with mortar and pestle to generate micro-particles. The grounded HA/CC powder was subsequently passed through a multi-layered sieve cloth to obtain particles within the size range of 200-300µm. The resultant micro-scale particles were aseptically transferred into glass vials and steam sterilised by autoclaving at 121°C for 15

minutes. Following sterilisation, the treated particles were immersed in the culture medium (DMEM) under strict aseptic conditions for 24 h for later use.

2 AlamarBlue Assay

After 24h of incubation in DMEM, 20-30 particles of the scaffold material were introduced in quadruplicate into wells in a 96-well plate containing previously cultured HUMSCs at 80% confluency (added 5000 cells in 100µl per well and cultured3Y days to achieve 80% confluency). In the control group, no particles were added to the cell wells. The cells and particles were co-cultured by incubating in an incubator at 37°C and 5% CO2. The culture medium was refreshed every three days. At specific time points (0h, 24h, 48h, 72h, 96h, 120h and 144h) after adding the scaffold particles, the cell culture medium of both groups was replaced with a fresh culture medium containing 10% Alamar Blue. The plates were then incubated for 4 hours in an incubator at 37°C and 5% CO2. The fluorescence of the culture medium was measured at 560 nm excitation and 590 nm emission using a fluorescence plate reader (BMG LABTECH, Germany) (Eilenberger et al., 2018). The average fluorescence intensity obtained for each time point was used to construct an Alamar Blue assay graph for analysis by using relative fluorescence units (RFU) on the Y-axis and the incubation time on the X-axis.

3 CCK-8 Assay

20-30 microspheres that had been pre-soaked in cell culture medium (DMEM) for 24h were introduced in quintuplicate into a 96-well plate containing previously cultured HUMSCs at 80% confluency. The control group's cell wells remained devoid of microspheres. Scaffold particles and cells were co-cultured at 5% CO2 and 37°C in an incubator. On the second, fourth, and sixth day of incubation, the treatment was terminated by replacing the cell culture medium microspheres or no microspheres with media containing 10% cell counting kit (CCK)-8 reagent. After returning the 96-well plate to the incubator for a 4-hour incubation period, the colour change was observed. Subsequently, the CCK-8 reaction

solution (100µl) was transferred from the 96-well plate into a new 96-well plate and the optical density (OD) at 450 nm (OD450) for each group at each time point was determined using a plate reader (BMG LABTECH, Germany). CCK-8 test curves were generated based on the OD450 values (Y-axis) and incubation time (X-axis).

4.2.4 Osteogenic differentiation

Three sets of HUMSCs (passage 4) grown in 24-well plates were established and categorised into three groups: In Group 1, cells were cultured using a standard growth medium (DEMEM supplemented with 10% FBS and 1% PS). In Group 2, MSCs were cultured in an osteogenic differentiation medium prepared from an Osteogenesis differentiation kit (Gibco™, UK, cat No: A1007201). In Group 3, MSCs cultured in an osteogenic differentiation medium supplemented with BMP-2 (100ng/ml). The cells were maintained in an incubator at 37°C with 5% CO_2. The culture medium was replaced every 3-4 days. Cell cultures in each group were terminated at specific time points, namely, 3, 7, 14, 21, and 28 days. Some cells were harvested for qPCR analysis, while others were preserved for subsequent staining assessments.

4.2.5 Alkaline Phosphatase (ALP) Staining

At the time points of 3, 7, 14, 21, and 28 days following the initiation of differentiation, the cellular samples were prepared for staining. The cells within each designated group were gently rinsed with PBS. Subsequently, 200 µL of the appropriate substrate solution (at working concentration) was added to each well to cover uniformly the cell monolayer. The staining process was carried out in dim light at room temperature for 30 minutes. The enzymatic reaction was stopped by adding 50 µl of 0.1 M ethylenediaminetetraacetic acid (EDTA) (20 mM final concentration) to the reaction mixture. Visual examination and image acquisition of the stained cells were conducted using a light microscope of the ZEISS brand.

4.2.6 Oil Red O Stain

HUMSCs were cultured in adipogenic differentiation medium, which was made from an Adipogenic differentiation kit (Gibco™, UK, cat No: A1007001), and a standard growth medium (control) for 14 days. Following the completion of adipogenic differentiation, the cells residing in a 6-well plate were subjected to a delicate washing procedure utilising 2.4 ml of PBS. Subsequently, fixation was carried out at room temperature for 15 minutes by adding 2.4 ml of 4% paraformaldehyde (PFA) solution. Oil Red O (0.5% made in isopropanol) was diluted in deionised water at a ratio of 6:4 to obtain the working Oil Red O solution. The cells were subsequently subjected to PBS washing, followed by a brief rinsing step involving 2.4 ml of 60% isopropanol. The adipocytes were subjected to staining through the application of 1 ml of the Oil Red O working solution, maintained at room temperature for 30 minutes. After the staining process, the cells underwent four consecutive washes with deionised water. Finally, the Oil Red O stained cells were observed utilizing phase-contrast microscopy at a magnification of x10 and images were acquired.

4.2.7 Alizarin Red Stain

After 28 days of inducing cellular differentiation of HUMSCs, the culture medium was removed and the cells were gently rinsed with PBS. Subsequently, the cells were stained with (250 µl per well) of Alizarin Red Staining solution (Millipore, UK, cat No:2003999) for 30 minutes at room temperature in the absence of light. Following this incubation, the Alizarin Red Stain solution was aspirated and replaced with 250 µl of PBS to cover the cell surface. The Alizarin Red staining was then examined using optical microscopy and photographic documentation of the staining outcomes was performed.

4.2.8 q-PCR

At a specific time point during the osteogenic differentiation process, cells were collected for the procedure of q-PCR to assess the Runx2 and Osteocalcin expressions. The details of the test can be seen in **section 3.2.12.**

4.2.9 Statistics

Graphs were generated using GraphPad Prism software version 9.5.1 (GraphPad Software, LLC) to analyse the data. The data were as presented as mean ± standard deviation (SD) and statistically analysed by using multiple or paired two-tailed t-tests and considering $p > 0.05$ as statistically not significant (ns).

4.3 Results

4.3.1 HUMSC Isolation and Culturing

The examination of MSCs isolated from the umbilical cord under a light microscope (**Figure 4.1A-E**) showed the cells with elongated and spindle-shaped morphology, a clear morphological feature consistent with the well-established criteria for undifferentiated MSCs (Gottipamula et al., 2016).

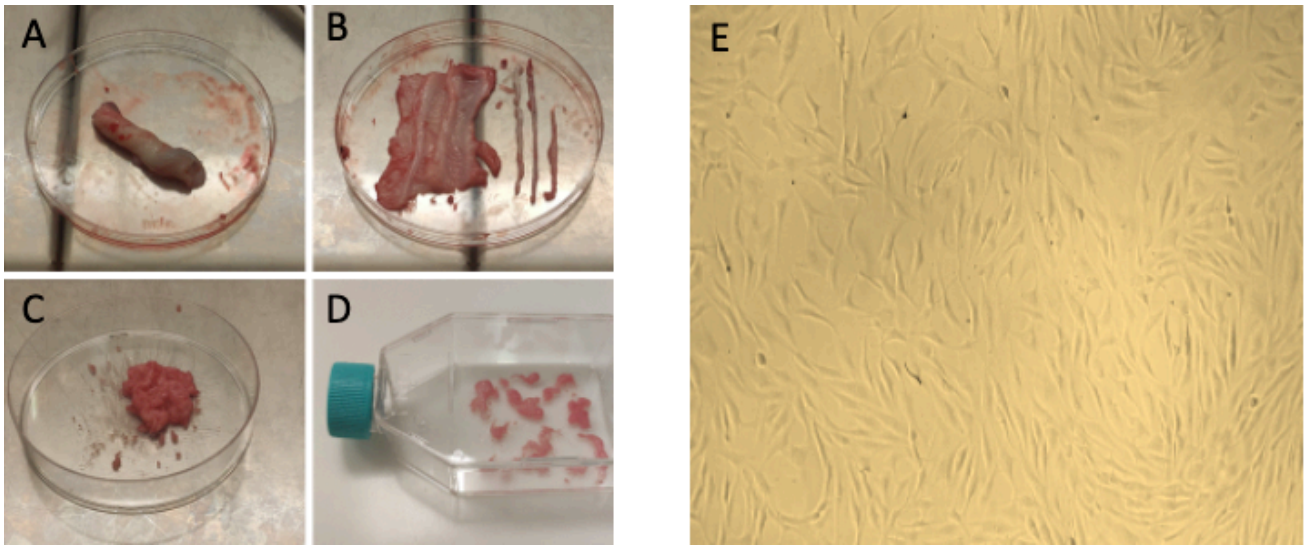

Figure 4.1. Visualisation of the umbilical cord, its dissection and isolation of MSCs from it.
The isolation of MSCs from the umbilical cord (HUMSCs) and isolated HUMSCs were visualised using a light microscope at 10x magnification. A piece of umbilical cord (**A**) was longitudinally dissected (**B**) and sliced into small (1-2mm in size) fragments after removing the blood vessels (**C**) and transferred the fragments into a T25 culture flask by autoclaved medicine spoon (**D**) and incubated the flask at 37°C/5% CO2 for 7 days. (**E**) Photomicrograph of the morphology of cultured HUMSCs.

4.3.2 MSC growth curve

Figure 4.2 shows cell growth over 6 days with initial cell seeding densities of $0.5x10^3$, $1x10^3$, $2x10^3$, $4x10^3$, $8x10^3$, $1.6x10^4$, and $3.2x10^4$ per well of a 96-well plate. This was done to identify the optimal cell density required for optimal cell proliferation. The Alamar Blue assay was used to measure cell proliferation in each well. Results indicate that when MSC-TERT cells were seeded at 16,000 cells per well, their proliferation started from day 2 and

peaked on day 4, thus emphasising that the initial seeding density has an influence on cell proliferation over time. Telomerase-immortalized human mesenchymal stromal cells (MSC-TERT) are derived from human MSCs and have been demonstrated to possess identical characteristics to MSCs, including cell morphology, surface markers, growth rate, and differentiation potential. In this experiment (Altmann et al., 2021), the MSC-TERT cell line was utilised to assess numerous properties of UCMSCs.

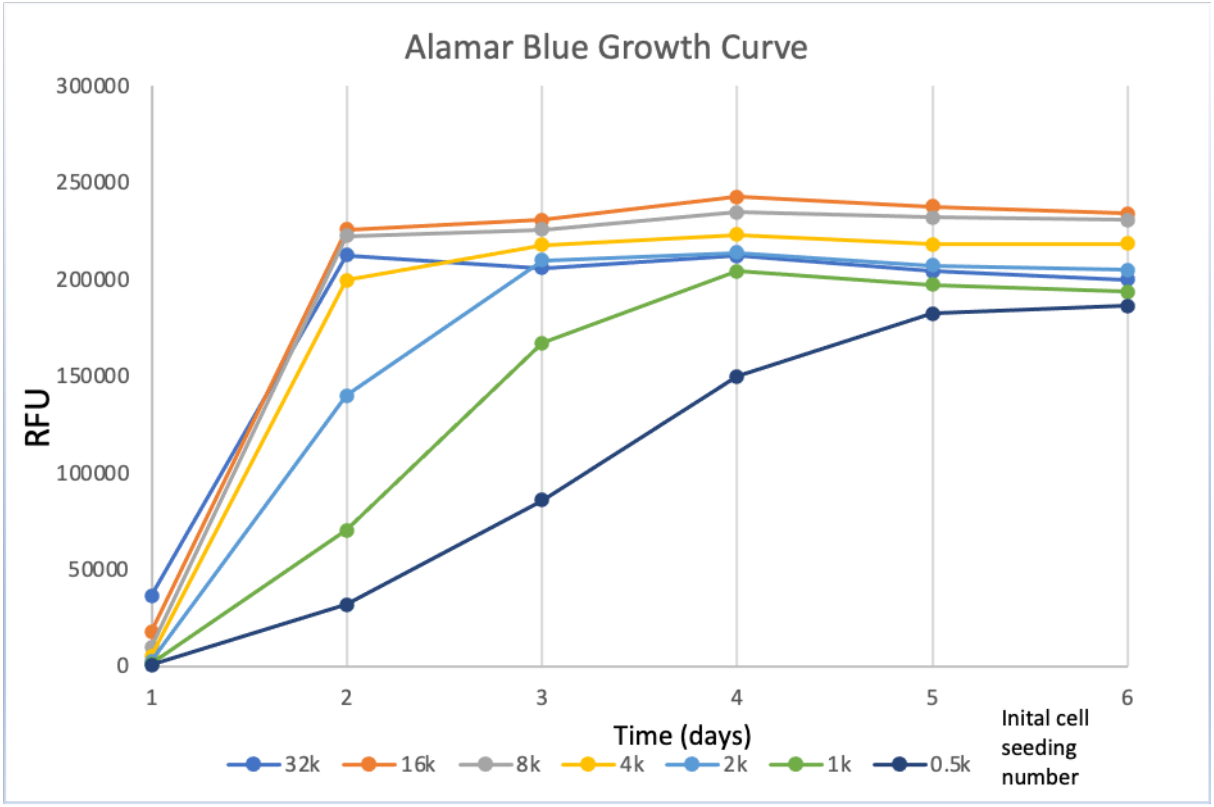

Figure 4.2. The growth of MSCs with varying initial cell seeding densities over 6 days.
The cells were seeded 500-32,000 cells per well of a 96-well plate and the proliferation of cells was assessed using the Alamar Blue assay (see 4.2.3.1) every day for 6 days.

4.3.3 Scaffold Biocompatibility

After growing HUMSCs to 80% confluency in a 96-well plate, HA/CC particles were placed into the wells containing HUMSCs and co-culturing for 10 days. The scaffold particles adhered by cells were fixed, dehydrated, and dried for SEM (**Figure 4.3**). The surface of the HA/CC particles appears to be rough and irregular under microscopic examination. There are visible pores and crevices distributed across the surface (**Figure 4.3A & B**). A large

number of UCMSC cells were observed adhering to and aggregating on the surface of the particles, with cell extensions penetrating the interstices of the scaffold surface (**Figure 4.3C**). The three-dimensional (3-D) structure of the scaffold particles vividly displayed the aggregation of MSC cells onto the scaffold and their migration to the non-contact surface of the particles, demonstrating the cells' migratory capacity and showcasing the excellent interfacial affinity of HA/CC.

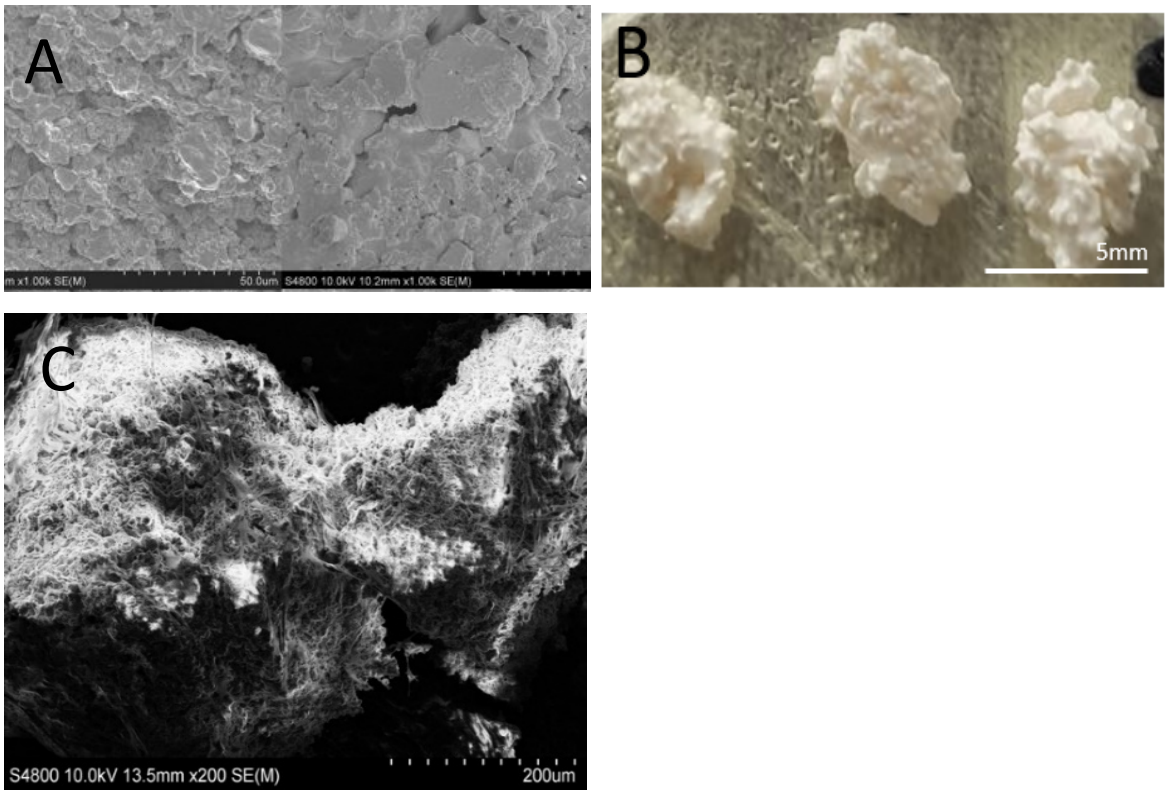

Figure 4.3 Visualising the HA/CC scaffold surface structure using SEM.
The surface HA/CC without or with cultured HUMSCs were fixed using glutaraldehyde was analysed using SEM. The surface structure of the HA/CC scaffold at (**A**) and (**B**) magnifications. (**C**) displays an SEM image illustrating HUMSCs cultured for 10 days on the HA/CC scaffold.

The Biocompatibility of HA/CC

The Alamar blue assay was used to assess the viability of HUMSCs cultured with the HA/CC for 144 hours. This was done to analyse the biocompatibility of the scaffold with HUMSCs. This test comprised a control group, consisting of only HUMSCs, and a group of HUMSCs seeded onto the HA/CC scaffold. The fluorescence intensity (RFU) measures, were taken at regular intervals of 24 hours, starting from hour 0 to 144 hours. The results (**Figure 4.4A**)

showed a consistent upward trend in the RFU observed in both groups, which indicates an overall increase in cell proliferation over time. Although statistically not significant ($p > 0.05$), the lack of difference between cells cultured on their own and with the scaffold suggests that the presence of the HA/CC scaffold did not induce cellular toxicity as MSCs were able to proliferate continuously at a rate like that of the control group.

In addition to the Alamar Blue assay, the CCK8 test was used to assess the viability of cells growing on the scaffold by comparing the proliferation of cells cultured without or with the scaffolds for 6 days (**Figure 4.4B**). The optical density at 450 nm (OD450) of each group was recorded on 2, 4 and 6 days to analyse cell proliferation over time. Both groups exhibited a consistent increase in OD450 values during the experimental period, indicating a rise in cell proliferation. The experimental group, where cells were cultured on the scaffold, demonstrated an OD450 increase comparable to that of the control group. Similarly to the Alamar Blue assay, these findings suggest that the presence of HA/CC does not result in a statistically significant difference in cell proliferation relative to the control group.

Both assays have suggested that HA/CC possesses favourable biocompatibility with HUMSCs, thus confirming that it is not toxic to cells and that it is a promising candidate for future applications in skeletal tissue regeneration.

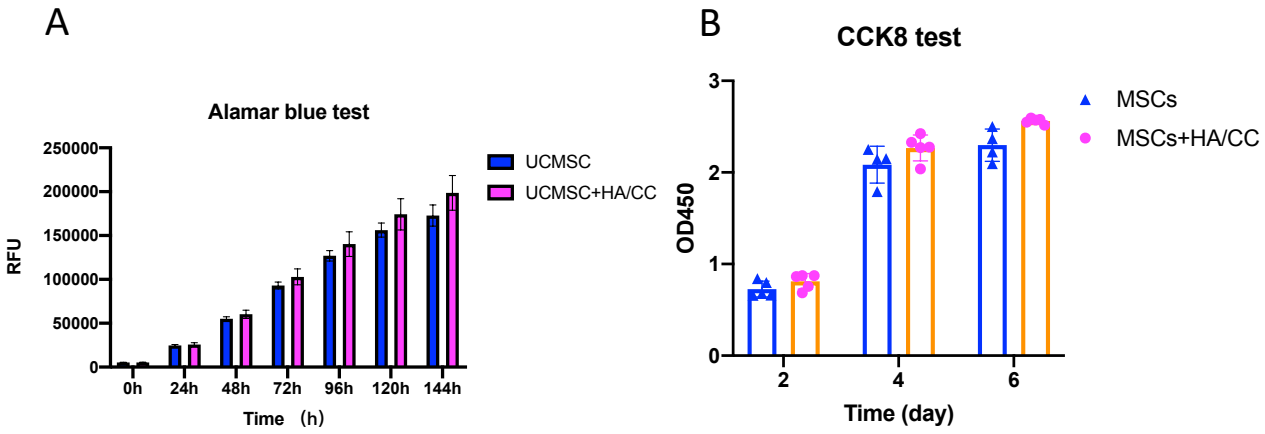

Figure 4.4 Effect of HA/CC scaffold on the viability of HUMSCs.
The viability of HUMSCs co-cultured with HA/CC scaffolds was assessed by Alamar Blue (**A**) and CCK8 (**B**) assays. Each bar represents the mean value of the test done in quadruplicate and error bars indicate SD. A paired two-tailed t-test was conducted to determine the statistical significance of the overall effect. The results of the t-test revealed no significant difference between the two groups (ns,$p > 0.05$, $t = 3.378$, $df = 2$, $n = 4$).

4.3.4 Analysing Osteogenic Differentiation of HUMSCs

The progression of osteogenic differentiation of HUMSCs when cultured in an osteogenic medium without or with BMP-2 (100ng/ml) for 28 days was investigated by measuring ALP activity using ALP staining (**Figure 4.5**) and Runx2/Osteocalicin biomarker expression by qPCR (**Figure 4.6**). BMP-2 is included in the differentiation medium since it potentiates osteogenesis induced by osteogenic medium. In the control group, HUMSC cultured in the normal cell medium for 3-28 days exhibited low ALP activity, as shown by their lighter red colour staining (the intensity of staining is directly proportional to the activity). In contrast to this, both groups A (differentiated using osteogenesis medium) and B (differentiated using osteogenesis medium with 100ng/ml BMP-2 protein) displayed a gradual increase in the intensity of the stain up to day 28. These results might indicate that the ALP activity acts as an early marker for osteoblastic activity. Taking together, HUMSC were in the process of successfully differentiating in differentiation medium without or with BMP-2 (100ng/ml). Interestingly, HUMSCs cultured in a differentiation medium with BMP-2 showed enhanced ALP activity, notably by the cells differentiated for 21 or 28 days, where the staining intensity was more pronounced than in the control group. The enhanced intensity of the ALP staining in the presence of BMP-2 suggests an increase in the ALP activity and, thus, a more robust osteogenic response under these conditions. Therefore, these results suggest that HUMSCs cultured in osteogenic medium can successfully differentiate into osteoblasts, which is further enhanced by the addition of BMP-2.

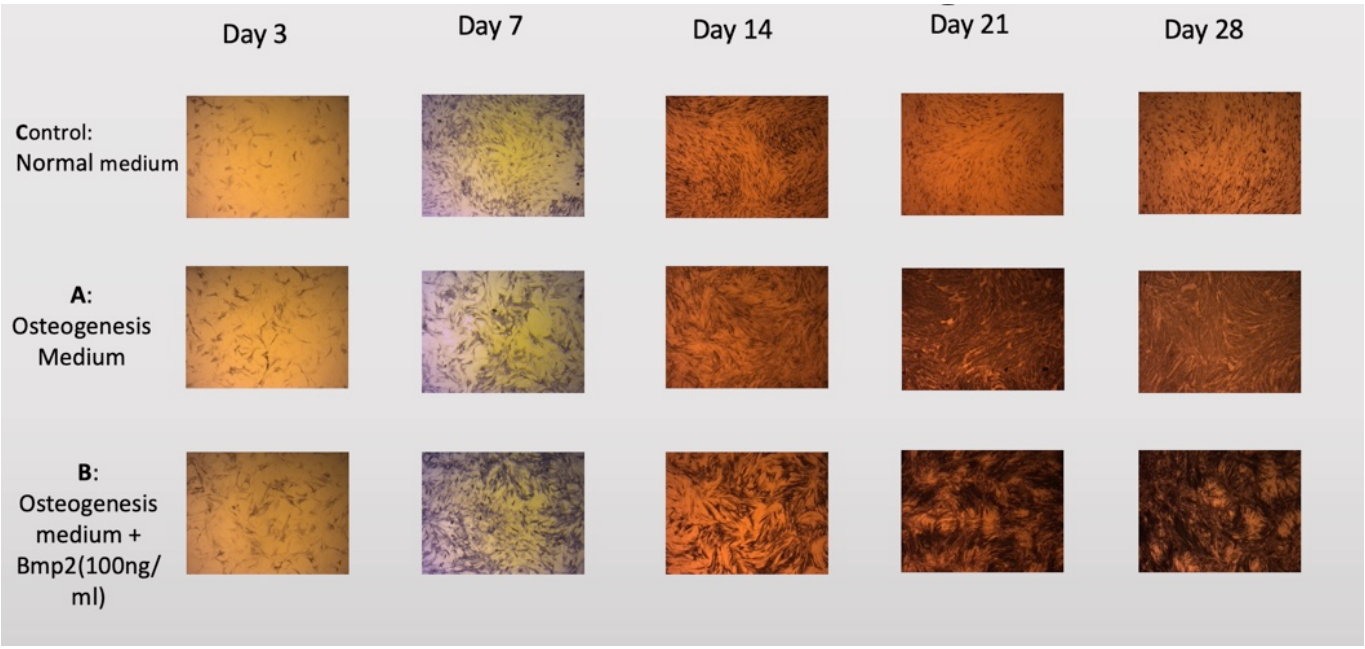

Figure 4.5. Assessing time-dependent differentiation of HUMSCs by ALP staining.
HUMSCs were cultured in DMEM culture medium (**control**), osteogenic medium (**A**), or osteogenic medium containing 100ng/ml BMP-2 (**B**) for 3-28 days. After differentiation, cells were stained using an ALP staining solution. Images were then taken using ZEISS PrimoVert (Carl Zeiss Microscopy, GmbH) and analysed using ZEISS ZEN CORE version 3.5.6.

Runx2 - When HUMSCs cultured in osteogenic differentiation medium (ODM) in the presence and absence of BMP-2 (100ng/ml) for 3-28 days, the increase in *Runx2* gene expression, assessed by qPCR, in HUMSCs treated with ODM started on day 21 and reached maximum on day 28. In contrast, the increase in Runx2 gene expression in HUMSCs treated with OMD+BMP-2 started on day 14 (4.33 $\pm$ 1.6 fold) and peaked on day 28 of the treatment (7.32 $\pm$ 2.35) (**Figure 4.6A**). Similarly, using qPCR, osteocalcin gene expression was measured over 28 days in HUMSCs treated with and without BMP-2 protein in the osteogenesis differentiation medium (**Figure 4.6B**). Results illustrated an increase of osteocalcin mRNA in both groups from day 3 to day 28. Osteocalcin mRNA expression peaked at day 14 in the presence or absence of BMP-2 protein. In the absence of BMP-2, osteocalcin mRNA expression was 2.864 (SD = 1.98), while in the presence of BMP-2, osteocalcin mRNA expression showed a significantly higher mean of 24.564 (SD = 13.067) at day 14. In contrast to the Runx2 gene expression, Osteocalcin gene expression for both groups decreased on days 21 and 28. However, the experimental group containing BMP-2 maintained a higher concentration of Osteocalcin than its control counterpart throughout

the 28-day treatment. Therefore, these findings suggest that the addition of BMP-2 to the osteogenic medium exhibited a higher expression of the Runx2 and Osteocalcin genes, suggesting enhanced differentiation in HUMSC cells. Therefore, it might be beneficial to incorporate BMP-2 to enhance the promotion of osteogenic differentiation in HUMSCs in future studies.

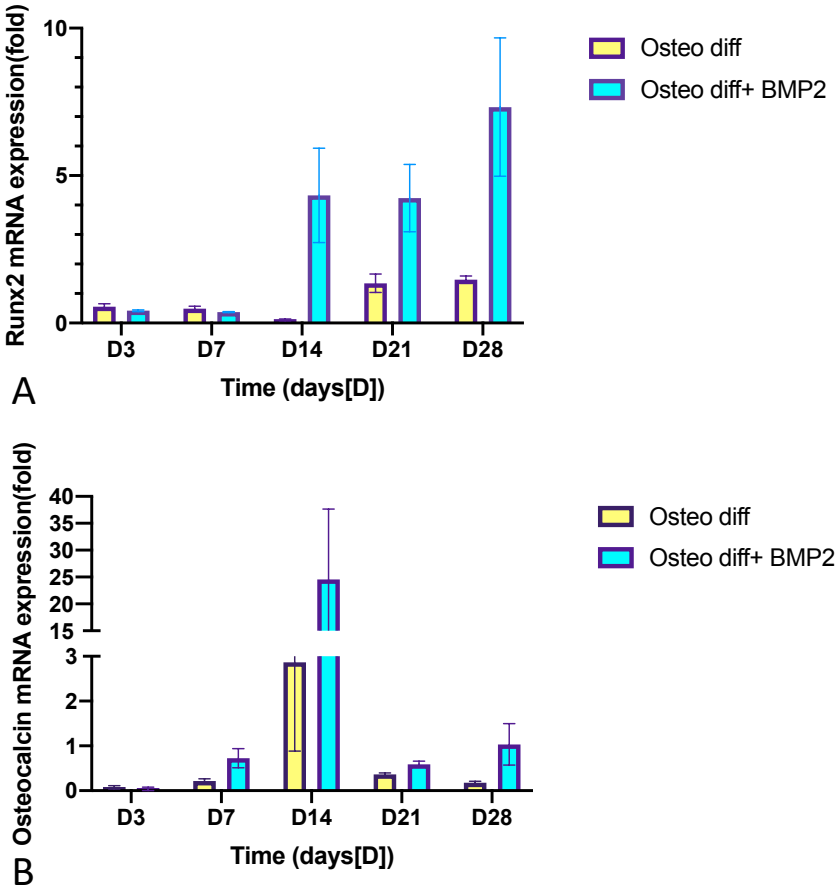

Figure 4.6. Analysis of the expression of Runx2 and Osteocalcin genes in osteogenically differentiated HUMSCs.

Total RNA isolated from HMSCs differentiated in osteogenic medium without or with BMP-2 protein for 3-28 days was converted to cDNA by using reverse transcription. The cDNA was used to analyse the expression of Runx2 (**A**) and Osteocalcin (**B**) by using qualitative PCR (qPCR). The fold increase in the expression in differentiated HUMSCs relative to the control group (undifferentiated HUMSCs) is shown on the Y-axis. Statistical analysis revealed that there was a statistically significant difference between the two groups from day 14 (p value (*p)*< 0.001, t value of t-test (t)=5.304, Degree of Freedom (DF)=20), on day 21 (*p*=0.0083, t=3.630, DF=20) and day 28 (*p*=0.0001, t=7.357, DF=20,n=3) (**Figure 4.6A**). Runx2 expression was higher starting from day 14 and continued to increase until day 28 in differenciation group. There was also a significant between the two groups for the expression of osteocalcin on day 14

($p < 0.001$, t=5.859, DF=17, n=3), **(Figure 4.6B)**. Osteocalcin gene expression was higher in the differentiation group at day 14, reaching its peak at that time, and then decreased after 2 weeks.

4.3.5 Analysis of HUMSCs differentiation to adipocytes and Osteocytes

To confirm the adipogenic differentiation potential, one of the various differentiation capabilities of MSC cells, HUMSC cells were treated with adipogenic induction medium for 14 days, followed by Oil Red O staining. Control group cells were cultured in regular culture medium for 14 days followed by Oil Red O staining too. **Figure 4.7A** shows the overview image of osteogenic differentiated MSCs stained by Alison Red into red colour, the adipose differentiated MSCs only got pink colour. **Figure 4.7B** displayed the adipo-differentiated MSC cells stained in Oil Red. The results indicate that HUMSCs have osteogenic differentiation and adipogenic differentiation potentials.

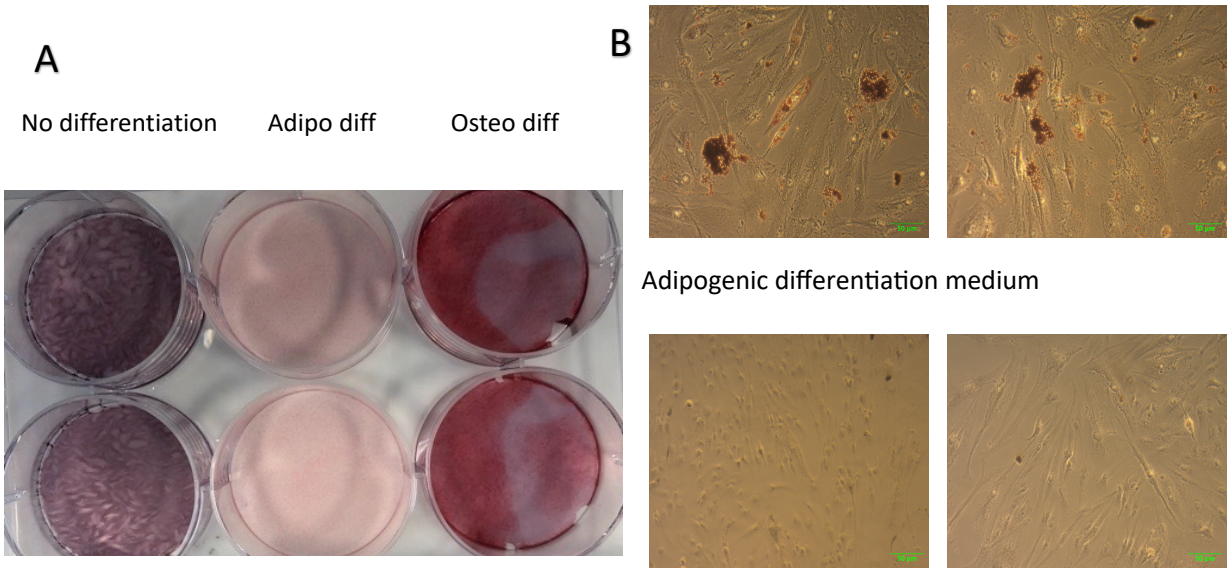

Figure 4.7. Osteogenic and adipogenic differentiation of HUMSC cells.
The cells were treated with Adipogenic differentiation media (Gibco™, UK, cat No: A1007001) and normal culture media, respectively**,** for 14 days. HUMSC cells were stained with Alizarin Red for

adipogenic and osteogenic (**A**) and Oil Red for adipogenic-only (**B**) differentiation. In panel B, the upper two images displayed the adipogenic-differentiated MSC cells stained with Oil Red O. The lower two control group images show no Oil Red O staining. The scale bar is 50 μm.

4.4 Discussion

MSCs can be isolated from various human and animal organ tissues and propagated *in vitro*. For instance, MSCs can be isolated from bone marrow, muscle and kidney cells (Samsonraj et al., 2017). However, HUMSCs are relatively easier to isolate and expand compared to MSCs isolated from other sources and they possess multiple differentiation potentials as well as the potential for multiple passages while retaining stem cell characteristics. Nevertheless, due to ethical concerns, HUMSCs are difficult to obtain in many research centres and are therefore less frequently used as a source for research studies.

4.4.1 Isolation, Culture, and Growth Characteristics of HUMSCs

Han et al. obtained a greater yield of cells from umbilical cord tissue by employing an improved enzymatic digestion of tissue procedure (Han et al., 2013). However, some researchers are inclined to use enzymatic digestion to obtain a higher cell yield. This is due to concerns exist among researchers regarding whether enzymatic digestion may affect the characteristics of the obtained cells (Skog et al., 2019). Xin et al. conducted comparative experiments to assess cell viability, surface antigen expression, and cell growth curves between enzymatically digested and non-digested cells, finding no significant abnormalities in either group (Xin et al., 2013). So, in our studies, MSCs were obtained through natural cell migration and their stem cell characteristics after passaging were assessed (Xia et al., 2005). The method chosen in this experiment ensured that MSCs were obtained naturally without interference, fully meeting the requirements of subsequent experiments. Following finely minced umbilical cord tissue placed in a tissue culture flask, MSCs adhered to the culture flask surface and proliferated in a spindle-shaped morphology. When viewed under a light microscope, spindle-shaped MSCs were uniformly distributed at the bottom of the culture dish (**Figure 4.1**). Different numbers of HUMSCs were seeded per well to compare the subsequent growth patterns associated with varying initial seeding densities, ultimately identifying an optimal initial seeding density for proliferation (**Figure 4.2**).

4.4.2 Biocompatibility of HA/CC

Biocompatibility refers to the ability of a material to interact with biological systems without causing harmful effects. In the case of scaffold materials, biocompatibility is crucial to ensure that the scaffold does not trigger adverse reactions or immune responses when implanted into living organisms. Factors related to the biocompatibility of the HA/CC material were evaluated in this study. Scanning electron microscopy (SEM) was used to examine the surface microstructure of the scaffold, revealing that its pore structure is more conducive to cell adhesion and growth. The smooth surface of the material may impede cell adhesion. For instance, agarose, a natural polysaccharide polymer with a smooth surface, is commonly synthesised into hydrogels for use in tissue engineering scaffolds or as coating materials, yet it does not facilitate cell attachment to its surface (Latfi et al., 2019). In order to enhance the adhesive properties of the smooth surface, auxiliary materials such as extracellular matrix components need to be added to improve the material's interface. In our study, the rough-surfaced HA/CC scaffolds were used to improve the attachment of cells. SEM analysis of HUMSCs cultured on HA/CC scaffolds confirmed that HUMSC cells could adhere naturally to the material surface and proliferate normally. Our work assessed the surface structure of the material, the affinity of its ultrastructure, its immunocompatibility, and the stability of the material within a certain time frame. Stability entails the material remaining intact without undergoing dissolution or degradation following coculture in the culture medium for around 10 days. In the in vitro cell culture studies, it was observed that HA/CC particles could remain unchanged as granules (100-500 µm in size) in the medium for an extended period, exceeding one month, indicating no loss of viability of cells, suggesting the excellent biocompatibility of the HA/CC material used in this experiment (Shard & Tomlins, 2006).

Implantable materials for bone must undergo *in vitro* experimental testing and screening before clinical use to minimise adverse reactions (Willershausen et al., 2013). The material should demonstrate low cytotoxicity and high biocompatibility (Kehoe et al., 2012). For the biocompatibility assessment of orthopaedic materials, there are numerous experimental methods available, including common viability assays such as 3-(4,5-dimethylthiazol-2-yl)-

2,5-diphenyl-2H-tetrazolium bromide (MTT) assay, CCK-8 assay and Alamar Blue assay. In this study, CCK-8 and Alamar Blue assays were chosen to jointly evaluate the material's compatibility with cells in different ways (**Figure 4.4**). Comparable outcomes were observed with the Alamar Blue and CCK-8 assays, indicating that the inclusion of HA/CC does not yield a statistically notable variance in cellular proliferation when compared to that of cells cultured without HA/CC particles. The results consistently indicated that HUMSCs cultured with HA/CC exhibited growth patterns similar to those cultured solely in the medium, suggesting the excellent biocompatibility of the HA/CC material used in this study.

4.4.3 Osteogenetic differentiation potential of MSCs

MSCs are a heterogeneous population of adult stem cells found in various tissues, including bone marrow, adipose tissue, and umbilical cord. They have the unique ability to differentiate into multiple cell lineages, such as osteoblasts, adipocytes, and chondrocytes, as well as other cell types including myocytes, neurons, and endothelial cells (Mushahary et al., 2018). This multipotent differentiation potential, coupled with their immunomodulatory properties and secretion of trophic factors, makes MSCs a promising candidate for regenerative medicine therapies, including the repair and regeneration of damaged tissues and organs (Ji et al., 2020).

Several investigations have substantiated the critical involvement of BMP-2 in the osteogenic differentiation process of HUMSCs (De Biase & Capanna, 2005). Beyond the direct administration of recombinant BMP-2 proteins, studies have confirmed the capacity of adenoviral vector-mediated BMP-2 gene transfer to initiate bone formation both *in vitro* and *in vivo* (Virk et al., 2008). Runx2 is a key osteogenic transcription factor. It could be one of the initial master transcription factors guiding the differentiation of MSCs into osteoblasts (Komori, 2018). It is conceivable that BMP-2 may not exclusively serve as the primary initiator of Runx2 expression during the osteogenic differentiation process of HUMSCs. A previous study has indicated that several developmentally significant ligands, including transforming growth factor (TGF)-β1, fibroblast growth factors (FGFs) and BMP9,

possess the capacity to stimulate Runx2 expression and augment ALP expression in new bone generation (Narayanan et al., 2019).

ALP plays a critical role in the process of osteogenesis, which is the formation of bone tissue. ALP is an enzyme involved in the mineralisation of bone matrix, where it hydrolyses inorganic pyrophosphate, a potent inhibitor of mineralisation, to promote the deposition of calcium and phosphate ions, essential components of HA crystals found in bone (Mikami et al., 2016). Additionally, the ALP activity is often used as a biomarker of osteoblastic differentiation, as its expression increases during the early stages of osteogenesis of MSCs. Therefore, monitoring ALP activity is routinely used to assess the progression of osteogenic differentiation *in vitro* and *in vivo*. In this section of the study, HUMSCs were induced to differentiate using BMP-2 and osteogenic differentiation medium to assess their osteogenic differentiation potential. The ALP staining of HUMSCs at multiple time points of differentiation indicated that the ALP expression is increased over time following osteogenic differentiation of MSCs. Furthermore, the BMP-2 + osteogenesis medium enhanced the ALP activity in MSCs was much higher than that increased in MSCs in the presence of osteogenesis medium (see **Figure 4.5**). Our findings indicated that treatment with BMP-2 significantly augmented the osteogenic differentiation efficiency of HUMSCs, as evidenced by the increased intensity of ALP staining.

Consequently, the expression levels of osteogenic marker genes were also elevated in HUMSCs following BMP-2 treatment. The increase in expression of Runx2 and Osteocalcin in HUMSCs treated with BMP-2 and osteogenesis medium was significantly higher compared to that in MSCs treated with osteogenesis medium alone, although the timing of peak expression varied (see **Figure 4.6**). It is noteworthy that the highest expression level of Runx2 in MSCs cultured with osteogenic differentiation medium with or without BMP-2 was detected on day 28. Similarly, Osteocalcin expression was also enhanced by BMP-2. Compared to Runx2, the peak of Osteocalcin expression occurred at day 14, regardless of the presence or absence of BMP-2. Marupanthorn et al. also observed the peak of the Runx2 expression on day 28. However, the different time points

of the peak for the Osteocalcin expression (Marupanthorn et al., 2017). The reason for the difference may lie in the varying sources of derived MSCs.

To validate the osteogenic differentiation potential of HUMSCs, cells induced with osteogenic medium (+ BMP-2) were stained with ALP for observation. Furthermore, a semi-quantitative analysis of the staining images could provide more intuitive results. Additionally, comparing the expression levels of more osteogenesis-related genes could be validated. The similarity between the increase in ALP activity and the expression of osteogenic genes (Runx2 and Osteocalcin) by osteogenic medium + BMP-2 provides evidence that the HUMSCs isolated by us possess a robust osteogenic differentiation potential. Additionally, the findings from the cells cultured in the medium with BMP-2 suggest that under the influence of BMP-2, osteogenic differentiation of MSCs is enhanced and augmented. This observation aligns with the osteogenic effects of BMPs.

This investigation illustrated that BMP-2 treatment augmented the osteogenic differentiation potential of HUMSCs, as indicated by elevated expression levels of ALP (Manassero et al., 2013) and osteogenic genes. Our work carried out in this chapter still has some limitations. Determining the optimal concentration of BMP-2 remains a topic of consideration in augmenting the osteogenic potential of HUMSCs. The biocompatibility of the HA/CC material was evaluated through in vitro experiments. However, the evaluation methods may be limited, and future studies could employ additional mechanistic testing methods, such as viability staining assays and confocal imaging. Additionally, the characterisation of material degradation properties could be included. Additionally, some researchers argue that in vitro experiments may not fully reflect *in vivo* performance, as certain materials may exhibit excellent *in vitro* results but fail to meet requirements *in vivo* due to immune reactions (He et al., 2015). Nevertheless, the results of this *in vitro* study have provided foundational promise for subsequent *in vivo* experiments.

4.5 Summary

In this chapter, HUMSCs were successfully isolated and propagated, confirming their cellular characteristics. Biocompatibility testing of the HA/CC material produced favorable results, facilitating subsequent in vivo experiments. Furthermore, the osteogenic induction potential of the obtained MSCs was validated, demonstrating the positive stimulatory effect of BMP-2 in promoting osteogenic differentiation. The experimental techniques learned and mastered in this chapter lay the foundation for subsequent chapters' work.

CHAPTER 5: Osteogenesis Enhancement by Constructs for Osteogenetic Bone Allografts

5.1 Introduction

The objective is to augment the osteogenic characteristics of the HA/CC scaffolds by applying bioactive substances aimed at elevating the levels of BMP-2/7. While pure HA/CC typically contains minimal BMPs (Ripamonti, 2017), optimal artificial grafts often require substantial amounts of BMPs (Sun et al., 2020). Therefore, our objective is to evaluate various methods to transfect MSCs for the overexpression of BMP-2 and BMP-7. MSCs can be readily extracted from various sources, including muscle tissues, bone marrow, adipose tissue, and the umbilical cord. Through *in vitro* or *ex vivo* cultivation, these cells can be expanded on a substantial scale while preserving their stem cell characteristics. The clinical deployment of MSCs for therapeutic purposes offers several modalities, including localised transplantation, systemic delivery, or integration with tissue engineering strategies.

Moreover, MSCs exhibit a broad spectrum of differentiation capabilities. Prior research has extensively demonstrated their capacity to differentiate into diverse cell types, including muscle cells, osteocytes, chondrocytes, adipocytes, and neural cells. This versatile transdifferentiation potential positions MSCs as promising candidates for effective gene delivery in gene therapy applications targeting various tissues and organs. In addition to their differentiation capabilities, MSCs possess immunomodulatory advantages that allow them to effectively modulate *in vivo* immune responses. Their low-level expression of major histocompatibility complex (MHC) class I and the absence of MHC-II contribute to mitigating immune reactions following allograft treatments.

Furthermore, MSCs exhibit inherent homing capabilities, enabling them to migrate towards sites of inflammation or injury. This intrinsic ability, likely mediated by specific signalling cues, can be harnessed for precise and targeted gene delivery to specific locations, offering a strategic advantage in therapeutic applications. The inherent characteristics of MSCs and their differentiation potential have garnered widespread attention in osteogenesis research. Modifying MSCs to express or overexpress osteogenic-related genes and proteins can overcome the current limitations in bone research. Even the extracellular matrix of

MSCs itself can facilitate the effective osteogenic differentiation of surrounding cells and the recruitment of osteogenic cells.

The purpose of gene transfection is to introduce exogenous DNA or RNA into cells through various methods to alter gene expression. This may involve upregulating specific target genes or downregulating and silencing certain antagonistic genes. The challenges to be addressed in this process include the efficiency and safety of transfection. One approach to gene delivery is through virus-mediated delivery systems, where genes are delivered via a viral delivery system with integration into the genome of target cells to achieve sustained expression. Typically, viral vectors with replication defects are used to reduce pathogenicity. While virus-mediated gene delivery is highly efficient, it presents limitations, especially in mammalian stem cells. Safety concerns are also associated with viral transfection, particularly in light of the recent COVID-19 pandemic. Lentivirus vectors, derived from human immunodeficiency virus (HIV) and utilised in this study, are widely used despite having replication defects. However, products before the 4th generation still pose some risks. Additionally, viral vectors exhibit antigenicity, potentially eliciting immune responses in *in vivo* experiments, leading to experimental interference.

Non-viral gene transfection includes various physical and chemical methods for genetic material delivery. Physical methods include microinjection, electroporation, ballistic injection, magnetofection, sonoporation, optical transfection, and localized hyperthermia. Chemical methods include lipofection, polyfection, gold complexation, and carbon-based methods (Ledley, 1994). Non-viral gene transfection is considered safer than viral transfection, but its primary drawback is the transfection efficiency, particularly in the case of MSCs, which exhibit relatively low transfection rates (Sum et al., 2018). Furthermore, even if successful transfection is achieved, gene expression is limited due to the cellular mechanisms within MSCs. Comparative analysis of inert promoters for transfection suggests that even the highest expressing cytomegalovirus (CMV) promoter cannot fulfil the required overexpression criteria (Qin et al., 2010). These limitations highlight the need for further research and development of novel transfection methods and promoters tailored specifically for MSCs. Additionally, advancements in gene editing technologies, such as CRISPR/Cas9, offer promising avenues for improving gene expression in MSCs by

precisely targeting and modifying their genomic sequences. Moreover, strategies that enhance cellular uptake and intracellular trafficking of nucleic acids, such as the use of cell-penetrating peptides or nanoparticle-based delivery systems, hold potential for overcoming the barriers to efficient gene delivery in MSCs. Continued efforts in these areas are essential for realizing the full therapeutic potential of gene therapy approaches in regenerative medicine and other biomedical applications involving MSCs.

5.2 Hypothesis and Objectives

In recent years, genetically engineered modification of MSCs has emerged as a focal point of research interest. Many studies leverage the multi-lineage differentiation potential of MSCs, aiming to enhance specific cellular characteristics through transfection for application in diverse fields of research. Therefore, it is hypothesized, within this chapter, that MSCs can be augmented through transfection to enhance the expression and secretion of BMP-2/7, thereby strengthening their capacity to promote osteogenic differentiation.

Objectives

1. Generate transfectable quantities of plasmid expression vectors, verified for fidelity.
2. Isolate MSC cells and transfect or transduce them using various methods (chemical transfection, viral transduction, electroporation). Monitor efficiency and quantify the expression levels of BMPs.
3. Transfect HEK-293T cells and assess their expression level of target genes (BMP-2/7).
4. Preserve and culture-modified MSCs and HEK-293T cells to support subsequent *in vivo* experiments.

5.3 Materials and methods

5.3.1 Materials

The materials required for this chapter are detailed in **Chapter 3.**

5.3.2 Methods

5.3.2.1 Bacterial transformation

Thawed XL1-Blue bacterials were used in the procedure. The detailed procedure can be found in **section 3.2.12.1.**

5.3.2.2 Osteogenic differentiation

Passage 4 involved the detachment and enumeration of cells through established methodologies. Three sets of 6-well plates were established and categorised into three cohorts: exclusive cell cultures (n=2), cell populations of $2x10^5$ were cultured by osteogenesis differentiation medium (n=2), and cell populations of $2x10^5$ seeded onto 3D-BGS (n=6). Subsequently, the plates were incubated within an environment of 37°C and 5% CO_2 in the incubator. Following a one-hour incubation period, 500 µL of DMEM medium was administered to each well, after which the plate was repositioned within the incubator to facilitate cellular proliferation. Monitoring of cellular confluence occurred periodically using optical microscopy. Upon reaching an approximate confluence of 70%, the cultivation medium was substituted with 500 µl of DMEM/F12 supplemented with 10% FBS, 1% penicillin-streptomycin, and 10% commercial StemPro osteogenic supplement (ThermoFisher Scientific, UK). This osteogenic medium was changed approximately every 3-4 days. At the intervals of 1, 7, 14, 21, and 28 days of differentiation, the cells underwent lysis for quantification of Alkaline phosphatase (ALP) activity and fixation for ALP stain.

5.3.2.3 Small scale plasmid DNA isolation

Plasmids were extracted from previously transformed *E. coli* cultures using the GenElute™ Plasmid Miniprep Kit, following the detailed procedure in **section 3.2.12.2** (Mini-prep).

5.3.2.4 Medium-scale plasmid DNA isolation

The Endotoxin-free Plasmid Midiprep Kit (Sigma-Aldrich, UK) was utilized to purify plasmids after transformation, following the detailed procedure in **section 3.2.12.3** (Midi-prep).

5.3.2.5 Restriction Enzyme Digestion of plasmid DNA

Plasmid authenticity was confirmed by digesting 1 µg of DNA with Nco I enzyme and H buffer at 37°C for 4 hours, followed by agarose gel electrophoresis, as described in **section 3.2.12.4**.

5.3.2.6 Agarose gel electrophoresis

After plasmid digestion, samples were analyzed by agarose gel electrophoresis. A 1% agarose gel (1g agarose in 100 ml TAE buffer) was prepared, loaded, and run at 250V for 5 minutes, then at 100V for 40 minutes. The gel was visualized under UV light. Details are provided in **section 3.2.12.5**.

5.3.2.7 Chemical transfection methods

HEK-293T cells and MSCs were transfected using DNA Transfection Reagents (jetOPTIMUS®, Polyplus®, UK, cat No: 101000025). Initially, 2 µg of plasmid DNA was combined with 200 µL of JetOpti buffer in Microfuge tubes. The tube was then briefly vortexed for 1 second and centrifuged. Subsequently, 3 µL of JetOptimus Reagent was added to the Microfuge tube, followed by another brief vortexing for 1 second and centrifugation. The mixture was allowed to stand for 10 minutes and was then transferred to the cells to be transfected in culture plates.

The transfected cells were incubated in an incubator at 37°C with 5% CO_2 for 24 hours. The following day, the cells were examined under a microscope or a fluorescence microscope for evaluation.

5.3.2.8 Neon™ electroporation transfection method

Plasmids were prepared at a concentration of 5 µg/µl in TE buffer (as supplied by the kit). Simultaneously, a control plasmid containing GFP was also prepared at the same concentration.

On the day of transfection, cells were harvested when they reached 80% confluence. Following cell counting, they were suspended in PBS to achieve a final density of 1.0 x 10^7 cells per ml. A 24-well plate was used, with each well containing 0.5 ml of DMEM supplemented with 5% FBS but devoid of penicillin-streptomycin. The plate was preheated in an incubator set at 37°C with 5% CO_2.

An Electrolytic Buffer, provided by the kit, was introduced into the Neon™ tube. Subsequently, 5 µg of plasmid was transferred to a sterile Microfuge tube. Cells were then added to the Microfuge tube containing plasmids and gently mixed. A new Neon™ tip was affixed to the Neon™ pipette, as per the manual's guidance. The tip was immersed into the mixture of plasmids and cells, drawing up 10 µl of the mixture. Following this, the entire pipette, with cells and plasmids, was inserted into the Neon™ tube and placed in the Neon™ Pipette station.

The appropriate voltage and pulse duration were set, and upon pressing the start button, an electric pulse was delivered. After the display indicated "complete," the Neon™ Pipette was promptly removed, and the cell mixture was transferred into the previously prepared 24-well plate. The plate was gently shaken to ensure even cell seeding. Subsequently, the cells were incubated at 37°C with 5% CO_2 overnight.

The following day, the medium was replaced with regular DMEM supplemented with 5% FBS and 1% penicillin-streptomycin. Cell transfection efficiency was observed via a fluorescence microscope (Zeiss, Germany).

5.3.2.9 Lentivirus method

For the transfection of each plasmid, HEK-293T cells were cultured in 10cm culture plates and subsequently incubated at 37°C with 5% CO_2 overnight. Once the cells had reached 80% confluence, they were deemed suitable for the assembly of viral particles. Upon

readiness of the HEK-293T cells, they were subjected to two washes with PBS and their culture medium was replaced with DMEM/10% FBS devoid of antibiotics. Subsequently, 600 µL of OPTI-MEM was dispensed into a centrifuge tube, into which DNA was pipetted following the prescribed amounts provided in Table 5.1. The contents were homogenised either by gentle swirling or by careful agitation of the tube. The mixture was then allowed to incubate for 5 minutes in a hood at room temperature. Following this, PEI (**Table 5.1**) was added to each tube and the resultant mixture was incubated for 20 minutes at room temperature.

Table 5.1 Transduce Reagents Amounts for this study

PEI:DNA 3:1 ratio

Dish size	Surface area (cm_2)	HEK293 Cell density	DMEM/ 10%FBS no ABs (Ganguli et al.)	Opti-mem in tube (uL)	PEI (uL)	pRSV-rev (ug)	VSV-G (ug)	pMDLg/ pRRE (ug)	pLKO (ug)	[DNA] plasmid (ug)
100 mm dish	55	3 $x10^6$	10	600	54	1.8	2.7	4.5	9.0	18

Subsequently, the DNA:PEI mixture was added dropwise to the cells in the culture plate, with caution to avoid contact with the plate's walls. The contents were gently swirled to ensure even dispersion, and the cells were further incubated at 37 °C with 5% CO_2 for 16 hours. The culture medium was then replaced with standard growth medium (DMEM), and the medium containing viral particles was transferred to a waste container treated with Virkon. The cells were once again incubated at 37 °C with 5% CO_2 for an additional 48 hours.

After this period, the medium containing viral envelope particles was harvested from the cells and transferred to a polypropylene storage tube. The medium was subsequently filtered through a 0.45 µm filter to remove any cellular debris. The collected medium was

employed for lentivirus particle titration and transfection of target cells, while any remaining particles were stored in a -80°C freezer. When MSCs reached a confluence of 50-60%, polybrene (Santa Cruz Biotechnology, cat No: sc-134220) was added at a dilution ratio of 1:1000 to the lentivirus particle medium, which was then transferred to the MSCs. The cells were incubated at 37 °C with 5% CO_2 for 4 hours before being replenished with DMEM medium. After 24 hours of incubation, the cells were examined using a fluorescence microscope, and images were captured via confocal microscopy. Subsequently, the cells were harvested for ELISA assays and cell selection.

5.3.2.10 Enzyme-linked immunosorbent assay (ELISA)

The media from the transfected HEK-293T cells was collected at 72 hours and assayed using the Human BMP-2 Elisa Test Kit and Human BMP-7 Elisa Test Kit (DuoSet® R&D SYSTEM, USA, cat No: DY355); (DuoSet® R&D SYSTEM, USA, cat No: DY357). The MSCs after transfected were collected (around 2 x 105 cells) and the cell lysates also were assayed by the above kits. The details of the procedures can be seen in **section 3.2.16**.

5.3.2.11 Clonal selection for the stable cell line

Puromycin can induce cell death across a range of cell types but the concentration required to do that is different for different cell types. As a result, it was imperative to establish the minimum concentrations required to eliminate all untransfected cells for the establishment of stable cell lines. To accomplish this, both MSCs and HEK-293T cells were separately cultured in 24-well plates until they reached an 80% confluence. Subsequently, a series of gradient concentrations of puromycin (0, 0.25, 0.5, 0.75, 1.0, 1.25, 1.5, 2.0 2.25 and 2.5 mg/ml) were introduced into the wells containing the cells. These cells were then incubated for 1-2 weeks to ascertain the concentration that results in the minimum puromycin concentration that results in complete cell death. Throughout this period, the culture media containing different concentrations of puromycin were refreshed every 3 days to sustain the drug's effect on the cells. Daily observations were conducted to monitor the cells in the plates and construct a puromycin dose-response curve for both MSCs and HEK-293T cells.

5.3.2.12 Confocal microscopy

Confocal microscopy was employed for the assessment of transfected MSCs and HEK-293T cells cultured on 13 mm coverslips. The cells were cultured on these coverslips in the presence of a medium obtained from the transfection and selection processes. Subsequently, the slides were meticulously examined and imaged using a confocal microscope equipped with a 20x objective lens. Emission wavelengths were specifically set at 405 nm for DAPI, 488 nm for GFP, and 647 nm for RFP or Cherry.

5.3.2.13 Flow cytometry

In preparation for flow cytometry analysis, cells were initially collected using trypsin. After centrifugation at 300 RCF and resuspension in PBS, cell counts were determined using trypan blue. Subsequently, 100,000 cells were seeded into U-bottom 96-well plates and gently washed with PBS. The cells were then resuspended in FACS buffer (comprising PBS, 0.05% sodium azide, and 0.2% bovine serum albumin) and incubated on ice for one hour. Following incubation, the cells were incubated with either test antibodies or isotype controls on ice, while avoiding exposure to light, for another hour. Gentle PBS washes and subsequent centrifugation steps (repeated thrice) were performed to eliminate any unbound antibodies. Finally, after the last wash, the cells were resuspended in FACS buffer and analyzed using a NOVOCyte flow cytometer (NOVOCyte, ACCELA, US). The resulting data was then processed and analysed using FlowJo.

5.3.2.14 qPCR assay

Total RNA extraction from the transfected MSCs was conducted using TRI Reagent (Sigma-Aldrich, UK, Cat No: T9424). After RNA extraction, reverse transcription was conducted using the Reverse Transcription Kit (RETROscript™, UK, cat No: AM1710). The reaction was maintained at 37°C for 15 minutes, followed by a denaturation step at 85°C for five seconds before gradual cooling. The resulting DNA, in conjunction with water and primers, was

introduced into the SYBR Green PCR Master Mix and subjected to 40 amplification cycles. The details of the primers employed, along with their respective sequences, are provided in the results section below.

5.4 Results

5.4.1 Restriction Digestion

Before carrying out expression analysis using these plasmids, they were subjected to restriction enzyme digestion for their authentication. For this purpose, the plasmids are amplified by transforming them into *E. coli*, culturing the plasmids carrying *E. coli* and isolating the plasmids from bacterial culture. Thus isolated plasmid DNAs were subjected to restriction digestion using NcoI and BglII (**Figure 5.1A**). The plasmids exhibited distinct fragment sizes after restriction digestion as predicted by the virtual digest of the plasmid DNA sequence (**Figure 5.1B**). This conformation makes them suitable for subsequent transfection procedures.

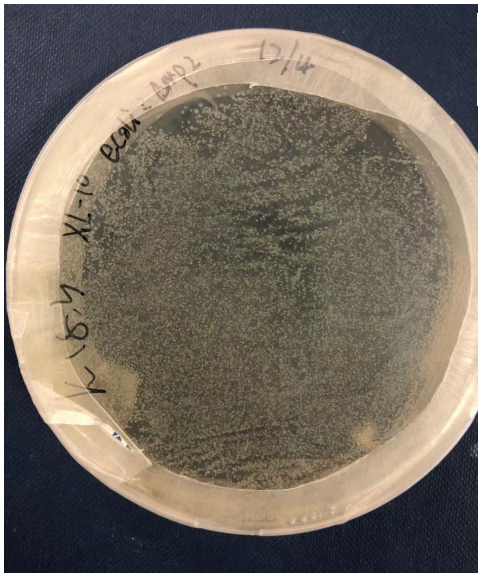

A

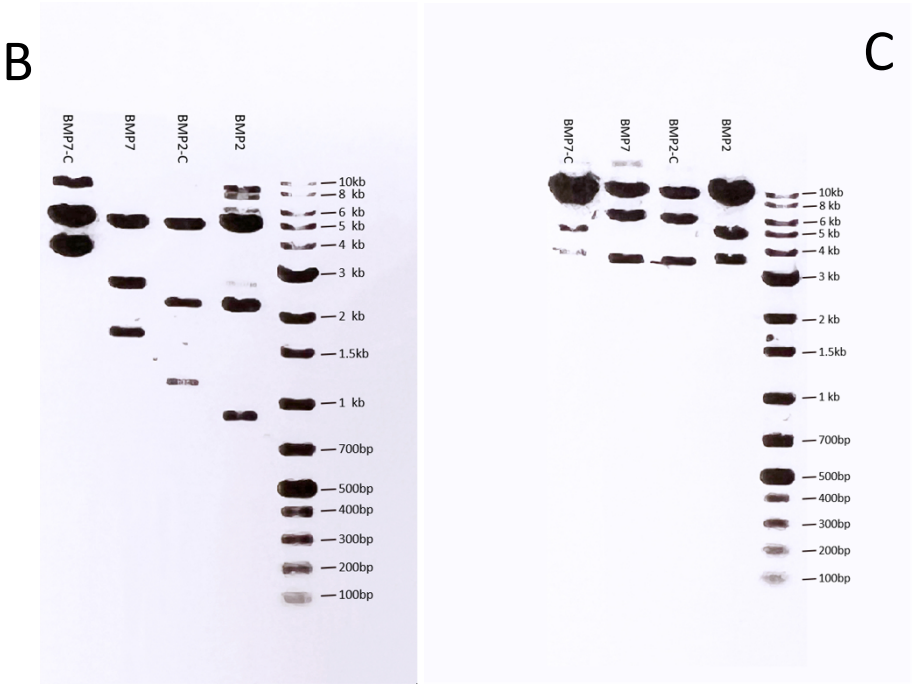

Figure 5.1 Plasmid transformed bacteria growth on LB-agar+kanamycin plate and restricted digestion results.
Panel A, the growth of XL-10 (E. coli) on the LB-agar (containing kanamycin) plates after transformation. **Panel B**, the gel electrophoresis results following restriction enzyme (NcoI) digestion of the plasmid extracted through mini-preparation post-transformation. **Panel C** shows the digestion result by using BglII enzyme. After restriction enzyme digestion with NcoI and BglII, the band sizes observed corresponded with the restriction site information provided in the plasmid map.

5.4.2 Transduced MSC cells

Various transfection methods, including chemical transfection (jetOPTIMUS), electroporation, and lentiviral transduction, were employed using expression vectors to express BMP-2 or BMP-7 in MSCs. The transfection efficiency was quite low when jetOPTIMUS or electroporation were used for the transfection of MSCs. However, successful transduction was ultimately achieved using the lentivirus method. Following cell selection, fluorescence microscopy was conducted to confirm the success of the procedure. The obtained results were as follows. The presence of BMP-2 can be seen in **Figure 5.2A**, using the GFP marker indicated by the green. The flow chart seen in **Figure 5.2B** demonstrates that 98% of the MSCs were transfected. The red of the mCherry marker is seen in **Figure 5.2C**, showing 55.45 % of BMP-7. Since both GFP or mCherry and BMP-2

or BMP-7 are expressed using a single promoter (EF-1α), the fluorescent signal within cells is directly proportional to the expression of the target BMP gene in those cells. The expression of relevant fluorescent proteins within the cells was visualised using confocal microscopy, while the fluorescent signals were detected and quantified by using flow cytometry.

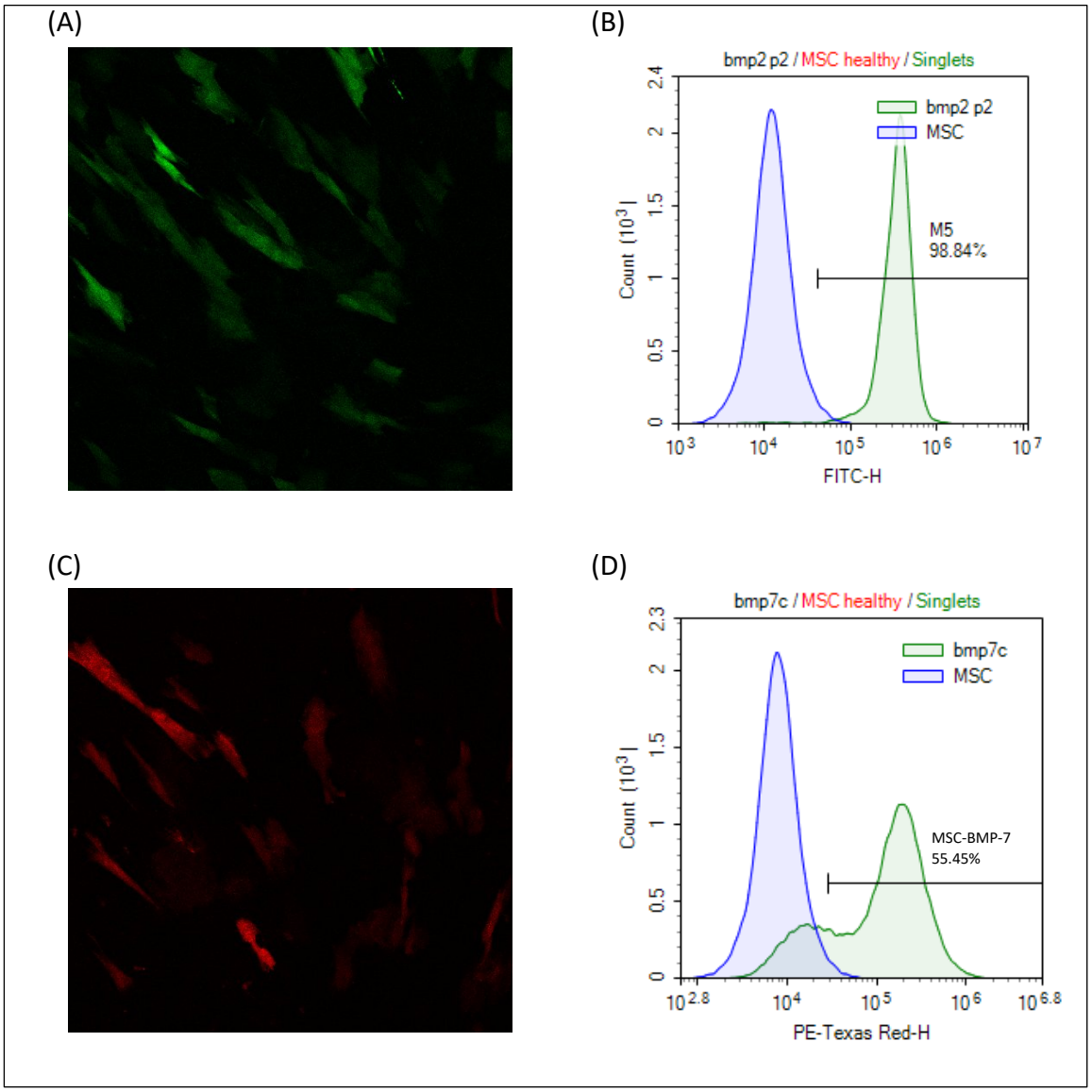

Figure 5.2 Expression of BMP-2 & BMP-7 in MSCs through lentiviral transduction.
MSCs were transduced with lentiviral particles carrying BMP-2/GFP or BMP-7/mCherry. After 48 hours, the fluorescent protein expression was visualised by Confocal microscopy (**A** and **C**) and quantified by flow cytometry (**B** and **D**). **A** and **C**, images of GFP (corresponding to BMP-2) and mCherry (corresponding to BMP-7) respectively, the magnification is 20X. The control of untransfected MSCs was used that showed no flourecence colour. B and D, the flow cytometry histogram showing the percentage of MSCs that were successfully transfected by GFP (BMP-2) and mCherry (BMP-7), respectively. The plots represent three independent experiments.

5.4.3 The transduced MSCs expression of BMPs

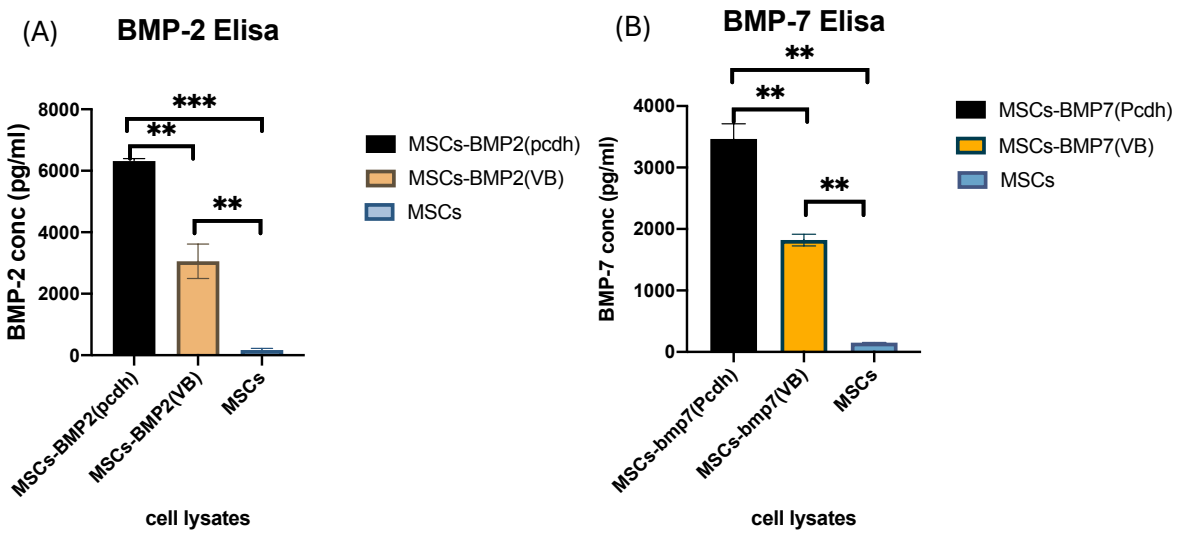

Figure 5.3 Analysing the expression of BMP-2/7 in MSCs by ELISA.
The lysates of MSCs transduced without (MSCs) or with BMP-2 (MSCs-MBP2 [pcdh]/MSCs-BMP2 [VB]) or BMP-7 (MSCs-BMP7 [pcdh]/MSCs-BMP7 [VB]) lentiviral particles were used in ELISA to asses BMP-2 (**A**) or BMP-7 (**B**) expression (**: p<0.01, ***: p<0.001). The concentration of MSCs-MBP-2 [pcdh] = 6317 ± 79.05 pg/ml; MSCs-BMP2 [VB] = 3057.0625 ± 557.71; MSCs-BMP7 [pcdh] = 3463.575 ± 248.583 and MSCs-BMP2 [VB] = 1820.55 ± 95.53.

Two different plasmids of BMP-2 were tested (VB and pcdh), and ELISA tests were done to detect which were more abundant, and therefore which had been more successfully transfected. As displayed in **Figure 5.3A**, the BMP-2 (pcdh) had a statistically higher concentration (>6000pg/ml/0.25 million cells) compared to BMP-2 (VB), (p=0.0044, one-way ANOVA). BMP-7 also had these two plasmids, and as **Figure 5.3B** shows, the BMP-7 (pcdh) similarly had a significantly higher concentration compared to BMP-7(VB), (p=0.0034, one-way ANOVA); demonstrating that in both cases the pcdh was more successful in transducing.

Furthermore, for both growth factors, the two plasmids had significantly higher concentrations than the controls –showing that the transfections of BMP-2 & BMP-7 were successful. MSCs-BMP-2(pcdh) and MSCs demonstrated a significant difference, with MSCs-BMP-2(pcdh) exhibiting a higher mean expression than MSCs (p = 0.0007, one-way ANOVA). Additionally, MSCs-BMP-7(pcdh) and MSCs exhibited a significant difference, with MSCs-BMP-7 (Pcdh) demonstrating a higher mean expression compared to MSCs (p = 0.0005, one-way ANOVA).

5.4.4 Transfection of HEK-293T cells

HEK-293T cells were also selected for transfection because our previous work showed the expression of BMP-2/BMP-7 in these cells (see **Chapter 4**). The lentiviral particles carrying BMP-2/GFP or BMP-7/mCherry were once again used to transduce HEK-293 cells and fluorescence microscopy was employed to determine transfection efficiency. The GFP expression in **Figure 5.4A** indicates that there is BMP-2 expression and, therefore, that the transfection was successful. This is corroborated by the ELISA (**Figure 5.4B)**, where the concentration of BMP-2 is higher in each of the tests than in the control. Similarly, **Figure 5.4C** displays the mCherry expression (which corresponds to the BMP-7 expression) and the ELISA test in **Figure 5.4D** confirms the successful transfection with the BMP-7 vector. Figure 5.5B illustrates that HEK-293T cells transfected with the Addgene BMP-2 plasmid secreted 26.038±5.594 ng/ml at 48 hours and 23.89±0.722 ng/ml at 96 hours of BMP-2. HEK-293T cells transfected with the BMP-2 (pcdh) plasmid showed a BMP-2 concentration of 7.54 ± 0.302 ng/ml in the media at 48 hours, decreasing to 2.33 ± 0.285 ng/ml at 96 hours. **Figure 5.4C** shows the presence of BMP-7 using the mCherry marker and **Figure 5.4 D** displays the concentrations of BMP-7 in different samples. **Figure 5.4D** depicts that HEK-293T cells transfected with the Addgene BMP-7 plasmid secreted 131.038 ± 16.906 ng/ml at 48 hours and 92.121 ± 2.238 ng/ml at 96 hours of BMP-7 in the media. HEK-293T cells transfected with the Addgene BMP-2/7 plasmid secreted 116.626 ± 2.279 ng/ml in the media at 48 hours and 96.111 ± 2.368 ng/ml at 96 hours of BMP-7.

(A)

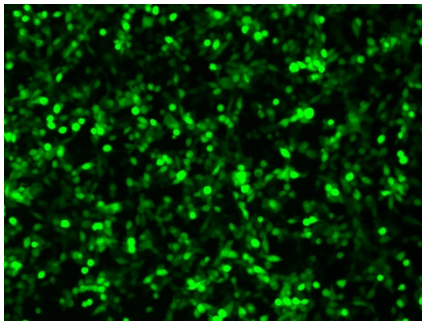

(B)

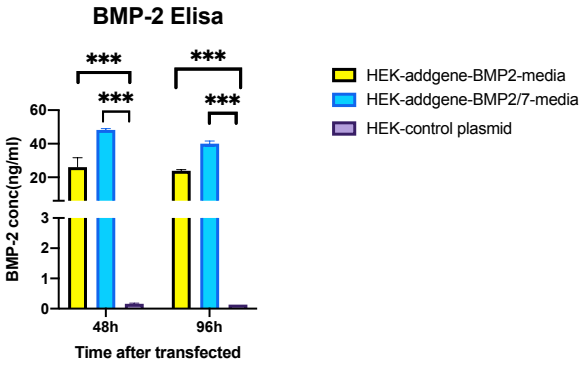

(C)

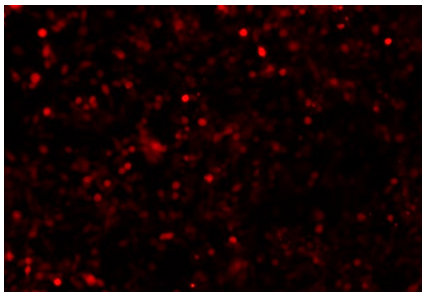

(D)

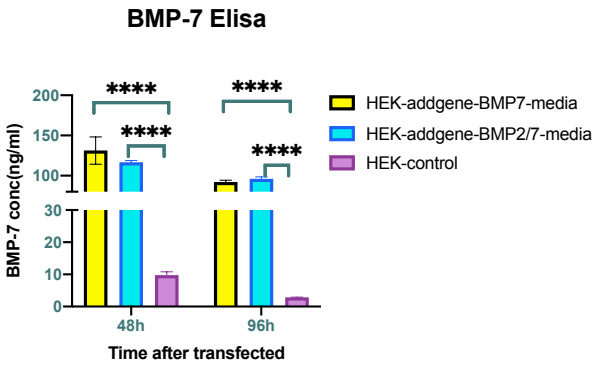

Figure 5.4 Analysis of BMP-2 and BMP-7 expression in HEK-293T cells.
HEK-293T cells were transfected with the Addgene plasmids of BMP-2, BMP-7 or BMP-2/7 and analysed the expression after 96 hours of transfection (**A** and **C**) and secretion after 48 hours and 96 hours of transfection (**B** and **D**). Results show mean ± SD, n=2. The statistical analysis was performed used a two-way ANOVA where *** $p < 0.001$ and **** $p < 0.0001$.

Panel **A** shows the presence of BMP-2 using a GFP marker and fluorescence microscopy, and Panel **B** displays the concentrations of BMP-2 in group of HEK transfected with pVAX-BMP-2 plasmid, group of HEK cells transfected with pVAX-BMP2/7 plasmid and HEK-control (without plasmid) gourp. There were significant differences between the transfected groups and the control group ($p < 0.001$). Panel **C** shows the presence of BMP-7 using assessing mCherry marker expression using fluorescence microscopy, and Panel **D** displays the concentrations of BMP-7 in the group of HEK cells transfected with pVAX-BMP-7 plasmid, group of HEK cells transfected with pVAX-BMP2/7 plasmid and HEK-control (untransfected) group.

5.5 Discussion

This chapter focused on assessing the expression of BMP2/7 in MSCs. The transduction efficiency of BMP2/7 plasmids in MSCs was evaluated by examining the expression levels of BMP-2 and BMP-7. Similar procedures were applied to HEK cells. Early attempts to extract BMP-2 from bone yielded very low yields (1–2 μg/kg cortical bone) (Viljanen et al., 1996). Subsequently, recombinant human BMP-2 (rhBMP-2) was produced using Chinese hamster ovary (CHO) cells, albeit with significant cost implications, limiting its widespread clinical application (Israel et al., 1992). Large-scale production of BMP-2 using *E. coli* reduced costs, but non-glycosylation of the protein resulted in diminished osteoinductive effects (Vallejo et al., 2002). High or supra-physiological doses of BMP-2 may lead to clinical side effects such as widespread swelling, seroma formation, cystic bone changes, and cancer development, raising concerns about its direct clinical application (Vallejo et al., 2002). Therefore, genetic modification of MSCs to produce BMP-2 has emerged as an alternative approach.

The Investigation detailed in this chapter represents an exploration into the development and assessment of gene-based constructs tailored for the enhancement of bone regeneration. After vector construction, plasmids were transformed into *E. coli* and plasmid DNA were prepared and analysed by restriction digestion to confirm that they were the correct plasmids. This evaluation validated the identification of the plasmid constructs, ensuring their suitability for downstream applications in gene delivery. Xueqin Gao et al. demonstrated successful overexpression of BMP-2 in muscle-derived cells (MDC) through lentiviral transduction, with efficiency of 50%. Additionally, they achieved high expression of BMP4 and green fluorescent protein (GFP) in MSC cells using retroviral transduction with BMP4 and GFP. The secretion level of BMP4, measured by ELISA, was approximately 6.19 ng/million cells/24 h (X. Gao et al., 2013). Other literature reports rAAV gene vector transfection of hBMSCs, with transfection efficiencies ranging from 8% to 52% (Stender et al., 2007; H. Zhang et al., 2018). This is lower than the transfection efficiency observed in other cell types using viral transfection methods (Gill & Denham, 2020). Viral transfection

methods typically yield higher transfection efficiencies compared to other transfection methods such as lipofection and electroporation.

The functional efficacy of the engineered constructs was further elucidated through comprehensive cellular assays, beginning with confocal microscopy analysis of HEK293T cells post-transfection. The successful expression of GFP and Cherry fluorescent proteins within the transfected cells served as a tangible indicator of BMP-2 and BMP-7 presence, respectively, confirming the suitability of the constructs for the expression in HEK293T cells. Following validation using ELISA assays, quantitative analysis revealed higher concentrations of BMP-2 and BMP-7 in transfected cell populations compared to control groups, highlighting the efficacy of the gene-based approach in enhancing osteogenesis. Images of confocal microscopy for the selected MSCs after transduced showed that MSCs were transduced successfully (see **Figure 5.2**), and the FACs results quantitively confirmed the expression. However, the ELISA assay showed the concentration of the expressed BMP-2 and BMP-7 was not high enough (see **figure 5.3**) compared with clinical requirements. The measured levels of BMP-2 varied across studies, with reported values ranging from 21.4 ± 12.0 ng/g to 20.2–120.6 ng/g. In contrast, BMP-7 exhibited slightly more consistent measurements, with values of 84.1 ± 34.4 ng/g in one study and 54.2–226.8 ng/g in another. (Bae et al., 2006; Pietrzak et al., 2006). The possible reasons for the low expression of BMPs in MSCs contrast with other studies as follows:
Firstly, the cell membrane of MSCs itself poses a barrier to transfection, resulting in low transfection efficiency regardless of the method used (Yang et al., 2022). Secondly, both liposomes and viral particles are prone to enzymatic degradation upon entry into MSCs (Patil et al., 2019). Thirdly, the size of plasmids themselves is relatively large and has some limitations of transfection (Z. Wu et al., 2010). Larger plasmids may exceed the capacity limit of viral particles, preventing them from being fully packaged. This results in fewer copies of the exogenous gene within the generated viral particles, leading to reduced transfection efficiency and lower levels of target gene expression. Larger plasmids can reduce packaging efficiency, resulting in lower levels of exogenous gene content within viral particles. This could be due to the difficulty in effectively packaging larger plasmids into viral particles or structural instability leading to decreased packaging efficiency. For

instance, the lentiviral vector used in this study can only carry gene fragments up to 12kb, whereas the size of the designed BMP-2 or BMP-7 combined with fluorescent markers GFP or Cherry is close to 10kb, hindering packaging efficiency (Truong et al., 2015). Fourthly, different promoters in mammalian cells lead to varying gene expression efficiencies, thereby affecting the expression levels of BMPs. This study employed CMV and EF1α promoters, known for their high expression efficiency in stem cells, yet failed to achieve satisfactory gene expression (Qin et al., 2010). Finally, the fluorescent emission of GFP and mCherry is highly sensitive and therefore it is easy to assess their expression even at very low levels. So, their expression could be an indication of BMP2/7 expression but not necessarily mean at high levels (Feklistov, 2013).

In this study, the lentivirus method was utilized to transduce MSCs to achieve a high transfection rate and overexpression of BMPs. Additionally, attempts were made to transfect MSCs using lipofectamine and electroporation methods. Confocal imaging results indicated that lentivirus-transfected cells achieved successful transfection, while other non-viral methods failed to produce similar outcomes (see **Figure 5.2**). Besides low transfection efficiency, non-viral methods also inflict damage on cells. For instance, electroporation creates temporary pores on the cell membrane through electrical pulses, which are later repaired by the cell membrane. During the electrical pulse, some cells may be damaged to the point of death. Additionally, almost all non-viral transfection methods result in transient expression of target genes and cannot sustain long-term expression.

Viral transfection methods offer advantages over non-viral methods in terms of higher transfection efficiency, minimal cell damage and the ability to integrate into the MSC genome for long-term expression of target gene proteins. However, they also have limitations. The primary concern lies in safety, including the potential pathogenicity caused by gene insertions (Giacca & Zacchigna, 2012). Due to the random nature of gene insertion sites, controlling this random insertion and its resulting pathogenicity is challenging. Additionally, the capacity of viral particles may limit the size of the target gene insertions, with genes larger than approximately 12kb potentially struggling to be encapsulated and enter the cell (Yin et al., 2014). Moreover, viral antigens may trigger immune responses in the host (Chan et al., 2006).

Due to insufficient BMP expression from the transfected MSCs, HEK-293T cells were transfected to achieve high levels of BMPs for subsequent studies. HEK-293T are an immortalised cell line derived from human embryonic kidney tissue. HEK293T is a sublineage of the original HEK293 cell line, transfected with a plasmid carrying the SV40 T-antigen origin of replication that can lead to large copy numbers of mRNA transcripts to produce large quantities of recombinant proteins (Pulix et al., 2021).
Based on these characteristics, in this experiment, an adequate amount of BMPs was provided by transfecting HEK cells. Considering the rapid self-replication and viral transfection properties of HEK cells, BMPs or active growth factors directly provided by HEK cells for *in vivo* experiments are seldom considered. Our accidental discovery in this experiment revealed that HEK cells can be co-cultured harmoniously with MSC cells. Building upon this, a bold attempt was made to use transfected HEK cells to provide adequate BMP-2/7 to support bone induction and ossification research in the next chapter (chapter 6). The studies in the subsequent chapter circumvent the safety issues that HEK cells may bring about by decellularisation. This innovative approach requires further experiments to validate its effectiveness, and determine potential genetic safety, and necessitates longer-term experimental observations for confirmation and potential improvement.

These comprehensive findings collectively underscore the immense potential of gene-based approaches in augmenting bone repair processes. While the results demonstrate significant promise in enhancing osteogenic outcomes, further optimisation may be necessary to achieve clinically relevant levels of BMP expression. For instance, improvements in plasmid size could enhance their packing efficiency and protein expression. While it is feasible to overexpress BMPs in MSCs, the level of detectable BMPs in the media is insufficient to exert biological effectiveness. Additionally, selecting cell lines with higher BMP expression and expanding their use through longer cell screening periods could be beneficial. Overexpression of BMPs in HEK293T cells results in much higher expression levels, and therefore 'conditioned media' from HEK293T cells could be used to stimulate MSCs.

Nonetheless, the functional validation presented herein provides a solid foundation for the continued advancement and refinement of gene-based strategies for bone tissue engineering and regenerative medicine applications, offering new avenues for addressing the unmet clinical needs associated with bone defects and fractures.

5.6 Summary

1. Lentivirus technology was utilised to successfully transduce MSC-Tert cell line, enabling them to express BMP-2/7 which were not sufficient and fluorescent proteins to a certain extent.

2. Plasmid transfection of HEK-293T cells led to successful overexpression of BMP-2/7, which is sufficient to facilitate MSCs to enhance bone formation.

5.7 Conclusion

Lentiviral transduction enabled BMP-2/7 expression in MSC-TERT cells but at insufficient levels for strong bone formation. Plasmid transfection in HEK-293T cells achieved higher BMP-2/7 expression.

Chapter 6: *In vivo* Assessment of the Osteogenic Potential of Exogenous BMP-enhanced HA/CC in Mice

6.1 Introduction

Currently, patients may present with bone defects as a result of various medical conditions such as severe open or closed fractures, bone tumours, or chronic inflammation. The treatment of bone defects and non-unions requires suitable implants to fill voids and facilitate bridging bone tissue growth. Bone engineering has been heralded as an alternative strategy of the twenty-first century to regenerate bone. In essence, the discipline aims to combine cells with scaffolds, or with appropriate growth factors, to initiate repair and regeneration.

The objective is to enhance the osteogenic capacity of HA/CC scaffolds by incorporating bioactive agents that increase BMP-2 and BMP-7 levels. HA/CC scaffolds were selected due to their strong biocompatibility, porosity, and structural resemblance to natural bone, which support cell attachment and growth. Additionally, the combination of hydroxyapatite (HA) with collagen (CC) creates a scaffold that mimics the mineral-organic composition of bone, providing a favorable environment for osteogenesis. While pure HA/CC scaffolds typically contain low levels of BMPs (Ripamonti, 2017), boosting BMP content is essential for effective bone regeneration (Sun et al., 2020). Thus, we aim to evaluate transfection methods for MSCs to overexpress BMP-2 and BMP-7, further enhancing scaffold performance for bone healing.

MSCs are ideal for this approach, as they can differentiate into various cell types, including bone cells, and have immunomodulatory and homing capabilities, allowing them to migrate to injury sites. MSCs can also be expanded in vitro, making them suitable for large-scale applications in tissue engineering. By integrating MSCs with HA/CC scaffolds, we aim to create a highly osteogenic system for advanced bone regeneration.

Gene transfection techniques enable us to modify MSCs to upregulate osteogenic genes like BMP-2 and BMP-7. Viral delivery systems, such as lentivirus vectors, offer efficient gene delivery, although they pose certain safety challenges. Ensuring stable gene expression and

minimizing immune responses are critical in using viral vectors, particularly for therapeutic applications in bone tissue engineering.

The *in vitro* studies confirmed that co-culturing HEK 293T cells and HUMSCs after transfection can provide sufficient BMP-2 and BMP-7 to promote bone proliferation and induce osteogenic differentiation (see results of **Chapter 5**). These results encouraged further *in vivo* experiments.

In vivo assessment is an essential process to evaluate the osteogenic capacity of bone graft materials (Fu et al., 2013). It serves as a pivotal stage in bridging the gap between promising *in vitro* results and the complex biological milieu encountered within living organisms. Therefore, *in vivo* assessment stands as an important step in the comprehensive exploration of bone graft substitutes, providing critical information to evaluate the usefulness of new therapeutic techniques. For example, micro-CT analyses give panoramic views while histological examinations unravel the microscopic intricacies, and quantitative polymerase chain reaction (qPCR) allows us to delve into genetic responses so that each facet contributes to a nuanced understanding of how bone grafts interact with the living environment (C. Chen & Kim, 2020; Peyrin, 2011). This multifaceted approach ensures that the translation from promising laboratory findings to clinical efficacy is grounded in a thorough and rigorous evaluation of osteogenic potential.

The hypothesised that the integration of BMP2-transfected HEK 293T cells and HUMSCs into an HA/CC scaffold, followed by a meticulous decellularisation process, would yield a graft with osteogenic potential. The rationale behind this hypothesis lay in the synergistic effects anticipated from the combination of BMP-transfected HEK 293T cells, known for their ability to produce osteogenic proteins, and MSCs, versatile cells capable of differentiating into various cell lineages, including osteoblasts. The strategic integration of these cellular components within the scaffold aimed to overcome the limitations associated with natural bone grafts, offering a bioactive construct that not only provided structural support but also fostered an environment conducive to enhanced osteogenesis.

The aim of the study described in this chapter was to comprehensively investigate in *in vivo* the performance of the MSCs+HEK+HA/CC bone graft, providing research evidence and support for the development of future effective bone grafts.

The objectives of this chapter are:

1. To produce a cell/HA/CC bone graft through *in vitro* engineering
2. To decellularise the construct so that it mimics an artificial allograft
3. To evaluate the osteogenic potential of the decellularised matrix/HA/CC bone graft by implantation in mice (*in vivo).*

6.2 Materials and Methods

6.2.0. Materials

The materials required for this chapter are detailed in **Chapter 3**.

6.2.1. Preparation of MSC+HEK+HA/CC bone graft for implantation

1. Co-culture of HEK 293T-MSCs on HA/CC

HA/CC particles with a size range of 300–400 µm were prepared as described in **Chapter 4**. A total of 10–15 mg of particles was first added to wells of a 96-well plate. Subsequently, 2 x 10^5 MSCs and 2 x 10^5 HEK-293T cells/well, mixed at a 1:1 ratio, were seeded into the wells. The medium was changed every 3 days and scaffold nodules were observed under a microscope. After 1 week, the cells and nodules were harvested by scraping into Microfuge tubes. Several wells of nodules were maintained for 2 weeks. On days 1, 7, and 14, cells cultured with the scaffold were stained with 50 µg/ml Hoechst (Invitrogen, Carlsbad, CA, USA) and 4 µM Calcein AM (Invitrogen) and then imaged by confocal microscopy.

2. Decellularisation

The harvested scaffolds were decellularised by undergoing three cycles of freezing at -80°C followed by thawing. The scaffolds were finally dried in a freeze dryer (Scanvac Coolsafe 110, LaboGene A/S, Allerød, Denmark).

3. Characterisation of MSCs and HEK 293T-MSCs

The decellularised scaffolds were hydrated in 500 µl PBS/well, then the concentrations of BMP-2 and BMP-7 in the solution were evaluated using ELISA kits (DuoSet® cat No: DY355; DuoSet®, cat No: DY354, both from R&D Systems, Minneapolis, MN, USA); details are provided in **Chapter 3**.

4. Fabrication of implanting material

After the above preparation, the materials were compressed into dense, elongated cuboids then divided into small blocks (1 x 2 x 2 mm^3) for implantation. The blocks were then sterilised with ethylene oxide and sealed for later use.

6.2.2 Animal preparation

The *in vivo* tests were performed at Huazhong University animal centre (research ethics number: [2023] IACUC Number:3294). Thirty-six male mice (C57BL/6J) aged 9 weeks (Shulaibao Biotechnology Co., Ltd, Wuhan, China) were randomly divided into three groups (**Table 6.1**). In this experiment, the Resource Equation Method was selected for power calculation. Measurements indicated that using 4 animals per time point per group yielded an E value greater than 20. After grouping, ear punching was performed for identification and recording purposes. The mice were housed in the animal experimental facility, and the animal cages were regularly cleaned (every 3 days). They were provided with food and water on a scheduled basis, and their activity was observed.

Table 6.1 Experimental mouse groups

	A: Control HA/CC	B: HA/CC + MSC matrix	C: HA/CC + HEK-BMP-2/7+MSC matrix
Day 7	4	4	4
Day 14	4	4	4
Day 28	4	4	4

6.2.3 Implantation

The mice were anaesthetised with 0.3% sodium barbiturate (cat No: 4390-16-3; Sigma-Aldrich; Merck-Millipore, Darmstadt, Germany)**,** and the fur on both hind limbs was carefully shaved, followed by disinfection with 0.2% Iodophor Sanitizer (Jiangxi Caoshanhu

disinfection supplies Co. Ltd., Nanchang, China). The muscle gap in the anterior tibial region was dissected until the tibia was adequately exposed, facilitating the subsequent insertion of a scaffolding block into each leg (see **Figure 6.1**). The muscle and skin were meticulously sutured and disinfected with 0.2% Iodophor Sanitizer. After anaesthetic recovery, the mice were returned to labelled cages for ongoing care and maintenance at Huazhong Science and Technical University animal centre.

6.2.4 Sample Harvesting

At designated time-points, specifically on days 7, 14, and 28, a cohort of four mice was chosen from each experimental group. Following humane euthanasia via cervical dislocation, the left tibia and surrounding muscle were harvested, then fixed and stored in 4% formaldehyde in PBS for further analysis. The right tibias were used for RNA extraction and subsequent qPCR.

6.2.5 Micro-CT Scan

After fixation, each left tibia with associated muscle was wrapped in parafilm and scanned using a SkyScan X-ray microtomography system (SkyScan 1176, Bruker MicroCT, Kontich, Belgium) at a voltage of 58 kV and a current of 431 µA. The scanning process employed an image pixel size of 9 and a rotation of 0.3, with a high-resolution exposure time of 1,000 ms. After scanning, the appendages were unwrapped and returned to a 10% formalin solution and stored at a temperature of 4°C. Subsequently, the samples were prepared for histological staining and analysis. The obtained CT data were used for 3D modelling and quantitative analysis of bone formation.

6.2.6 q-PCR

The right limbs of each mouse were processed upon collection. The gastrocnemius muscles and fibula were excised, and the tibia along with the surrounding tissue around the scaffold were trimmed, then 1 g tissue fragments were rapidly frozen using liquid nitrogen and crushed in a mortar. The tissue was homogenised using a sonicator (VCX150, SONICS &

MATERIALS INC., Newtown, CT, USA). The q-PCR process followed the steps outlined in detail in **Section 3.2.11**.

6.2.7 Histology of Undecalcified Samples

The left limb from each group at a particular time-point (D7, D14, D28) was embedded in poly (methyl methacrylate) (PMMA) following serial dehydration. The embedded samples were cut into 10 μm sections using a microtome (EXAKT 300 CP Band System, Norderstedt, Germany), and undecalcified sections were subjected to Toluidine Blue and Masson-Goldner's trichrome stainings. These processes were outsourced from AICA Sci-tech Ltd. (Beijing, China). The histology sections were then imaged using a light microscope (Zeiss; Carl Zeiss Microscopy GmbH, Jena, Germany). The overall gross appearance of the specimens was imaged using a TM-DM10 imaging system (TOMLOV, Los Angeles, CA, USA).

6.2.8 Statistical Analysis

Statistical analyses were performed using IBM SPSS Statistics software (IBM Corp., Armonk, NY, USA) and GraphPad Prism (GraphPad Software Inc., San Diego, CA, USA). All data are presented as mean ± standard deviation. T-tests were used when comparing two groups, and a 2-way analysis of variance (ANOVA) was performed for comparisons between multiple groups. A p-value < 0.05 was considered statistically significant.

6.3 Results

6.3.1 Characterisation of the MSC+HEK+HA/CC bone graft by confocal microscopy

Cells cultured on the HA/CC scaffold are shown in **Figure 6.2**. On the first day following the attachment of MSCs and HEK 293T cells (expressing BMP-2/7) to the HA/CC scaffold surface, complete coverage was not achieved. By day 7, increased cell proliferation resulted in more extensive cell attachment to the scaffolds. By day 14, nearly the entire scaffolds were enveloped by cells. The blue colour represents DAPI staining, while the green colour indicates Calcein AM. The red colour corresponds to the autofluorescence of the scaffold.

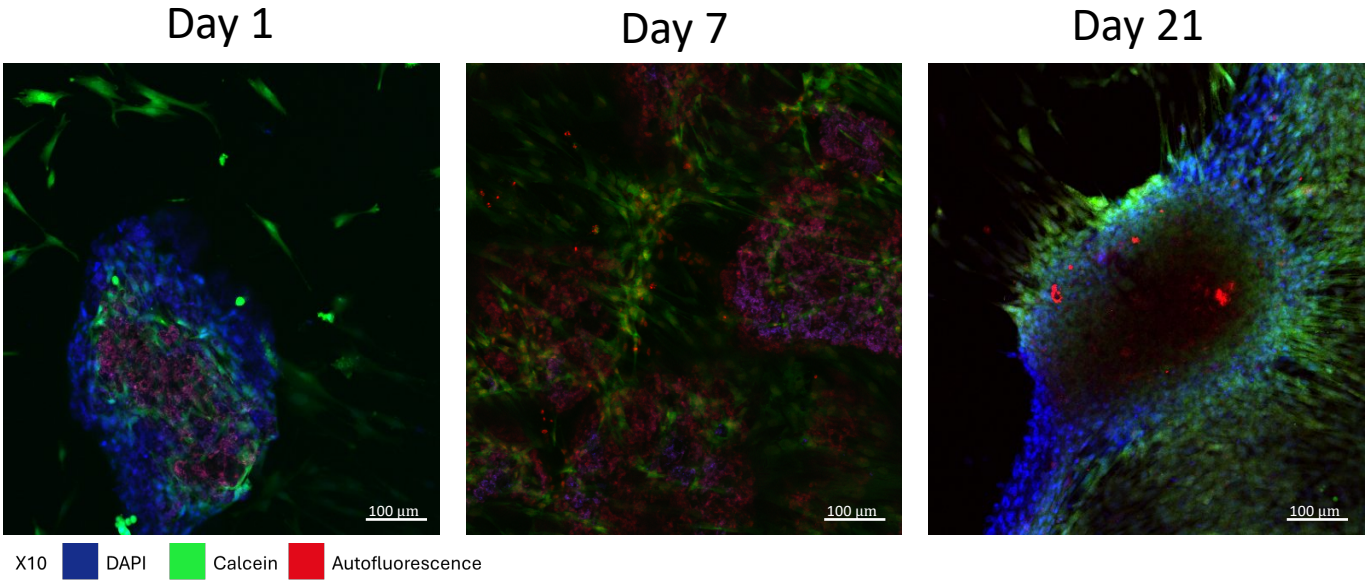

Figure 6.1 Morphological changes of HUMSCs adhering to scaffolds grown in cell culture medium. The cell morphology of HUMSCs and HEK 293T cells co-cultured on scaffolds in a normal growth medium for 1, 7 or 14 days was imaged by using confocal fluorescence microscopy.

6.3.2 The effect of decellularisation

Scanning electron microscopy (SEM) was employed to elucidate the microstructural details of the osteogenic scaffold surfaces. The images effectively illustrate the surfaces of scaffolds bearing adherent cells which formed multiple layers, highlighting discernible morphological differences. At a magnification of 2,000x (**Figure 6.3**), distinctive fibre-shaped and spherical structures were observable. In the decellularised samples, the

collagen fibres exhibited a slenderer appearance compared to their previous aspect, and the spherical structures were no longer evident. The ELISA outcomes for the decellularised osteogenic scaffolds indicate a substantial presence of both BMP-2 and BMP-7.

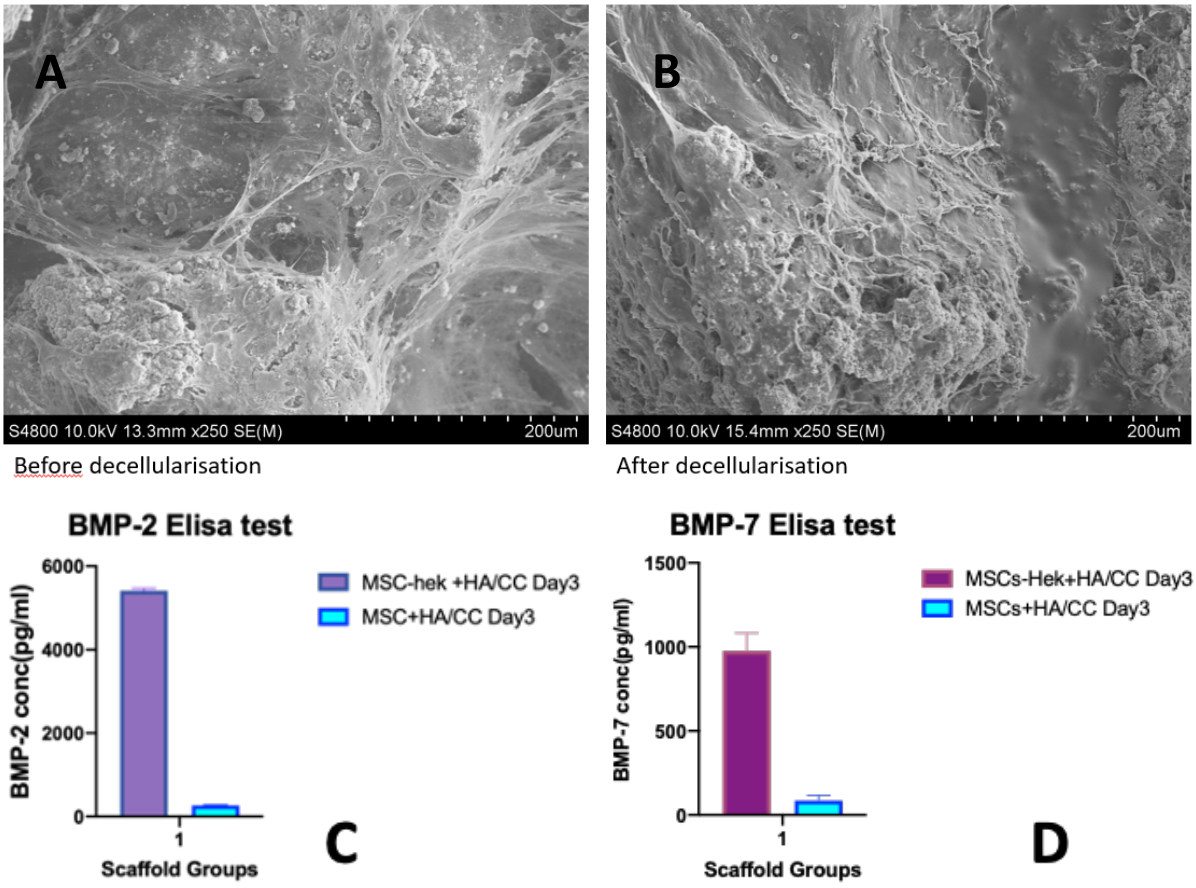

Figure 6.2 SEM images of the surface of MSC-HEK+HA/CC before and after decellularisation.
The surface of the HA/CC scaffold co-cultured with MSCs+HEK-293T (BMP2/7) for 14 days is subjected to SEM before (**A**) and after decellularisation (**B**). The SEM images shown are at 2000 times magnification. The BMP-2 (**C**) and BMP-7 (**D**) levels in the spent media in which the HA/CC scaffold co-cultured with MSCs or MSCs+HEK-293T (BMP2/7) for 3 days and decellularised were analysed by ELISA.

6.3.3 Analysis of gross appearance and micro CT of the implanted MSC+HEK+HA/CC bone graft

The gross appearance of sections of the implants (HA/CC scaffold, HA/CC scaffold co-cultured with MSCs [MSC+HA/CC] or MSCs and HEK293T cells expressing BMB2/7

[MSCs+HEK+HA/CC]) in tissue is shown in **Figure 6.4**. The surface views reveal the presence of the scaffold material, which remains visible, along with callus formation at various time-points, specifically on day 1, day 7, day 14, and day 28. Notably, the group implanted with MSCs+HEK+HA/CC bone graft exhibited a more pronounced yellowish stain, indicating the presence of osteogenic scaffold, characterised by a richer tissue colouration and a greater influx of migrating cells.

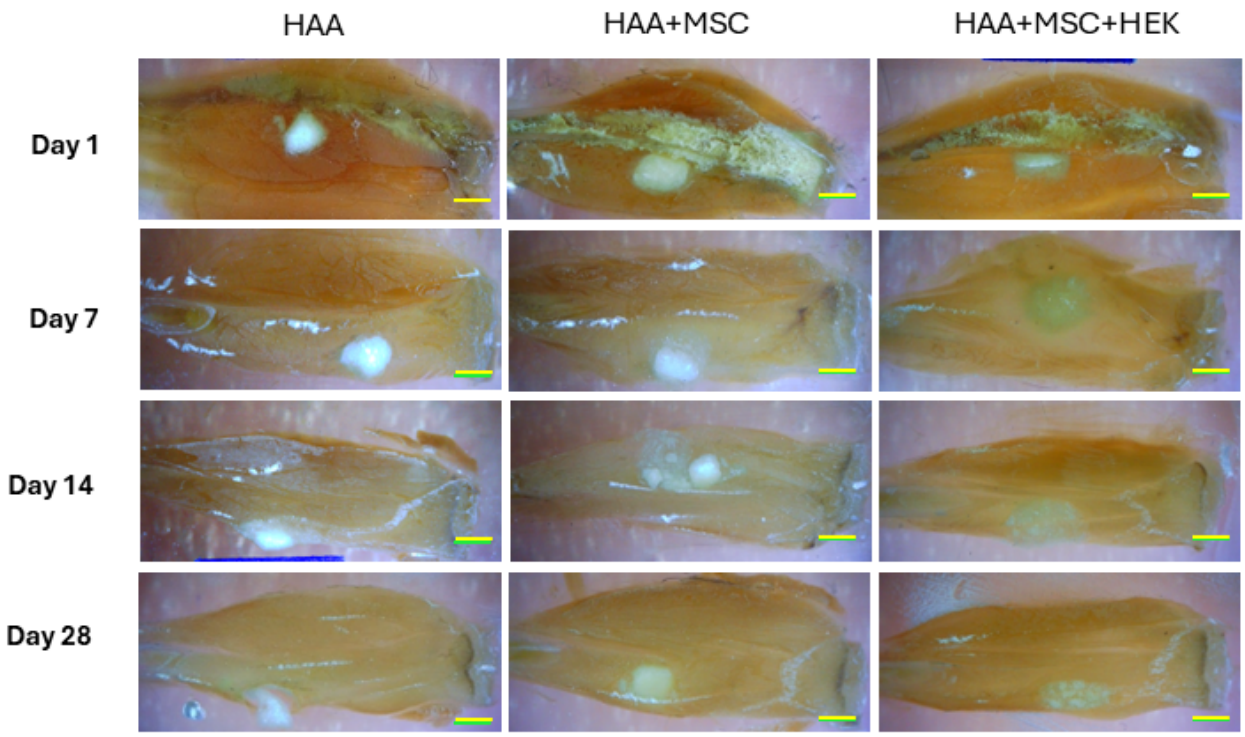

Figure 6.3 Gross observations of new bone formation in mice.
These images depict the skeletal structures and newly-formed callus within specimens that have been embedded in resin. The images display the different specimens at specific time-points in each group. The scale bar is 2 mm.

Micro-CT imaging demonstrated varying degrees of callus formation around osteogenic scaffolds of different compositions in different groups within the tibiae of mice (see **Figure 6.5**). The quantity of bone formed, as well as the quality and density of newly-formed callus, varied at different time points. Overall, there was a progressive increase in new bone formation across all groups. In comparison to the HA/CC group, the MSC+HA/CC and MSC+HEK+HA/CC groups displayed a richer and denser peri-nodular osteogenesis, validated through subsequent software-based quantitative analyses. Additionally, it was

observed that in the HA/CC group, Osteogenic scaffolds exhibited higher density, shrinking in size over time with minimal changes in density. Conversely, the MSC+HA/CC and MSC+HEK+HA/CC groups showed lower osteogenic scaffold density, implying cellular and soft tissue ingrowth. This suggested that osteogenic scaffolds subjected to cell adhesion and decellularisation processes attracted cell adhesion and ingrowth, with the decrease in density indicating a faster degradation rate compared to the unmodified HA/CC scaffold.

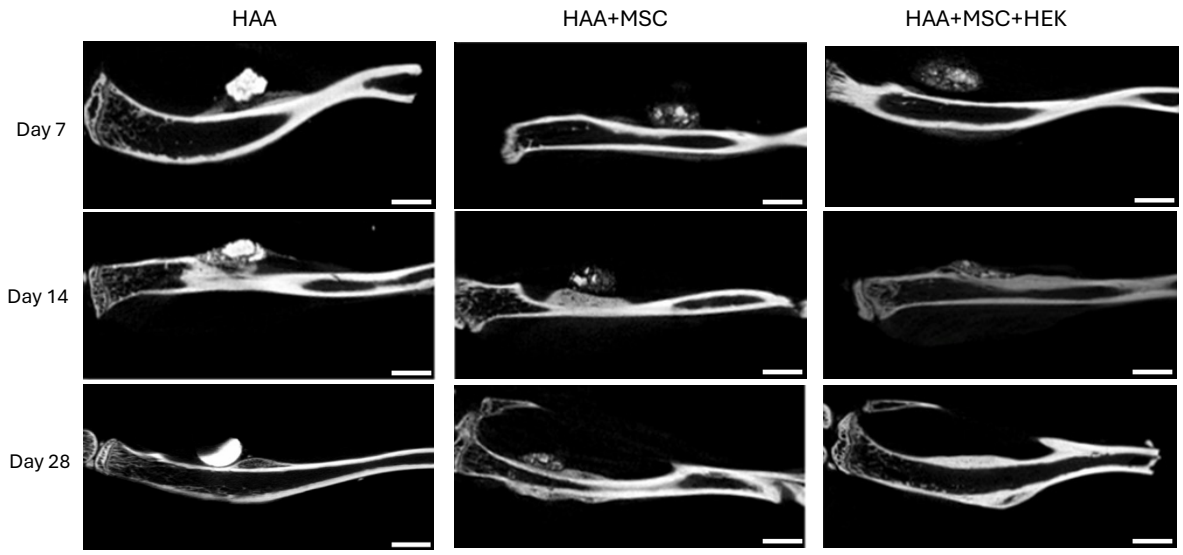

Figure 6.4 Bone and calluses of mice post-operation scanned by micro-CT.
Representative images of bone specimens and the development of calluses in the different experimental groups at designated time intervals, specifically on days 1, 7, 14, and 28 after surgical intervention. The scale bar is 2mm. In the control group, the implants were absorbed slowly and showed stronger density, which could be explained by the lack of the cells on the implants and HA/CC making it less porous, therefore, more density.

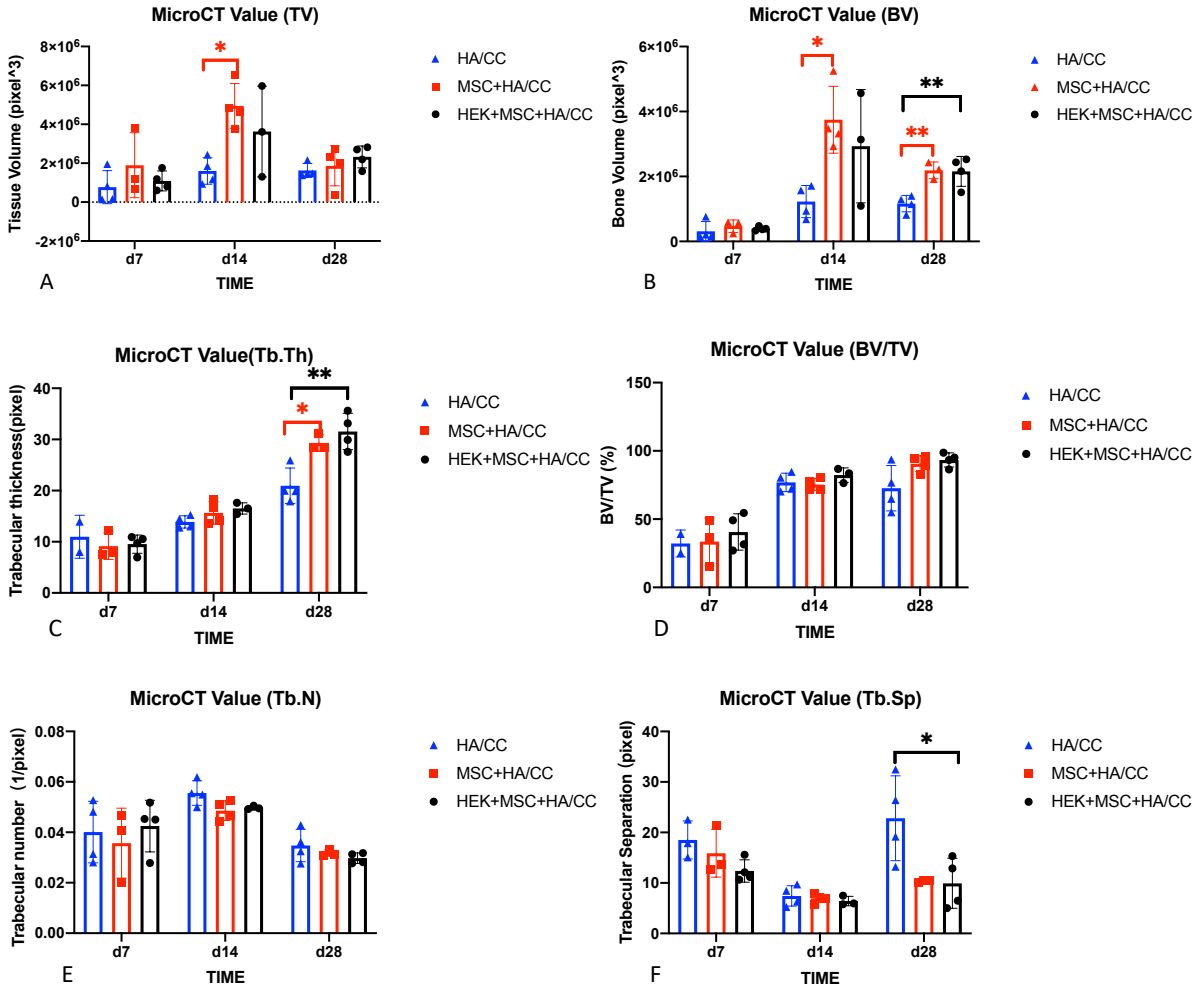

Figure 6.5 Analysis of quality of bone formation through micro-CT in mice implanted with HA/CC+MSC+HEK bone grafts.

Various qualities (A-F) of bone formation were assessed by mcro-CT amongst the test groups of mice consisting of the control HA/CC, MSC+HA/CC, and HEK+MSC+HA/CC groups on the day (d)7, d14 and d21 of the implantation. The qualities of bone formation explored are tissue volume (**A**), bone volume (**B**), trabecular thickness ([Tb.Th] **C**), bone volume/tissue volume ([BV/TV] **D**), trabecular number ([Tb.N] **E**) and trabecular separation ([Tb.Sp] **F**). *, $p < 0.05$; **, $p < 0.01$.

On day 7, the MSC+HA/CC group exhibited the highest mean bone volume, calculated at approximately 471,309.27 pixel^3. A one-way ANOVA conducted at this stage yielded a *p*-value of 0.6291, indicating the absence of statistically significant differences in bone volume among the three groups (**Figure 6.6**). This trend persisted on day 14, where once again, the MSC+HA/CC group exhibited the highest bone volume, with a mean of 374,7681.5 pixel^3, and this difference was significant, with a *p*-value of 0.0351 by ANOVA. To identify the specific pairwise comparison responsible for this statistical variation, Tukey's

multiple comparisons test was used. The results revealed a significant difference in bone volume between the HA/CC control group and the MSC+HA/CC group. Furthermore, by day 28, the HEK+MSC+HA/CC group showed an increase in bone volume, leading to two instances of statistically significant differences among the groups ($p = 0.0054$). Subsequent analysis using Tukey's multiple comparisons tests identified statistically significant differences between the HA/CC group and the MSC+HA/CC group ($p = 0.0117$), as well as between the HA/CC group and the HEK+MSC+HA/CC group ($p = 0.0090$).

On day 7, the HEK+MSC+HA/CC group was found to have the highest percentage of bone volume/tissue volume (BV/TV) at approximately 40.6%, however, one-way ANOVA revealed no statistically significant difference between the groups ($p = 0.7387$). Similarly on day 14, there was no significant difference between groups although the *p*-value decreased to 0.3090. However, it was observed that BV/TV increased among all three groups and their percentages all fell within a similar range between 70–90%. On day 28, significant differences were observed between the groups ($p = 0.0437$). Similarly, in agreement with the bone volume data, a significant difference was specifically observed between the HA/CC group relative to the MSC+HA/CC group ($p = 0.0519$).

Regarding trabecular thickness (Tb.Th), no statistically significant differences were observed among the groups on either day 7 or day 14 of the study. However, a notable trend emerged, showing an increase in Tb.Th measurements across the three time-points. For instance, on day 7, the MSC+HA/CC group displayed a mean Tb.Th value of approximately 9.81, which consistently rose to reach a mean of 31.81 by day 28. Day 28 was the sole time point at which statistically significant differences materialised ($p = 0.0034$). Further analysis utilising Tukey's multiple comparisons tests revealed significant disparities, specifically between the HA/CC and MSC+HA/CC groups ($p = 0.0198$) and between the HA/CC and HEK+MSC+HA/CC groups ($p = 0.0035$). Collectively, these findings suggest that HA/CC alone possesses the capacity to improve bone growth characteristics such as bone volume and Tb.Th, supplementing it with MSCs and establishing a co-culture with MSCs and HEK 293T cells offers the potential for further enhancements in bone regeneration at fracture sites.

Thus, these results underscore HA/CC as a promising biomaterial with considerable potential for use as a scaffold in regenerative applications.

The analytical outcomes also revealed changes in parameters such as trabecular number (Tb.N) and trabecular separation (Tb.Sp), wherein the Tb.Sp at day 28 exhibited contrasting results to bone volume (BV). Specifically, the HA/CC group exhibited a significant difference compared to the HEK+MSC+HA/CC group (p = 0.0376). The disparity in Tb.Sp, which was inversely related to osteogenesis, reflects larger gaps between trabeculae, indicative of lower-quality callus formation. These findings suggest favourable osteogenic outcomes in the HEK+MSC+HA/CC group. Although statistical analysis did not reveal significant intergroup differences in Tb.N, potential recognition biases in statistical calculations may exist, a phenomenon less frequently encountered in the results of other researchers (Hsu et al., 2014; Poilliot et al., 2023).

6.3.4 Histological observations

Masson-Goldner's trichrome staining was used to assess the progress of osteogenesis in the various experimental groups at different time points. Little difference was observed among the HA/CC, HA/CC+MSCs, and HA/CC+MSCs+Hek groups on days 1 and 7. Notably, at these time points, voids could be seen at the scaffold implantation sites due to the scaffold washing out during section staining, accompanied by mild tissue reactions and cell aggregations, demonstrating similar patterns across the groups. By days 14 and 28, all three groups showed cellular ingress at the scaffold sites, displaying fibrous proliferation and new bone formation indicated by green staining. Increased deposition of collagen fibres (green colour) by day 28 suggests a progression in cellular differentiation or increased osteoblastic activity, despite the emergence of smaller voids. Inter-group differences notably manifest, with increased green staining and reduced voids in the HA/CC+MSCs and HA/CC+MSCs+HEK groups compared to the control, indicating less cellular ingress at the implantation sites. Further suggesting that the two treatment groups had more cellular ingrowth and bone formation than the control group. The

HA/CC+MSCs+HEK group showed more cellular tissue at the implantation site with an increase in bluish-green staining, suggesting greater osteogenesis.

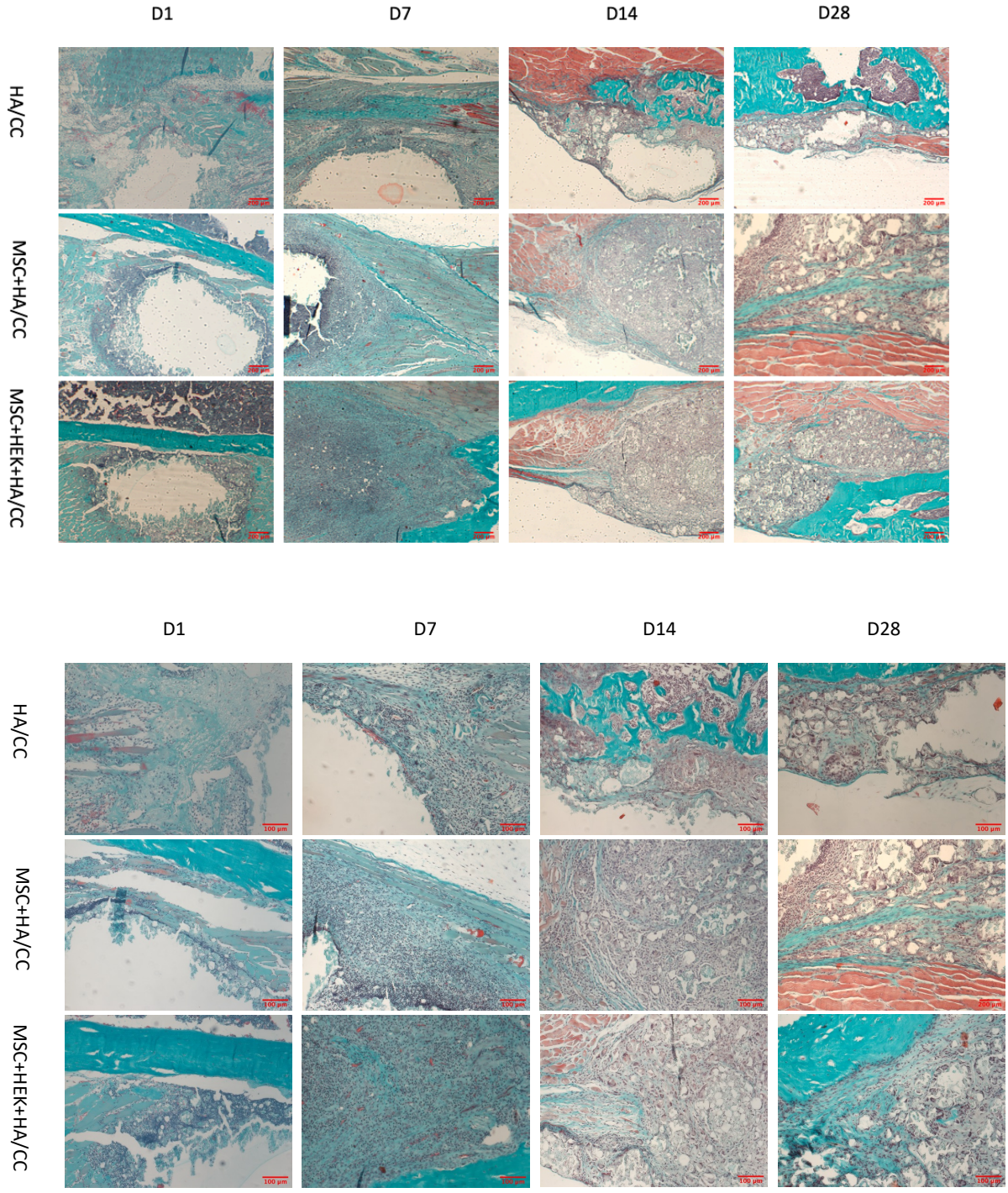

Figure 6.6 Analysing time-dependent osteogenesis by Masson Goldner's trichrome-staining.
Masson-Goldner's trichrome staining (indicative of osteogenesis) of tibial scaffold grafts in three groups mentioned above on day (D1), D7, D14 and D28 of the implantation. The staining was visualised using a Zeiss light microscope (Carl Zeiss Microscopy GmbH, Jena, Germany), revealing muscle fibres stained in

red, cell nuclei in a grey-blue hue, and fibres and newly-formed bone highlighted in green. Scale bars (100-200 µm) are shown in red in each image.

Toluidine Blue-staining of tibial scaffold grafts revealed comparable osteogenic conditions among the HA/CC, HA/CC+MSCs, and HA/CC+MSCs+Hek groups on days 1 and 7. Similarly, unstained voids appeared at the implantation sites due to detachment of scaffold material during staining. Increased cellular ingress, fibrous proliferation, and heightened osteogenic activity were observed in these areas, implying a greater potential for subsequent new bone formation. Inter-group comparisons indicated that both the HA/CC+MSCs and HA/CC+MSCs+Hek groups exhibited enhanced cellular ingress and deeper bluish-purple staining in the later stages compared to the HA/CC group. Groups implanted with cell-processed material demonstrated enhanced cell attraction and phagocytic absorption. Moreover, the increased presence of stimulated cells secreting fibrous tissue suggested potential osteoblastic differentiation.

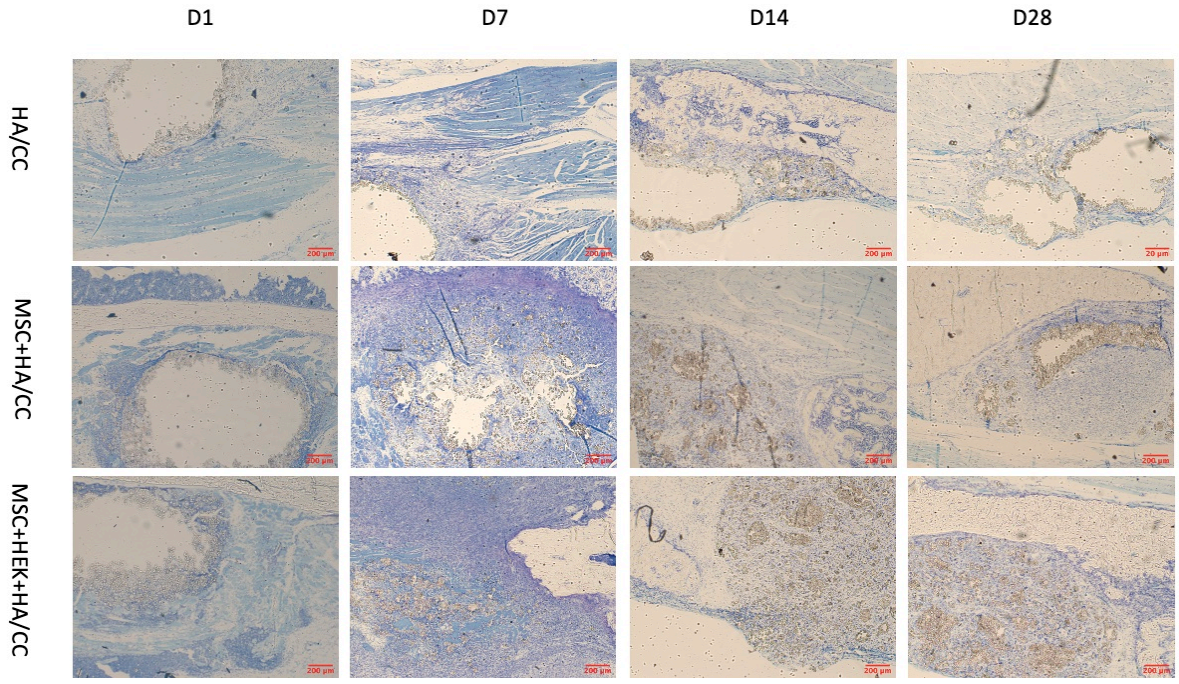

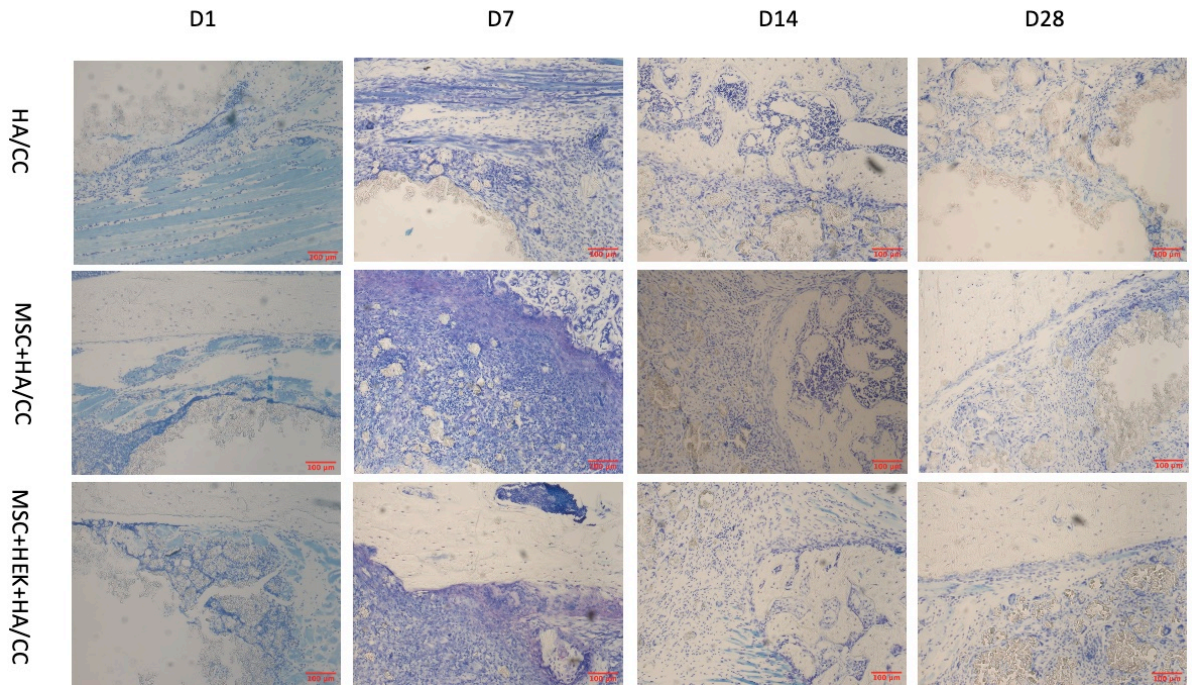

Figure 6.7 Toluidine Blue-staining of the implanted Tibial scaffolds.
Toluidine Blue staining of osteogenesis at the tibial scaffold implantation sites in mice across different experimental groups and time points. The sections were examined under an optical microscope, with chondrocytes and osteogenic cells appearing bluish-purple against a pale blue background. Scale bars (100-200 μm) are shown in red in each image.

6.3.5 Expression of osteogenic markers: RUNX2, BMP-2 and BMP-7

Osteogenic biomarker gene expression was analysed by qPCR at three time points (days 7, 14, and 28) after implantation (**Figure 6.9**). The primary objective was to assess the concentration of BMP-2 within the control HA/CC group in relation to the MSC+HA/CC and HEK+MSC+HA/CC groups. On day 7, it was observed that the HA/CC group exhibited the highest BMP-2 expression level, reflecting a mean value of 1.160×10^{-4}, this was followed by the co-culture group HEK+MSC+HA/CC, with a mean relative BMP-2 expression level of 0.7332×10^{-4}, and the MSC+HA/CC group displaying the lowest relative BMP-2 expression, with a mean of 0.3893×10^{-4}. One-way ANOVA on day 7 yielded a *p*-value of 0.192, showing the absence of a statistically significant difference among the groups. Subsequently, on day 14, there was a reduction in relative BMP-2 expression within the HA/CC group, which exhibited a mean expression level of 0.6335×10^{-4}. Conversely, the MSC+HA/CC group showed the highest relative BMP-2 expression at 1.400×10^{-4}, while the HEK+MSC+HA/CC

group also experienced an increase, recording a relative expression of 1.125×10^{-4}. This shift in BMP-2 expression level was accompanied by a reduction in the *p*-value to 0.1564. Significant differences between the groups were only identified on day 28 of the investigation. At this time point, the HEK+MSC+HA/CC group showed significantly higher relative expression of BMP-2 than the other groups as shown by further analysis using Tukey's multiple comparisons test, which revealed no significant difference between the control HA/CC and MSC+HA/CC groups ($p = 0.9979$). However, a significant difference was observed between the control HA/CC group and the HEK+MSC+HA/CC culture, with a *p*-value of < 0.0001. The same significant difference was also observed between the MSC+HA/CC and HEK+MSC+HA/CC groups.

The procedures used to analyse BMP-7 expression levels were identical to those employed for studying BMP-2 expression and the results exhibited congruent data trends from day 7 to day 28, paralleling the patterns observed with BMP-2. On day 7, the HA/CC control group showed the highest relative BMP-7 expression, yielding a calculated mean of 0.4860×10^{-4}. It was followed closely by the HEK+MSC+HA/CC group, displaying a mean of 0.4525×10^{-4}, while the MSC+HA/CC group recorded a mean of 0.2980×10^{-4}. A one-way ANOVA of day 7 results yielded a *p*-value of 0.4722, signifying the absence of statistically significant differences in relative BMP-7 expression among the groups at this time point. This trend continued into day 14, where the *p*-value was 0.0762, reflecting a considerable decline from the day 7 assessment but still failing to reach statistical significance. It is worth noting that, similar to the BMP-2 findings, a recurrent pattern emerged, with the MSC+HA/CC group demonstrating the highest relative BMP-7 expression on day 14, amounting to 1.0542×10^{-4}. After this, BMP-7 expression levels continued to increase in the MSC+HA/CC group up to day 28, with a mean of 1.3752×10^{-4}. In contrast, the HEK+MSC+HA/CC group experienced a substantial surge in relative BMP-7 expression, with the mean increasing from 0.6282×10^{-4} on day 14 to 1.6576×10^{-2} on day 28. One-way ANOVA at this stage yielded a highly significant *p*-value of < 0.0001, indicating a notable significant difference. Subsequent analysis utilising Tukey's multiple comparisons test pinpointed the significance, revealing that the HEK+MSC+HA/CC group exhibited statistically significant differences from both the HA/CC control and MSC+HA/CC groups on day 28. This distinctive surge in

BMP-7 expression level within the co-culture HEK+MSC+HA/CC group on day 28 was a notable feature of the findings.

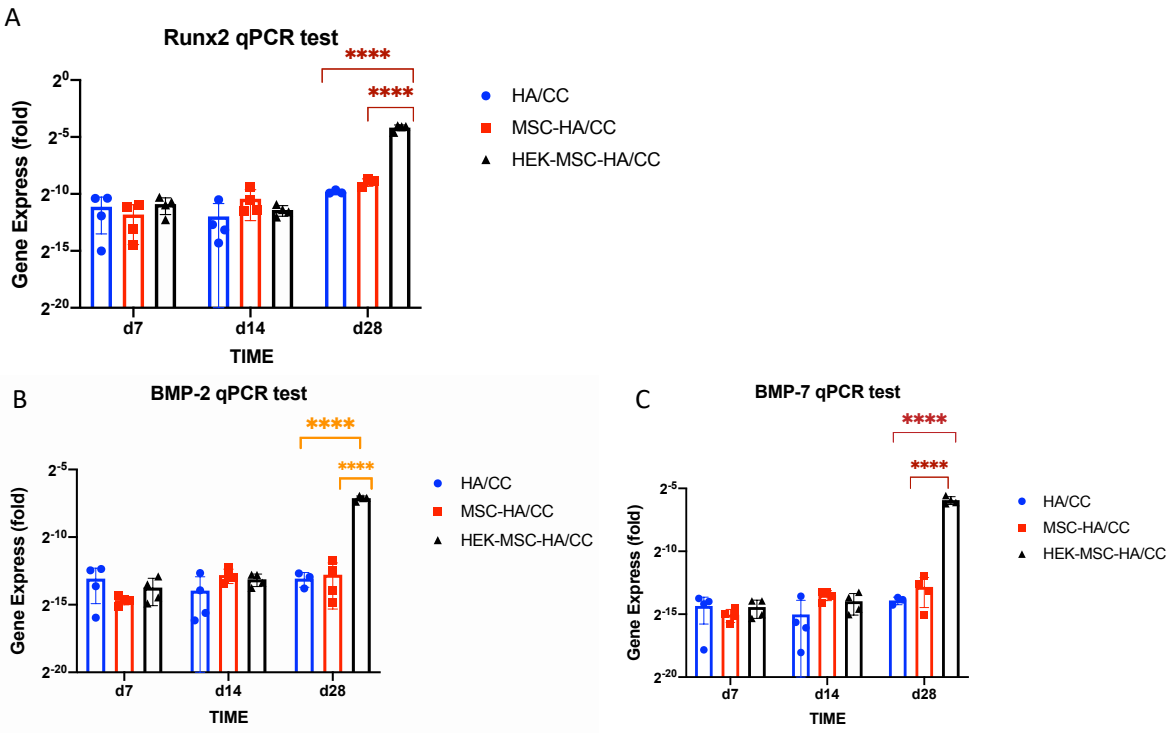

Figure 6.8 Analysis of the expression of the osteogenic markers RUNX2, BMP-2 and BMP-7 in implanted tissues.
Total RNA was isolated from the implanted region in the right tibia on the day (d)7, d14 and d28 of postimplantation in HA/CC, MSC-HA/CC and HEK-MSC-HA/CC groups and converted to cDNA and used the cDNA in the quantitative PCR (qPCR) to analyse the expression of Runx2 (**A**), BMP-2 (**B**) and BMP-7 (**C**). The expression values are normalised to the expression of housekeeping gene GAPDH.****, $p <$ 0.0001, N = 4.

In summary, both BMP-2 and BMP-7 assays exhibited consistent increases in expression, with the HEK+MSC+HA/CC group, displaying the highest expression of both BMP-2 and BMP-7 on day 28 of the study. Notably, BMP-7 exhibited higher expression levels, reaching a mean expression level of 1.6576×10^{-2}, surpassing the BMP-2 expression level on day 28 (7.1751×10^{-3}).

6.4 Discussion

In this part of the study, HEK/MSC+HA/CC and MSC+HA/CC scaffolds were successfully prepared, and the osteogenic capacity of the combined decellularized HEK/MSC with HA/CC was tested. The results were compared with those from the MSC+HA/CC group and the control group in vivo. Additionally, the expression levels of bone formation-related genes in the tissue post-implantation were analyzed.

Micro-CT results revealed an overall increasing trend in new bone formation in all three groups with time. In comparison to the HA/CC group, the MSC+HA/CC and MSC+HEK+HA/CC groups exhibited more abundant and denser bone formation surrounding the implants (**Figure 6.5**), and these findings were further validated by microCT quantification. This suggests dynamic changes in bone formation parameters over time, with distinct patterns emerging, particularly in the HEK+MSC+HA/CC group (**Figure 6.6**). These results may indicate that BMP-transfected HEK 293T cells played an important role in osteogenesis of this group.

BMP-2 was first isolated by Urist et al. in 1965 and is recognised as one of the inducer differentiation growth factors involved in bone formation (Urist, 1965). BMPs have been widely used to enhance osteogenesis. The earliest application was in demineralised bone matrix (DBM), which contained BMPs capable of inducing and regulating bone formation throughout embryonic development and into post-natal stages.

BMPs were first extracted from bovine bone in the 1980s and later applied to improve bone healing. However, these sources of BMPs were very expensive and the resource was also limited. In 1988, Wozney. et al. succeeded in cloning BMP-2 and BMP-4 (Wozney et al., 1988). Nowadays, human recombinant proteins can be produced in large quantities through genetic modification and manufacturing. Consequently, BMPs were produced for clinical application. However, very high doses were used to achieve a clinical effect.

In a clinical trial, the administered dose of BMP-2 in humans is typically 1 mg/60 kg. Some products even employ 20–40 mg BMP-2/60 kg weight. Clinical application of high doses of BMPs has a number of risks. While high doses of BMP-2 can indeed promote osteogenesis, it is acknowledged that, as a morphogen and growth factor, it may induce

side effects such as ectopic ossification. Devine et al. reported in clinical spine studies that a significantly higher cancer risk emerged in the treated group compared to the control group when a very high concentration of rhBMP-2, approximately 40 mg per patient, was used (Devine et al., 2012). They would therefore consider BMPs as carcinogenic, even with a lack of sufficient data to support this claim.

However, in our experiment, the BMP-2 dosage was approximately 30 ng/100 g in mice, representing a concentration 160–200 times less than that used in humans. Notably, Okubo et al. employed BMP-2 doses in animal experiments that were around 1,000 times higher than the amount used in this study (Okubo et al., 2001). Despite the substantial difference in dosage, the researchers observed remarkable osteogenic effects surpassing the clinical outcomes of bone fracture repair in humans. Our results suggest that the combination of HA/CC with MSCs and HEK cells may reduce the required dosage of BMP-2 and that BMP-7 may act in synergy with BMP-2 to enhance its osteogenic effects. Both BMP-2 and BMP-7 belong to the bone morphogenetic protein family and play crucial roles in various stages of bone development and repair. When applied together, BMP-2 and BMP-7 exhibit complementary and additive effects, enhancing the recruitment, proliferation, and differentiation of osteoprogenitor cells. Additionally, they stimulate the synthesis of extracellular matrix proteins and facilitate mineralisation, leading to the formation of mature bone tissue. This synergistic interaction between BMP-2 and BMP-7 amplifies their osteogenic properties, resulting in accelerated and more robust bone formation compared to individual administration (A. Bandyopadhyay et al., 2006). Overall, the combined effect of BMP-2 and BMP-7 represents a potent strategy for enhancing bone regeneration and treating bone defects in clinical settings.

Importantly, the subsequent histological tissue staining in this experiment did not reveal evident heterotopic ossification in the muscular tissues. This outcome suggests that the synergistic action of BMP-2 and BMP-7, along with the MSC-driven decellularisation of the extracellular matrix with HA/CC scaffold, markedly enhances new bone formation. This finding instils confidence in the potential for further investigation into the treatment of large bone defects, suggesting a direction for further exploration in this field.

The decellularised extracellular matrix derived from MSCs inherently contains growth factors that facilitate bone induction. This elucidates why, despite the comparatively lower

concentration of BMP in the materials used in this experiment compared to other studies, satisfactory osteogenic effects were still achieved. In contrast to other non-bioactive artificial bones, the requirement for BMP in this experiment was minimised, possibly owing to the rich growth factor content similar to that of DBM, allowing for synergistic interactions with BMP. Moreover, decellularised MSC-HEK-HA/CC are composed of type I collagen, calcium phosphate, and hydroxyapatite, which presents several advantages. Type I collagen naturally and effectively binds BMP, ensuring a sustained and gradual release. Reddi & Huggins found that the soluble extract of bone tissue alone, or insoluble residues alone, lose their capacity for induction of osteogenesis (Reddi & Huggins, 1972). This strongly supported the hypothesis that collagen together with HA/CC would further enhance the effect of BMPs.

The decellularized osteogenic scaffolds prepared are enriched with BMP-2 and BMP-7. The likely mechanisms underlying their promotion of bone regeneration may be as follows:

1. The degradation products of the absorbed scaffold material, such as Ca^{2+} and PO_4^{3-}, actively participate in bone formation and metabolism.
2. The nanoscale surface area of the scaffold facilitates enhanced cell adhesion, and the presence of BMP-2 and BMP-7 within the scaffold efficiently initiates the bone regeneration process.
3. The cell factors abundantly present within the extracellular matrix of the combined osteogenic scaffolds aid in recruiting surrounding cells, concurrently inducing the differentiation of stem cells into osteoblasts.

Natural bone is composed of both inorganic and organic extracellular matrix, with the organic matrix primarily consisting of collagen fibres and other non-collagenous proteins. Unlike other allogeneic or xenogeneic bone grafts, HA/CC does not contain collagen fibres, thus avoiding potential immunogenicity and pathogens associated with organic components (Xia et al., 2008). Our *in vitro* experiments demonstrate that MSCs and HEK cells can effectively adhere to and proliferate on HA/CC, likely due to the increased available surface area on HA/CC (**Figure 6.2**).

In comparison to non-bioactive scaffolds, decellularised MSC matrix preserves the natural environment for cell growth (**Figure 6.3**), and through decellularisation, retains intricate

biological molecules and physical cues that support cellular growth and vitality. Its immunogenic risk is minimal, as nearly all cellular DNA can be effectively removed.

The *in vivo* outcomes promoting new bone formation align broadly with expectations and are consistent with *in vitro* results. Well-processed HEK-MSC HA/CC scaffolds with BMP-2/7 demonstrated effective bone formation, and observations at various time-points revealed the simultaneous absorption of the osteogenic scaffolds, coupled with the recruitment of host mouse MSCs, accelerating the bone formation process. Additionally, the unexpected and robust cellular ingrowth within the osteogenic scaffolds was noted. Both the HA/CC+MSCs and HA/CC+MSCs+Hek groups exhibited a more rapid absorption and replacement by surrounding tissues. Due to the intact integrity of the mouse tibia, the bone formation in this experiment is predominantly considered to be a result of direct osteogenesis from stem cells, with a prevalence of osteogenic remodelling over endochondral ossification.

There are several limitations to this study. The accelerated healing rate of small animals like rodents, compared to humans, limits the direct translation of results to human scenarios due to ethical and practical constraints. Future studies may consider employing moderately larger animal models for better simulation. Additionally, the use of scaffold granules, while offering increased surface area for enhanced cell adhesion, lacks larger spatial structures found in 3D-printed scaffolds, which could better mimic bone defects. Research suggests that spatial structure influences bone cell behaviour, indicating a need for 3D-printed scaffolds with controlled structures for future clinical trials (Y. Shi, He, et al., 2020). In future investigations, 3D-printed HA/CC scaffolds with computer-controlled spatial structures should align more closely with the requirements of clinical trials.

6.5 Summary

1. Artificial allografts can be produced by culturing stem cells on an HA/CC scaffold.
2. HEK-MSC pre-culture enhanced the osteogenic potential of the HA/CC scaffold, resulting in a significant increase in new bone volume and osteogenic gene expression.
3. The MSC group also increased osteogenesis in comparison with the control group.

6.6 Conclusion

This study demonstrated that MSC and HEK cell integration with HA/CC scaffolds enhances osteogenesis, increasing bone formation and elevated osteogenic gene expression. Micro-CT and histological analyses confirmed that BMP-transfected HEK cells significantly improved bone density and distribution improvements. The scaffold's bioactive properties, combined with BMP-2 and BMP-7, enabled a reduced BMP dosage while maintaining efficacy. Future research should focus on larger animal models and 3D-printed scaffolds to better simulate human applications for bone defect treatment.

Chapter 7: General Discussion

7.1 Biocompatibility of HA/CC Scaffolds for Tissue Engineering

The biocompatibility of HA/CC material was investigated extensively in this study, focusing on its crucial role in ensuring the safety and efficacy of implantable scaffold materials. The evaluation encompassed various factors essential for biocompatibility, including surface microstructure, cellular interaction, stability, and immunocompatibility (Jamali et al., 2002).

The surface microstructure analysis, conducted through SEM imaging, revealed that the rough surface of the HA/CC scaffold facilitated cell adhesion and growth (**see Figure 4.3**). This finding is significant as it indicates the scaffold's ability to support cellular activities essential for tissue regeneration. In contrast, materials with smooth surfaces, like agarose, often require the addition of auxiliary components to improve cell attachment (Pae et al., 2014). By utilising rough-surfaced HA/CC scaffolds, this study demonstrated natural cell adhesion and proliferation, highlighting the material's favourable biocompatibility profile. The HA/CC material remained stable and intact over time, ensuring its suitability for long-term *in vivo* use. This durability is crucial for maintaining structural integrity during tissue regeneration (see **section 4.4.2**).

The biocompatibility assessment also included *in vitro* cell culture studies, where HA/CC particles showed no adverse effects on cell viability over an extended period (see **Figure 4.3**). This result confirms the excellent biocompatibility of the HA/CC material and suggests its compatibility with living tissues (N. Singh et al., 2021). Moreover, the choice of cell viability assays, such as the CCK-8 and Alamar Blue assays, provided consistent outcomes, further supporting the material's biocompatibility (see **Figure 4.4**).

Overall, the findings from this study underscore the favourable biocompatibility profile of HA/CC material, essential for its potential applications in tissue engineering and regenerative medicine. While the study addresses certain limitations, such as the need for further mechanistic testing and *in vivo* validation, it provides a solid foundation for future research endeavours aimed at harnessing the therapeutic potential of HA/CC scaffolds.

7.2 Differentiation Potential of BMP-2

The investigation into the differentiation potential of HUMSCs highlighted the critical role of BMP-2 in promoting osteogenic differentiation (Y. Li et al., 2022). MSCs possess remarkable multipotent differentiation capabilities, making them promising candidates for regenerative medicine therapies. BMP-2, a key regulator in osteogenesis, was found to significantly enhance the osteogenic differentiation efficiency of HUMSCs. This augmentation was evidenced by increased ALP staining intensity (see **Figure 4.5**) and elevated expression levels of osteogenic marker genes, such as Runx2 and Osteocalcin, following BMP-2 treatment.

The results demonstrated a time-dependent increase in ALP expression, particularly in HUMSCs treated with BMP-2 and osteogenic differentiation medium (X. W. Liu et al., 2021). Moreover, the expression patterns of Runx2 and Osteocalcin were significantly elevated in BMP-2-treated HUMSCs compared to those cultured in an osteogenic medium alone (see **Figure 4.6**).

Validation of the osteogenic differentiation potential was further supported by semi-quantitative analysis of ALP staining images and comparison of osteogenesis-related gene expression levels. The findings indicated robust osteogenic differentiation capabilities of HUMSCs under the influence of BMP-2, aligning with the known osteogenic effects of BMPs.

7.3 Exogenus Expression of BMP-2 and BMP-7 in HEK293T and MSCs

This part of the study aimed to validate BMP-2 and BMP-7 expression plasmids and transfect MSCs and HEK 293T cells to assess transfection efficiency and examine the expression levels of BMP-2 and BMP-7. The investigation involved the constructing expression plasmids for BMP-2 and BMP-7, followed by characterisation and validation of these constructs through analysis of distinct fragment patterns upon restriction enzyme digestion (see **Figure 5.1**). While previous attempts to extract BMP-2 from bone yielded

low yields, recombinant methods were explored as alternative approaches due to their potential for cost-effectiveness and scalability. The study detailed the use of lentiviral transduction and other viral transfection methods to achieve successful overexpression of BMP-2 and BMP-7 in MSCs (see **Figure 5.2**) and HEK 293T cells (see **Figure 5.4**).

Despite successful transfection observed in MSCs using green fluorescence protein (GFP) expression plasmid (easy to detect GFP even at very low levels by using confocal fluorescence microscopy), the expression levels of BMP-2 and BMP-7 were not as high as anticipated, posing several challenges (see **Figure 5.3**). These challenges included poor transducion, weak promoter and the size limitations of plasmids for efficient gene packing (Tamm et al., 2016). While adenoviral transfection methods offered advantages in terms of higher transfection efficiency, they also raised safety concerns and limitations related to gene insertion size and immune responses. Alternative approaches, such as electroporation and lipofection, were explored but failed to achieve satisfactory results (L. Gao et al., 2021).

To address the low expression levels of BMPs in MSCs, efforts were made to optimise transfection methods, including the use of lentivirus transfection, which demonstrated successful transfection with minimal cell damage. However, further optimisation is needed to achieve clinically relevant levels of BMP expression. Possible approaches for optimisation include improvements in plasmid size for easier entry into cells (Y. N. Lee et al., 2019), selection of more efficient promoters and longer screening periods for selecting cell lines with higher BMP expression.

Additionally, the study explored the potential of using HEK 293T stable cell line expressing adequate BMP-2/7 for bone induction and ossification research (see **Figure 5.4**). HEK 293T stable cell line expressing BMP-2 or BMP-7 is generated by transfecting HEK 293T cells with lentivirus carrying BMP-2 or BMP-7 and selecting the transfected cells using puromycin (Horikawa et al., 2021). While this innovative approach shows promise, further experiments are needed to validate its effectiveness, ensure genetic safety, and address potential immune reactions caused by viral antigens. Nonetheless, the functional validation presented in this study lays a solid foundation for the continued advancement of gene-

based strategies in bone tissue engineering and regenerative medicine, offering new avenues for addressing clinical needs associated with bone defects and fractures.

7.4 *In Vivo* Assessment of Exogenous BMP Enhanced Osteogenesis of HA/CC in Mice

This part of our study delves into the successful preparation and evaluation of hydroxyapatite/calcium carbonate (HA/CC) scaffolds cocultured with HEK293T-BMP-2 and MSC (MSC+HEK+HA/CC) or MSC (MSC+HA/CC) alone for their osteogenic potential *in vivo* by implanting them in mice and analysing the expression levels of bone formation-relevant genes in the implanted tissue.

Micro-CT analysis revealed a progressive increase in new bone formation over time across all three groups (see **Figure 6.5**) (Ganeshaaraj et al., 2022). Notably, both the MSC+HA/CC and MSC+HEK+HA/CC groups exhibited more abundant and denser bone formation surrounding the implants compared to the HA/CC group, indicating the enhanced osteogenic capacity of the combined scaffolds. Moreover, the quantitative analysis further corroborated these findings, highlighting distinct patterns of bone formation, particularly in the HEK+MSC+HA/CC group (see **Figure 6.6**). This suggests a significant contribution of BMP-transfected HEK cells to the osteogenesis observed in this group.

BMP-2, a key inducer of differentiation growth factors in bone formation, has long been recognised for its role in enhancing osteogenesis (Rogers et al., 2015). However, traditional sources of BMPs, such as demineralised bone matrix and bovine bone extracts, are expensive and limited in availability. The advent of recombinant technology has enabled large-scale production of human BMPs, albeit with the challenge of high dosage requirements in clinical applications. Our experiment, utilising a much lower BMP-2 dosage in mice compared to human clinical doses, still achieved remarkable osteogenic effects, suggesting a synergistic interaction between BMP-2 and BMP-7 (see **Figure 6.6**).

The co-delivery of BMP-2 and BMP-7, both belonging to the bone morphogenetic protein family, offers complementary and additive effects, enhancing the recruitment,

proliferation, and differentiation of osteoprogenitor cells (Qing et al., 2012). This synergistic action leads to accelerated and robust bone formation, surpassing outcomes observed in clinical settings. Importantly, histological tissue staining did not reveal evident heterotopic ossification, underscoring the safety and efficacy of this approach.

The decellularised extracellular matrix derived from MSCs, rich in growth factors, facilitates bone induction and minimises the requirement for exogenous BMPs. The composition of decellularised HA/CC scaffolds, comprising type I collagen, calcium carbonate (CC) and hydroxyapatite (HA), further enhances the osteogenic effects by effectively binding with BMPs and supporting sustained release (see **Figure 6.3**). Additionally, the nanoscale surface area of the scaffold promotes cell adhesion and initiates bone regeneration processes.

Overall, our findings underscore the potential of combined HEK/MSC+ HA/CC scaffolds in promoting bone regeneration, offering new avenues for addressing large bone defects and fractures in clinical settings. Further optimisation and validation are warranted to realise the full therapeutic potential of this approach.

7.5 Limitations of the Study

Despite the promising outcomes, this study acknowledged several limitations:
- Optimisation of BMP-2 concentration and the need for additional mechanistic testing methods were identified (Poon et al., 2016).
- Need for additional mechanistic testing, such as viability staining assays and confocal fluorescence imaging, to strengthen analysis.
- In vitro biocompatibility testing may not fully capture in vivo complexities, necessitating further in vivo studies.
- Uncertain scaffold degradation properties over time, calling for additional investigation into long-term stability.
- Challenges in transfection efficiency and BMP expression, with potential improvements in plasmid design and promoter selection.

- Reliance on small animal models limits direct translation to human outcomes; larger animal models may offer improved simulation.
- Scaffold granules lack spatial complexity of 3D-printed scaffolds, highlighting the need for controlled 3D structures to better replicate bone tissue environments.

7.6 Prospect

Future studies could benefit from using moderately larger animal models for improved simulation. While scaffold granules provide increased surface area to enhance cell adhesion, they lack the larger spatial structures characteristic of 3D-printed scaffolds, which may better replicate bone defects. Research indicates spatial structure impacts bone cell behaviour, suggesting the need for 3D-printed scaffolds with controlled architectures in upcoming clinical trials.

7.7 Summary

The results chapters in this thesis collectively represent a significant advancement in our understanding and application of regenerative medicine techniques.

In the initial chapter, the successful isolation and propagation of HUMSCs, coupled with the confirmation of their cellular characteristics, form a robust foundation for subsequent experiments. Biocompatibility testing of the HA/CC material further validates its suitability for *in vivo* applications, setting the stage for future investigations.

The utilisation of lentivirus technology and plasmid transfection in subsequent chapters demonstrates our ability to manipulate cellular behaviour effectively. This includes the successful transfection of MSCs to express BMP-2/7 and fluorescent proteins, as well as the overexpression of BMP-2/7 in HEK293T cells, providing crucial factors for bone formation.

The culmination of these efforts is observed in the final part, where artificial allografts are produced through *in vitro* culture of stem cells on HA/CC scaffolds. The synergistic effect of HEK293T-BMP-2/MSCs is particularly noteworthy, as evidenced by the significant increase in new bone volume and osteogenic gene expression. Additionally, the MSCs group also showed enhanced osteogenesis compared to the control group, underscoring the potential of these techniques for bone tissue engineering applications.

Collectively, these findings represent a significant step forward in the field of regenerative medicine, offering promising avenues for the development of novel therapies for bone defects and injuries. The mastery of experimental techniques demonstrated throughout these chapters lays a solid foundation for further exploration and application in future research endeavours.

7.8 Conclusion

In conclusion, this thesis significantly advances regenerative medicine by demonstrating the effective isolation and manipulation of HUMSCs, leading to enhanced bone formation through techniques like lentivirus transfection and artificial allograft production. These

findings provide a strong foundation for developing novel bone defects and injuries therapies.

Appendix 1

Ethical approval for formal review of experimental animal ethics, Huazhong University of Science and Technology

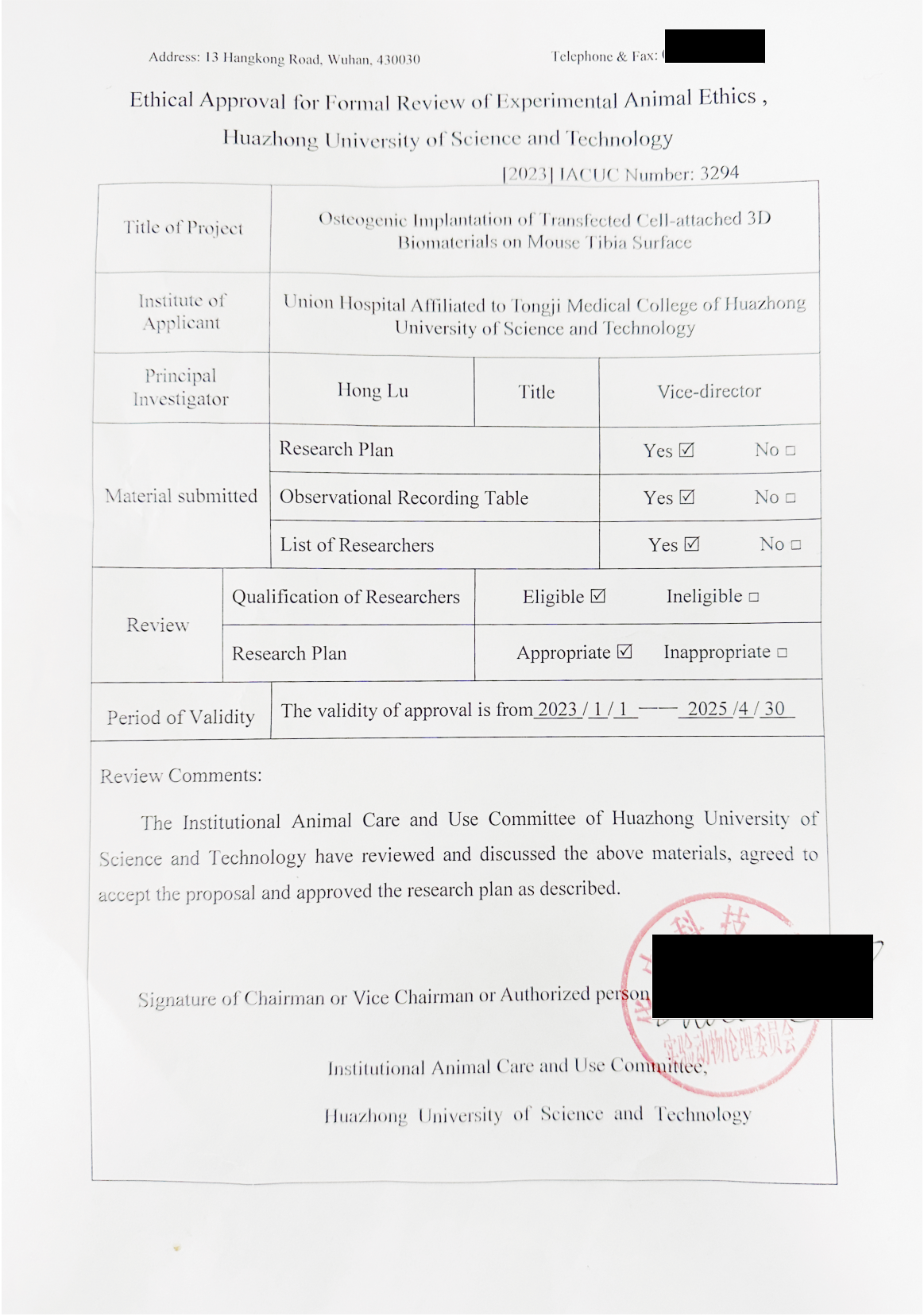

Address: 13 Hangkong Road, Wuhan, 430030 Telephone & Fax: [redacted]

Ethical Approval for Formal Review of Experimental Animal Ethics ,
Huazhong University of Science and Technology

[2023] IACUC Number: 3294

Title of Project	Osteogenic Implantation of Transfected Cell-attached 3D Biomaterials on Mouse Tibia Surface		
Institute of Applicant	Union Hospital Affiliated to Tongji Medical College of Huazhong University of Science and Technology		
Principal Investigator	Hong Lu	Title	Vice-director
Material submitted	Research Plan	Yes ☑	No □
	Observational Recording Table	Yes ☑	No □
	List of Researchers	Yes ☑	No □
Review	Qualification of Researchers	Eligible ☑	Ineligible □
	Research Plan	Appropriate ☑	Inappropriate □
Period of Validity	The validity of approval is from 2023 / 1 / 1 —— 2025 /4 / 30		

Review Comments:

The Institutional Animal Care and Use Committee of Huazhong University of Science and Technology have reviewed and discussed the above materials, agreed to accept the proposal and approved the research plan as described.

Signature of Chairman or Vice Chairman or Authorized person [redacted]

Institutional Animal Care and Use Committee,
Huazhong University of Science and Technology

Appendix 2

Certification of animal experiment

Reference

Agrawal, S., Galmarini, S., & Kröger, M. (2023). Voronoi tessellation-based algorithm for determining rigorously defined classical and generalized geometric pore size distributions. *Phys Rev E, 107*(1-2), 015307. doi:10.1103/PhysRevE.107.015307

Ahmed, M. F., El-Sayed, A. K., Chen, H., Zhao, R., Yusuf, M. S., Zuo, Q., . . . Li, B. (2019). Comparison between curcumin and all-trans retinoic acid in the osteogenic differentiation of mouse bone marrow mesenchymal stem cells. *Exp Ther Med, 17*(5), 4154-4166. doi:10.3892/etm.2019.7414

Akay, G., Birch, M. A., & Bokhari, M. A. (2004). Microcellular polyHIPE polymer supports osteoblast growth and bone formation in vitro. *Biomaterials, 25*(18), 3991-4000. doi:https://doi.org/10.1016/j.biomaterials.2003.10.086

Akin, F. A., Zreiqat, H., Jordan, S., Wijesundara, M. B. J., & Hanley, L. (2001). Preparation and analysis of macroporous TiO2 films on Ti surfaces for bone–tissue implants. *Journal of Biomedical Materials Research, 57*(4), 588-596. doi:https://doi.org/10.1002/1097-4636(20011215)57:4<588::AID-JBM1206>3.0.CO;2-Y

Aksyuk, A. A., & Rossmann, M. G. (2011). Bacteriophage assembly. *Viruses, 3*(3), 172-203. doi:10.3390/v3030172

Alghamdi, H. S., & Jansen, J. A. (2020). The development and future of dental implants. *Dent Mater J, 39*(2), 167-172. doi:10.4012/dmj.2019-140

Almalki, S. G., & Agrawal, D. K. (2016). Key transcription factors in the differentiation of mesenchymal stem cells. *Differentiation, 92*(1-2), 41-51. doi:10.1016/j.diff.2016.02.005

Altmann, S., Mut, J., Wolf, N., Meißner-Weigl, J., Rudert, M., Jakob, F., . . . Ebert, R. (2021). Metabolic Glycoengineering in hMSC-TERT as a Model for Skeletal Precursors by Using Modified Azide/Alkyne Monosaccharides. *Int J Mol Sci, 22*(6). doi:10.3390/ijms22062820

Andrzejowski, P., Masquelet, A., & Giannoudis, P. V. (2020). Induced Membrane Technique (Masquelet) for Bone Defects in the Distal Tibia, Foot, and Ankle: Systematic Review, Case Presentations, Tips, and Techniques. *Foot Ankle Clin, 25*(4), 537-586. doi:10.1016/j.fcl.2020.08.013

Arnold, P. M., Sasso, R. C., Janssen, M. E., Fehlings, M. G., Heary, R. F., Vaccaro, A. R., & Kopjar, B. (2018). i-Factor™ Bone Graft vs Autograft in Anterior Cervical Discectomy and Fusion: 2-Year Follow-up of the Randomized Single-Blinded Food and Drug Administration Investigational Device Exemption Study. *Neurosurgery, 83*(3). Retrieved from https://journals.lww.com/neurosurgery/Fulltext/2018/09000/i_Factor__Bone_Graft_vs_Autograft_in_Anterior.7.aspx

Arumugam, P., Kaarthikeyan, G., & Eswaramoorthy, R. (2024). Comparative Evaluation of Three Different Demineralisation Protocols on the Physicochemical Properties and Biocompatibility of Decellularised Extracellular Matrix for Bone Tissue Engineering Applications. *Cureus, 16*(7), e64813. doi:10.7759/cureus.64813

Bach, F. H., Winkler, H., Ferran, C., Hancock, W. W., & Robson, S. C. (1996). Delayed xenograft rejection. *Immunol Today, 17*(8), 379-384. doi:10.1016/0167-5699(96)10024-4

Bae, H. W., Zhao, L., Kanim, L. E., Wong, P., Delamarter, R. B., & Dawson, E. G. (2006). Intervariability and intravariability of bone morphogenetic proteins in commercially available demineralized bone matrix products. *Spine (Phila Pa 1976), 31*(12), 1299-1306; discussion 1307-1298. doi:10.1097/01.brs.0000218581.92992.b7

Bakhshandeh, B., Zarrintaj, P., Oftadeh, M. O., Keramati, F., Fouladiha, H., Sohrabi-Jahromi, S., & Ziraksaz, Z. (2017). Tissue engineering; strategies, tissues, and biomaterials. *Biotechnol Genet Eng Rev, 33*(2), 144-172. doi:10.1080/02648725.2018.1430464

Baldwin, P., Li, D. J., Auston, D. A., Mir, H. S., Yoon, R. S., & Koval, K. J. (2019). Autograft, Allograft, and Bone Graft Substitutes: Clinical Evidence and Indications for Use in the Setting of Orthopaedic Trauma Surgery. *J Orthop Trauma, 33*(4), 203-213. doi:10.1097/bot.0000000000001420

Bandyopadhyay, A., Bernard, S., Xue, W., & Bose, S. (2006). Calcium Phosphate-Based Resorbable Ceramics: Influence of MgO, ZnO, and SiO2 Dopants. *Journal of the American Ceramic Society, 89*(9), 2675-2688. doi:https://doi.org/10.1111/j.1551-2916.2006.01207.x

Bandyopadhyay, A., Tsuji, K., Cox, K., Harfe, B. D., Rosen, V., & Tabin, C. J. (2006). Genetic analysis of the roles of BMP2, BMP4, and BMP7 in limb patterning and skeletogenesis. *PLoS Genet, 2*(12), e216. doi:10.1371/journal.pgen.0020216

Banerjee, S. S., Bandyopadhyay, A., & Bose, S. (2010). Biphasic Resorbable Calcium Phosphate Ceramic for Bone Implants and Local Alendronate Delivery. *Advanced Engineering Materials, 12*(5), B148-B155. doi:https://doi.org/10.1002/adem.200980072

Batoon, L., Millard, S. M., Wullschleger, M. E., Preda, C., Wu, A. C., Kaur, S., . . . Pettit, A. R. (2019). CD169(+) macrophages are critical for osteoblast maintenance and promote intramembranous and endochondral ossification during bone repair. *Biomaterials, 196*, 51-66. doi:10.1016/j.biomaterials.2017.10.033

Bemenderfer, T. B., Harris, J. S., Condon, K. W., Li, J., & Kacena, M. A. (2021). Processing and Sectioning Undecalcified Murine Bone Specimens. *Methods Mol Biol, 2230*, 231-257. doi:10.1007/978-1-0716-1028-2_14

Ben Shabat, Y., & Fischer, A. (2015). Design of Porous Micro-Structures Using Curvature Analysis for Additive-Manufacturing. *Procedia CIRP, 36*, 279-284. doi:https://doi.org/10.1016/j.procir.2015.01.057

Benford, H. L., Frith, J. C., Auriola, S., Mönkkönen, J., & Rogers, M. J. (1999). Farnesol and Geranylgeraniol Prevent Activation of Caspases by Aminobisphosphonates: Biochemical Evidence for Two Distinct Pharmacological Classes of Bisphosphonate Drugs. *Molecular Pharmacology, 56*(1), 131. doi:10.1124/mol.56.1.131

Berendsen, A. D., & Olsen, B. R. (2015). Bone development. *Bone, 80*, 14-18. doi:10.1016/j.bone.2015.04.035

Blaudez, F., Ivanovski, S., Hamlet, S., & Vaquette, C. (2020). An overview of decellularisation techniques of native tissues and tissue engineered products for bone, ligament and tendon regeneration. *Methods, 171*, 28-40. doi:10.1016/j.ymeth.2019.08.002

Brydone, A. S., Meek, D., & Maclaine, S. (2010). Bone grafting, orthopaedic biomaterials, and the clinical need for bone engineering. *Proc Inst Mech Eng H, 224*(12), 1329-1343. doi:10.1243/09544119jeim770

Buser, Z., Brodke, D. S., Youssef, J. A., Meisel, H. J., Myhre, S. L., Hashimoto, R., . . . Wang, J. C. (2016). Synthetic bone graft versus autograft or allograft for spinal fusion: a systematic review. *J Neurosurg Spine, 25*(4), 509-516. doi:10.3171/2016.1.Spine151005

Canalis, E., McCarthy, T. L., & Centrella, M. (1989). Effects of platelet-derived growth factor on bone formation in vitro. *J Cell Physiol, 140*(3), 530-537. doi:10.1002/jcp.1041400319

Cao, H., & Kuboyama, N. (2010). A biodegradable porous composite scaffold of PGA/β-TCP for bone tissue engineering. *Bone, 46*(2), 386-395. doi:https://doi.org/10.1016/j.bone.2009.09.031

Caplan, A. I., & Correa, D. (2011). PDGF in bone formation and regeneration: new insights into a novel mechanism involving MSCs. *J Orthop Res, 29*(12), 1795-1803. doi:10.1002/jor.21462

Caputo, A. T., Eder, O. M., Bereznakova, H., Pothuis, H., Ardevol, A., Newman, J., . . . Adams, T. E. (2021). Structure-guided selection of puromycin N-acetyltransferase mutants with enhanced selection stringency for deriving mammalian cell lines expressing recombinant proteins. *Sci Rep, 11*(1), 5247. doi:10.1038/s41598-021-84551-9

Carbone, E. J., Jiang, T., Nelson, C., Henry, N., & Lo, K. W. H. (2014). Small molecule delivery through nanofibrous scaffolds for musculoskeletal regenerative engineering. *Nanomedicine: Nanotechnology, Biology and Medicine, 10*(8), 1691-1699. doi:https://doi.org/10.1016/j.nano.2014.05.013

Cattalini, J. P., Boccaccini, A. R., Lucangioli, S., & Mouriño, V. (2012). Bisphosphonate-Based Strategies for Bone Tissue Engineering and Orthopedic Implants. *Tissue Engineering Part B: Reviews, 18*(5), 323-340. doi:10.1089/ten.teb.2011.0737

Centrella, M., McCarthy, T. L., & Canalis, E. (1989). Effects of transforming growth factors on bone cells. *Connect Tissue Res, 20*(1-4), 267-275. doi:10.3109/03008208909023896

Challis, V. J., Roberts, A. P., Grotowski, J. F., Zhang, L.-C., & Sercombe, T. B. (2010). Prototypes for Bone Implant Scaffolds Designed via Topology Optimization and Manufactured by Solid Freeform Fabrication. *Advanced Engineering Materials, 12*(11), 1106-1110. doi:https://doi.org/10.1002/adem.201000154

Chan, J. L., Tang, K. C., Patel, A. P., Bonilla, L. M., Pierobon, N., Ponzio, N. M., & Rameshwar, P. (2006). Antigen-presenting property of mesenchymal stem cells occurs during a narrow window at low levels of interferon-gamma. *Blood, 107*(12), 4817-4824. doi:10.1182/blood-2006-01-0057

Chang, C. L., Chen, C. S., Huang, C. H., & Hsu, M. L. (2012). Finite element analysis of the dental implant using a topology optimization method. *Med Eng Phys, 34*(7), 999-1008. doi:10.1016/j.medengphy.2012.06.004

Charalambides, C., Beer, M., & Cobb, A. G. (2005). Poor results after augmenting autograft with xenograft (Surgibone) in hip revision surgery. *Acta Orthopaedica, 76*(4), 544-549. doi:10.1080/17453670510041547

Chen, C., & Kim, W. K. (2020). The application of micro-CT in egg-laying hen bone analysis: introducing an automated bone separation algorithm. *Poult Sci, 99*(11), 5175-5183. doi:10.1016/j.psj.2020.08.047

Chen, D., Ji, X., Harris, M. A., Feng, J. Q., Karsenty, G., Celeste, A. J., . . . Harris, S. E. (1998). Differential Roles for Bone Morphogenetic Protein (BMP) Receptor Type IB and IA in Differentiation and Specification of Mesenchymal Precursor Cells to Osteoblast and Adipocyte Lineages. *Journal of Cell Biology, 142*(1), 295-305. doi:10.1083/jcb.142.1.295

Chen, Z., Mao, X., Tan, L., Friis, T., Wu, C., Crawford, R., & Xiao, Y. (2014). Osteoimmunomodulatory properties of magnesium scaffolds coated with β-tricalcium phosphate. *Biomaterials, 35*(30), 8553-8565. doi:https://doi.org/10.1016/j.biomaterials.2014.06.038

Cheng, L., Suresh, K. S., He, H., Rajput, R. S., Feng, Q., Ramesh, S., . . . Ramalingam, M. (2021). 3D Printing of Micro- and Nanoscale Bone Substitutes: A Review on Technical and Translational Perspectives. *Int J Nanomedicine, 16*, 4289-4319. doi:10.2147/ijn.S311001

Cherukuri, A., Mehta, R., Sood, P., & Hariharan, S. (2018). Early allograft inflammation and scarring associate with graft dysfunction and poor outcomes in renal transplant recipients with delayed graft function: a prospective single center cohort study. *Transpl Int, 31*(12), 1369-1379. doi:10.1111/tri.13318

Clarke, B. (2008). Normal bone anatomy and physiology. *Clin J Am Soc Nephrol, 3 Suppl 3*, S131-139. doi:10.2215/CJN.04151206

Cui, Y., Zhu, T., Li, D., Li, Z., Leng, Y., Ji, X., . . . Ding, J. (2019). Bisphosphonate-Functionalized Scaffolds for Enhanced Bone Regeneration. *Adv Healthc Mater, 8*(23), e1901073. doi:10.1002/adhm.201901073

Damien, C. J., & Parsons, J. R. (1991). Bone graft and bone graft substitutes: A review of current technology and applications. *Journal of Applied Biomaterials, 2*(3), 187-208. doi:https://doi.org/10.1002/jab.770020307

Daniel, Alexander, Jeffrey, Thorsten, Ian, Patrick, . . . Bethany. (2019). Investigating the Osteoinductive Potential of a Decellularized Xenograft Bone Substitute. *Cells Tissues Organs, 207*(2), 97-113. doi:10.1159/000503280

De Biase, P., & Capanna, R. (2005). Clinical applications of BMPs. *Injury, 36 Suppl 3*, S43-46. doi:10.1016/j.injury.2005.07.034

del Rosario, C., Rodríguez-Évora, M., Reyes, R., Delgado, A., & Évora, C. (2015). BMP-2, PDGF-BB, and bone marrow mesenchymal cells in a macroporous β-TCP scaffold for critical-size bone defect repair in rats. *Biomedical Materials, 10*(4), 045008. doi:10.1088/1748-6041/10/4/045008

Denner, J. (2023). Systemic inflammation in xenograft recipients (SIXR) or undetected PCMV/PRV transmission? *Xenotransplantation, 30*(1), e12788. doi:10.1111/xen.12788

Devine, J. G., Dettori, J. R., France, J. C., Brodt, E., & McGuire, R. A. (2012). The use of rhBMP in spine surgery: is there a cancer risk? *Evid Based Spine Care J, 3*(2), 35-41. doi:10.1055/s-0031-1298616

Dias, M. R., Guedes, J. M., Flanagan, C. L., Hollister, S. J., & Fernandes, P. R. (2014). Optimization of scaffold design for bone tissue engineering: A computational and experimental study. *Medical Engineering & Physics, 36*(4), 448-457. doi:https://doi.org/10.1016/j.medengphy.2014.02.010

Ding, T., Cai, M., Wu, C. C., Bao, L. J., & Li, J. (2022). Distribution profiles of bisphenols in school supplies and implications for human exposure. *Sci Total Environ, 849*, 157938. doi:10.1016/j.scitotenv.2022.157938

Doktor, T., Valach, J., Kytyr, D., & Jiroušek, O. (2011). *Pore Size Distribution of Human Trabecular Bone - Comparison of Intrusion Measurements with Image Analysis*.

Dominici, M., Le Blanc, K., Mueller, I., Slaper-Cortenbach, I., Marini, F., Krause, D., . . . Horwitz, E. (2006). Minimal criteria for defining multipotent mesenchymal stromal cells. The International Society for Cellular Therapy position statement. *Cytotherapy, 8*(4), 315-317. doi:10.1080/14653240600855905

Donath, K., & Breuner, G. (1982). A method for the study of undecalcified bones and teeth with attached soft tissues. The Säge-Schliff (sawing and grinding) technique. *J Oral Pathol, 11*(4), 318-326. doi:10.1111/j.1600-0714.1982.tb00172.x

Dong, M., Jiao, G., Liu, H., Wu, W., Li, S., Wang, Q., . . . Chen, Y. (2016). Biological Silicon Stimulates Collagen Type 1 and Osteocalcin Synthesis in Human Osteoblast-Like Cells Through the BMP-2/Smad/RUNX2 Signaling Pathway. *Biol Trace Elem Res, 173*(2), 306-315. doi:10.1007/s12011-016-0686-3

Duan, Y., Huang, W., Zhan, B., Li, Y., Xu, X., Li, K., . . . Gu, Q. (2022). Bioink derived from human placenta supporting angiogenesis. *Biomed Mater, 17*(5). doi:10.1088/1748-605X/ac7b5b

Earl, V. J., & Badawy, M. K. (2019). Radiation Exposure to Staff and Patient During Videofluoroscopic Swallowing Studies and Recommended Protection Strategies. *Dysphagia, 34*(3), 290-297. doi:10.1007/s00455-018-9945-0

Eaves, C. J. (2015). Hematopoietic stem cells: concepts, definitions, and the new reality. *Blood, 125*(17), 2605-2613. doi:10.1182/blood-2014-12-570200

Eilenberger, C., Kratz, S. R. A., Rothbauer, M., Ehmoser, E.-K., Ertl, P., & Küpcü, S. (2018). Optimized alamarBlue assay protocol for drug dose-response determination of 3D tumor spheroids. *MethodsX, 5*, 781-787. doi:https://doi.org/10.1016/j.mex.2018.07.011

Endo, Y., Funayama, H., Yamaguchi, K., Monma, Y., Yu, Z., Deng, X., . . . Takahashi, T. (2020). [Basic Studies on the Mechanism, Prevention, and Treatment of Osteonecrosis of the Jaw Induced by Bisphosphonates]. *Yakugaku Zasshi, 140*(1), 63-79. doi:10.1248/yakushi.19-00125

Ezra, A., & Golomb, G. (2000). Administration routes and delivery systems of bisphosphonates for the treatment of bone resorption. *Advanced Drug Delivery Reviews, 42*(3), 175-195. doi:https://doi.org/10.1016/S0169-409X(00)00061-2

Feinberg, S., Hollister, S., Chu, T., & Halloran, J. (1999). An image-based approach to design and manufacture of scaffolds for maxillofacial reconstruction. *International Journal of Oral and Maxillofacial Surgery, 28*, 55. doi:https://doi.org/10.1016/S0901-5027(99)80817-0

Feklistov, A. (2013). RNA polymerase: in search of promoters. *Ann N Y Acad Sci, 1293*, 25-32. doi:10.1111/nyas.12197

Feng, Y., Zhu, S., Mei, D., Li, J., Zhang, J., Yang, S., & Guan, S. (2021). Application of 3D Printing Technology in Bone Tissue Engineering: A Review. *Curr Drug Deliv, 18*(7), 847-861. doi:10.2174/1567201817999201113100322

Ferretti, J. L., Cointry, G. R., Capozza, R. F., Mondelo, N., Peluffo, V., Chiappe, A., . . . Alippi, R. M. (1997). [Effects of bisphosphonates on the mechanical efficiency of normal and osteopenic bones]. *Medicina (B Aires), 57 Suppl 1*, 83-92.

Fu, K., Xu, Q., Czernuszka, J., Triffitt, J. T., & Xia, Z. (2013). Characterization of a biodegradable coralline hydroxyapatite/calcium carbonate composite and its clinical implementation. *Biomed Mater, 8*(6), 065007. doi:10.1088/1748-6041/8/6/065007

Ganeshaaraj, G., Kaushalya, S., Kondarage, A. I., Karunaratne, A., Jones, J. R., & Nanayakkara, N. D. (2022). Semantic Segmentation of Micro-CT Images to Analyze Bone Ingrowth into Biodegradable Scaffolds. *Annu Int Conf IEEE Eng Med Biol Soc, 2022*, 3830-3833. doi:10.1109/embc48229.2022.9870828

Ganguli, A., Pagan-Diaz, G. J., Grant, L., Cvetkovic, C., Bramlet, M., Vozenilek, J., . . . Bashir, R. (2018). 3D printing for preoperative planning and surgical training: a review. *Biomed Microdevices, 20*(3), 65. doi:10.1007/s10544-018-0301-9

Gao, L., Zhou, Q., Zhang, Y., Sun, S., Lv, L., Ma, P., . . . Zhan, L. (2021). Dimethyl Sulfoxide-Free Cryopreservation of Human Umbilical Cord Mesenchymal Stem Cells Based on Zwitterionic Betaine and Electroporation. *Int J Mol Sci, 22*(14). doi:10.3390/ijms22147445

Gao, X., Usas, A., Lu, A., Tang, Y., Wang, B., Chen, C. W., . . . Huard, J. (2013). BMP2 is superior to BMP4 for promoting human muscle-derived stem cell-mediated bone regeneration in a critical-sized calvarial defect model. *Cell Transplant, 22*(12), 2393-2408. doi:10.3727/096368912x658854

García-Gareta, E., Coathup, M. J., & Blunn, G. W. (2015). Osteoinduction of bone grafting materials for bone repair and regeneration. *Bone, 81*, 112-121. doi:10.1016/j.bone.2015.07.007

Ghosal, K., Chandra, A., G, P., S, S., Roy, S., Agatemor, C., . . . Provaznik, I. (2018). Electrospinning over Solvent Casting: Tuning of Mechanical Properties of Membranes. *Sci Rep, 8*(1), 5058. doi:10.1038/s41598-018-23378-3

Giacca, M., & Zacchigna, S. (2012). Virus-mediated gene delivery for human gene therapy. *J Control Release, 161*(2), 377-388. doi:10.1016/j.jconrel.2012.04.008

Gill, K. P., & Denham, M. (2020). Optimized Transgene Delivery Using Third-Generation Lentiviruses. *Curr Protoc Mol Biol, 133*(1), e125. doi:10.1002/cpmb.125

Gillman, C. E., & Jayasuriya, A. C. (2021). FDA-approved bone grafts and bone graft substitute devices in bone regeneration. *Materials Science and Engineering: C, 130*, 112466. doi:https://doi.org/10.1016/j.msec.2021.112466

Gómez Font, R., Martínez García, M. L., & Olmos Martínez, J. M. (2008). Osteochemonecrosis of the jaws due to bisphosphonate treatments. Update. *Med Oral Patol Oral Cir Bucal, 13*(5), E318-324.

Gómez, S., Vlad, M. D., López, J., & Fernández, E. (2016). Design and properties of 3D scaffolds for bone tissue engineering. *Acta Biomaterialia, 42*, 341-350. doi:https://doi.org/10.1016/j.actbio.2016.06.032

Gore, L. F., & Abbott, J. J. (1964). THE SECTIONING OF UNDECALCIFIED TISSUE USING A DIAMOND IMPREGNANTED CUTTING DISC. *J Med Lab Technol, 21*, 293-297.

Gottipamula, S., Muttigi, M. S., Chaansa, S., Ashwin, K. M., Priya, N., Kolkundkar, U., . . . Seetharam, R. N. (2016). Large-scale expansion of pre-isolated bone marrow mesenchymal stromal cells in serum-free conditions. *J Tissue Eng Regen Med, 10*(2), 108-119. doi:10.1002/term.1713

Götz, H. E., Müller, M., Emmel, A., Holzwarth, U., Erben, R. G., & Stangl, R. (2004). Effect of surface finish on the osseointegration of laser-treated titanium alloy implants.

Biomaterials, 25(18), 4057-4064. doi:https://doi.org/10.1016/j.biomaterials.2003.11.002

Grauss, R. W., Hazekamp, M. G., Oppenhuizen, F., van Munsteren, C. J., Gittenberger-de Groot, A. C., & DeRuiter, M. C. (2005). Histological evaluation of decellularised porcine aortic valves: matrix changes due to different decellularisation methods. *Eur J Cardiothorac Surg, 27*(4), 566-571. doi:10.1016/j.ejcts.2004.12.052

Groeneveld, E. H. J., van den Bergh, J. P. A., Holzmann, P., ten Bruggenkate, C. M., Tuinzing, D. B., & Burger, E. H. (1999). Mineralization processes in demineralized bone matrix grafts in human maxillary sinus floor elevations. *Journal of Biomedical Materials Research, 48*(4), 393-402. doi:https://doi.org/10.1002/(SICI)1097-4636(1999)48:4<393::AID-JBM1>3.0.CO;2-C

Gungor-Ozkerim, P. S., Inci, I., Zhang, Y. S., Khademhosseini, A., & Dokmeci, M. R. (2018). Bioinks for 3D bioprinting: an overview. *Biomater Sci, 6*(5), 915-946. doi:10.1039/c7bm00765e

Guoqing, Z., Junxin, L., Chengguang, Z., Juanjuan, X., Xiaoyu, Z., & Anmin, W. (2021). Design Optimization and Manufacturing of Bio-fixed tibial implants using 3D printing technology. *J Mech Behav Biomed Mater, 117*, 104415. doi:10.1016/j.jmbbm.2021.104415

Han, Y. F., Tao, R., Sun, T. J., Chai, J. K., Xu, G., & Liu, J. (2013). Optimization of human umbilical cord mesenchymal stem cell isolation and culture methods. *Cytotechnology, 65*(5), 819-827. doi:10.1007/s10616-012-9528-0

Hasegawa, T., Miwa, M., Sakai, Y., Niikura, T., Lee, S. Y., Oe, K., . . . Komori, T. (2010). Efficient cell-seeding into scaffolds improves bone formation. *J Dent Res, 89*(8), 854-859. doi:10.1177/0022034510370022

Hassan, E., & Calà Lesina, A. (2022). Topology optimization of dispersive plasmonic nanostructures in the time-domain. *Opt Express, 30*(11), 19557-19572. doi:10.1364/oe.458080

He, P., Zou, Y., & Hu, Z. (2015). Advances in aluminum hydroxide-based adjuvant research and its mechanism. *Hum Vaccin Immunother, 11*(2), 477-488. doi:10.1080/21645515.2014.1004026

Hellstein, J. W., & Marek, C. L. (2005). Bisphosphonate Osteochemonecrosis (Bis-Phossy Jaw): Is This Phossy Jaw of the 21st Century? *Journal of Oral and Maxillofacial Surgery, 63*(5), 682-689. doi:https://doi.org/10.1016/j.joms.2005.01.010

Hellstein, J. W., & Marek, C. L. (2006). Bisphosphonate induced osteochemonecrosis of the jaws: an ounce of prevention may be worth a pound of cure. *Spec Care Dentist, 26*(1), 8-12. doi:10.1111/j.1754-4505.2006.tb01503.x

Hettwer, W. (2017). [Synthetic bone replacement : Current developments and perspectives]. *Orthopade, 46*(8), 688-700. doi:10.1007/s00132-017-3447-x

Hofreuter, D., Odenbreit, S., Püls, J., Schwan, D., & Haas, R. (2000). Genetic competence in Helicobacter pylori: mechanisms and biological implications. *Res Microbiol, 151*(6), 487-491. doi:10.1016/s0923-2508(00)00164-9

Horikawa, M., Sabe, H., & Onodera, Y. (2021). Strategies for all-at-once and stepwise selection of cells with multiple genetic manipulations. *Biochem Biophys Res Commun, 582*, 93-99. doi:10.1016/j.bbrc.2021.10.016

Howell, J. D. (2021). The CT Scan after 50 years - Continuity and Change. *N Engl J Med, 385*(2), 104-105. doi:10.1056/NEJMp2033374

Hsu, J. T., Chen, Y. J., Ho, J. T., Huang, H. L., Wang, S. P., Cheng, F. C., . . . Tsai, M. T. (2014). A comparison of micro-CT and dental CT in assessing cortical bone morphology and trabecular bone microarchitecture. *PLoS One, 9*(9), e107545. doi:10.1371/journal.pone.0107545

Hulbert, S. F., Young, F. A., Mathews, R. S., Klawitter, J. J., Talbert, C. D., & Stelling, F. H. (1970). Potential of ceramic materials as permanently implantable skeletal prostheses. *Journal of Biomedical Materials Research, 4*(3), 433-456. doi:https://doi.org/10.1002/jbm.820040309

Ikarashi, A., Sano, H., Tanaka, M., & Ohshima, H. (2023). The accuracy of quantifying the degree of hard tissue calcification using an electron probe micro analyzer, micro-focus X-ray computed tomography, and tissue sectioning methods. *J Oral Biosci, 65*(3), 226-232. doi:10.1016/j.job.2023.06.001

Israel, D. I., Nove, J., Kerns, K. M., Moutsatsos, I. K., & Kaufman, R. J. (1992). Expression and characterization of bone morphogenetic protein-2 in Chinese hamster ovary cells. *Growth Factors, 7*(2), 139-150. doi:10.3109/08977199209046403

Jahani, D., Nazari, A., Ghourbanpour, J., & Ameli, A. (2020). Polyvinyl Alcohol/Calcium Carbonate Nanocomposites as Efficient and Cost-Effective Cationic Dye Adsorbents. *Polymers (Basel), 12*(10). doi:10.3390/polym12102179

Jamali, A., Hilpert, A., Debes, J., Afshar, P., Rahban, S., & Holmes, R. (2002). Hydroxyapatite/calcium carbonate (HA/CC) vs. plaster of Paris: a histomorphometric and radiographic study in a rabbit tibial defect model. *Calcif Tissue Int, 71*(2), 172-178. doi:10.1007/s00223-001-1087-x

James, A. W. (2013). Review of Signaling Pathways Governing MSC Osteogenic and Adipogenic Differentiation. *Scientifica (Cairo), 2013*, 684736. doi:10.1155/2013/684736

Jamshidinia, M., Wang, L., Tong, W., & Kovacevic, R. (2014). The bio-compatible dental implant designed by using non-stochastic porosity produced by Electron Beam Melting® (EBM). *Journal of Materials Processing Technology, 214*(8), 1728-1739. doi:https://doi.org/10.1016/j.jmatprotec.2014.02.025

Ji, X., Yuan, X., Ma, L., Bi, B., Zhu, H., Lei, Z., . . . Xiao, J. (2020). Mesenchymal stem cell-loaded thermosensitive hydroxypropyl chitin hydrogel combined with a three-dimensional-printed poly(ε-caprolactone) /nano-hydroxyapatite scaffold to repair bone defects via osteogenesis, angiogenesis and immunomodulation. *Theranostics, 10*(2), 725-740. doi:10.7150/thno.39167

Kajiwara, H., Yamaza, T., Yoshinari, M., Goto, T., Iyama, S., Atsuta, I., . . . Tanaka, T. (2005). The bisphosphonate pamidronate on the surface of titanium stimulates bone formation around tibial implants in rats. *Biomaterials, 26*(6), 581-587. doi:https://doi.org/10.1016/j.biomaterials.2004.02.072

Kehoe, S., Zhang, X. F., & Boyd, D. (2012). FDA approved guidance conduits and wraps for peripheral nerve injury: a review of materials and efficacy. *Injury, 43*(5), 553-572. doi:10.1016/j.injury.2010.12.030

Kim, H. S., Neugebauer, J., McKnite, A., Tilak, A., & Christian, J. L. (2019). BMP7 functions predominantly as a heterodimer with BMP2 or BMP4 during mammalian embryogenesis. *Elife, 8*. doi:10.7554/eLife.48872

Komori, T. (2018). Runx2, an inducer of osteoblast and chondrocyte differentiation. *Histochem Cell Biol, 149*(4), 313-323. doi:10.1007/s00418-018-1640-6

Koyama, C., Hirota, M., Okamoto, Y., Iwai, T., Ogawa, T., Hayakawa, T., & Mitsudo, K. (2020). A nitrogen-containing bisphosphonate inhibits osteoblast attachment and impairs bone healing in bone-compatible scaffold. *Journal of the Mechanical Behavior of Biomedical Materials, 104*, 103635. doi:https://doi.org/10.1016/j.jmbbm.2020.103635

Kuboki, Y., Jin, Q., Kikuchi, M., Mamood, J., & Takita, H. (2002). Geometry of Artificial ECM: Sizes of Pores Controlling Phenotype Expression in BMP-Induced Osteogenesis and Chondrogenesis. *Connective Tissue Research, 43*(2-3), 529-534. doi:10.1080/03008200290001104

Kuboki, Y., Jin, Q., & Takita, H. (2001). Geometry of Carriers Controlling Phenotypic Expression in BMP-Induced Osteogenesis and Chondrogenesis. *JBJS, 83*(1). Retrieved from https://journals.lww.com/jbjsjournal/Fulltext/2001/00002/Geometry_of_Carriers_Controlling_Phenotypic.5.aspx

Kuboki, Y., Takita, H., Kobayashi, D., Tsuruga, E., Inoue, M., Murata, M., . . . Ohgushi, H. (1998). BMP-Induced osteogenesis on the surface of hydroxyapatite with geometrically feasible and nonfeasible structures: Topology of osteogenesis. *Journal of Biomedical Materials Research, 39*(2), 190-199. doi:https://doi.org/10.1002/(SICI)1097-4636(199802)39:2<190::AID-JBM4>3.0.CO;2-K

Kumar, P., Nagarajan, A., & Uchil, P. D. (2019). Electroporation. *Cold Spring Harb Protoc, 2019*(7). doi:10.1101/pdb.top096271

Kusumbe, A. P., Ramasamy, S. K., & Adams, R. H. (2014). Coupling of angiogenesis and osteogenesis by a specific vessel subtype in bone. *Nature, 507*(7492), 323-328. doi:10.1038/nature13145

Latfi, A. S. A., Pramanik, S., Poon, C. T., Gumel, A. M., Lai, K. W., Annuar, M. S. M., & Pingguan-Murphy, B. (2019). Structural and bone marrow stem cell biocompatibility studies of hydrogel synthesized via chemo-enzymatic route. *J Biomater Appl, 33*(6), 854-865. doi:10.1177/0885328218812490

Lavrentieva, A., Hatlapatka, T., Neumann, A., Weyand, B., & Kasper, C. (2013). Potential for osteogenic and chondrogenic differentiation of MSC. *Adv Biochem Eng Biotechnol, 129*, 73-88. doi:10.1007/10_2012_133

Lebedev, A. E., Katalevich, A. M., & Menshutina, N. V. (2015). Modeling and scale-up of supercritical fluid processes. Part I: Supercritical drying. *The Journal of Supercritical Fluids, 106*, 122-132. doi:https://doi.org/10.1016/j.supflu.2015.06.010

Ledley, F. D. (1994). Non-viral gene therapy. *Curr Opin Biotechnol, 5*(6), 626-636. doi:10.1016/0958-1669(94)90085-x

Lee, J., Byun, H., Madhurakkat Perikamana, S. K., Lee, S., & Shin, H. (2019). Current Advances in Immunomodulatory Biomaterials for Bone Regeneration. *Advanced Healthcare Materials, 8*(4), 1801106. doi:https://doi.org/10.1002/adhm.201801106

Lee, Y. N., Lin, C. F., Chang, C. Y., Wu, Y. J., Tsai, C. H., Tseng, S. W., . . . Su, C. H. (2019). Enhanced Proliferation of Endothelial Progenitor Cells Post-Ultrasonic Microbubble Transfection Is Plasmid DNA Size Dependent and Contributed by Interleukin-6 Generation. *Ultrasound Med Biol, 45*(9), 2434-2443. doi:10.1016/j.ultrasmedbio.2019.05.009

Lennon, D., Solchaga, L. A., Somoza, R. A., Schluchter, M. D., Margevicius, S., & Caplan, A. I. (2018). Human and Rat Bone Marrow-Derived Mesenchymal Stem Cells Differ in

Their Response to Fibroblast Growth Factor and Platelet-Derived Growth Factor. *Tissue Eng Part A, 24*(23-24), 1831-1843. doi:10.1089/ten.TEA.2018.0126

León-Félix, C. M., Maranhão, A. Q., Amorim, C. A., & Lucci, C. M. (2024). Optimizing Decellularization of Bovine Ovarian Tissue: Toward a Transplantable Artificial Ovary Scaffold with Minimized Residual Toxicity and Preserved Extracellular Matrix Morphology. *Cells Tissues Organs*. doi:10.1159/000537838

Li, L., Yu, F., Shi, J., Shen, S., Teng, H., Yang, J., . . . Jiang, Q. (2017). In situ repair of bone and cartilage defects using 3D scanning and 3D printing. *Sci Rep, 7*(1), 9416. doi:10.1038/s41598-017-10060-3

Li, N., Guo, R., & Zhang, Z. J. (2021). Bioink Formulations for Bone Tissue Regeneration. *Front Bioeng Biotechnol, 9*, 630488. doi:10.3389/fbioe.2021.630488

Li, Y., Fu, G., Gong, Y., Li, B., Li, W., Liu, D., & Yang, X. (2022). BMP-2 promotes osteogenic differentiation of mesenchymal stem cells by enhancing mitochondrial activity. *J Musculoskelet Neuronal Interact, 22*(1), 123-131.

Liu, X. W., Ma, B., Zi, Y., Xiang, L. B., & Han, T. Y. (2021). Effects of rutin on osteoblast MC3T3-E1 differentiation, ALP activity and Runx2 protein expression. *Eur J Histochem, 65*(1). doi:10.4081/ejh.2021.3195

Liu, Z., Ge, Y., Zhang, L., Wang, Y., Guo, C., Feng, K., . . . Liu, F. (2020). The effect of induced membranes combined with enhanced bone marrow and 3D PLA-HA on repairing long bone defects in vivo. *Journal of Tissue Engineering and Regenerative Medicine, 14*(10), 1403-1414. doi:https://doi.org/10.1002/term.3106

Lode, A., Bernhardt, A., & Gelinsky, M. (2008). Cultivation of human bone marrow stromal cells on three-dimensional scaffolds of mineralized collagen: influence of seeding density on colonization, proliferation and osteogenic differentiation. *J Tissue Eng Regen Med, 2*(7), 400-407. doi:10.1002/term.110

Lomas, R., Chandrasekar, A., & Board, T. N. (2013). Bone allograft in the U.K.: perceptions and realities. *Hip Int, 23*(5), 427-433. doi:10.5301/hipint.5000018

Lorenz, M. G., & Wackernagel, W. (1994). Bacterial gene transfer by natural genetic transformation in the environment. *Microbiol Rev, 58*(3), 563-602. doi:10.1128/mr.58.3.563-602.1994

Lv, Y., Wang, B., Liu, G., Tang, Y., Liu, J., Wei, G., & Wang, L. (2022). Design of bone-like continuous gradient porous scaffold based on triply periodic minimal surfaces. *Journal of Materials Research and Technology, 21*, 3650-3665. doi:https://doi.org/10.1016/j.jmrt.2022.10.160

Lv, Y., Wang, B., Liu, G., Tang, Y., Lu, E., Xie, K., . . . Wang, L. (2021). Metal Material, Properties and Design Methods of Porous Biomedical Scaffolds for Additive Manufacturing: A Review. *Frontiers in Bioengineering and Biotechnology, 9*. doi:10.3389/fbioe.2021.641130

Ma, S., Song, K., Lan, J., & Ma, L. (2020). Biological and mechanical property analysis for designed heterogeneous porous scaffolds based on the refined TPMS. *Journal of the Mechanical Behavior of Biomedical Materials, 107*, 103727. doi:10.1016/j.jmbbm.2020.103727

Malladi, P., Xu, Y., Yang, G. P., & Longaker, M. T. (2006). Functions of vitamin D, retinoic acid, and dexamethasone in mouse adipose-derived mesenchymal cells. *Tissue Eng, 12*(7), 2031-2040. doi:10.1089/ten.2006.12.2031

Manassero, M., Viateau, V., Deschepper, M., Oudina, K., Logeart-Avramoglou, D., Petite, H., & Bensidhoum, M. (2013). Bone Regeneration in Sheep Using Acropora Coral, a

Natural Resorbable Scaffold, and Autologous Mesenchymal Stem Cells. *Tissue Engineering Part A, 19*(13-14), 1554-1563. doi:10.1089/ten.tea.2012.0008

Marks, S. C., & Odgren, P. R. (2002). Chapter 1 - Structure and Development of the Skeleton. In J. P. Bilezikian, L. G. Raisz, & G. A. Rodan (Eds.), *Principles of Bone Biology (Second Edition)* (pp. 3-15). San Diego: Academic Press.

Marsell, R., & Einhorn, T. A. (2011). The biology of fracture healing. *Injury, 42*(6), 551-555. doi:10.1016/j.injury.2011.03.031

Marupanthorn, K., Tantrawatpan, C., Kheolamai, P., Tantikanlayaporn, D., & Manochantr, S. (2017). Bone morphogenetic protein-2 enhances the osteogenic differentiation capacity of mesenchymal stromal cells derived from human bone marrow and umbilical cord. *Int J Mol Med, 39*(3), 654-662. doi:10.3892/ijmm.2017.2872

Marx, R. E. (2003). Pamidronate (Aredia) and zoledronate (Zometa) induced avascular necrosis of the jaws: a growing epidemic. *Journal of Oral and Maxillofacial Surgery, 61*(9), 1115-1117. doi:10.1016/s0278-2391(03)00720-1

Matai, I., Kaur, G., Seyedsalehi, A., McClinton, A., & Laurencin, C. T. (2020). Progress in 3D bioprinting technology for tissue/organ regenerative engineering. *Biomaterials, 226*, 119536. doi:10.1016/j.biomaterials.2019.119536

McGovern, J. A., Griffin, M., & Hutmacher, D. W. (2018). Animal models for bone tissue engineering and modelling disease. *Dis Model Mech, 11*(4). doi:10.1242/dmm.033084

Meyers, M. A., Chen, P.-Y., Lin, A. Y.-M., & Seki, Y. (2008). Biological materials: Structure and mechanical properties. *Progress in Materials Science, 53*(1), 1-206. doi:10.1016/j.pmatsci.2007.05.002

Murphy, S. V., De Coppi, P., & Atala, A. (2020). Opportunities and challenges of translational 3D bioprinting. *Nat Biomed Eng, 4*(4), 370-380. doi:10.1038/s41551-019-0471-7

Mushahary, D., Spittler, A., Kasper, C., Weber, V., & Charwat, V. (2018). Isolation, cultivation, and characterization of human mesenchymal stem cells. *Cytometry A, 93*(1), 19-31. doi:10.1002/cyto.a.23242

Narayanan, A., Srinaath, N., Rohini, M., & Selvamurugan, N. (2019). Regulation of Runx2 by MicroRNAs in osteoblast differentiation. *Life Sci, 232*, 116676. doi:10.1016/j.lfs.2019.116676

Neve, A., Corrado, A., & Cantatore, F. P. (2013). Osteocalcin: skeletal and extra-skeletal effects. *J Cell Physiol, 228*(6), 1149-1153. doi:10.1002/jcp.24278

Nie, R., Sun, Y., Lv, H., Lu, M., Huangfu, H., Li, Y., . . . Zhou, Y. (2022). 3D printing of MXene composite hydrogel scaffolds for photothermal antibacterial activity and bone regeneration in infected bone defect models. *Nanoscale, 14*(22), 8112-8129. doi:10.1039/d2nr02176e

Nishimura, R., Hata, K., Matsubara, T., Wakabayashi, M., & Yoneda, T. (2012). Regulation of bone and cartilage development by network between BMP signalling and transcription factors. *The Journal of Biochemistry, 151*(3), 247-254. doi:10.1093/jb/mvs004

O'Brien, M. J. M., Jones, D. M., Semciw, A. I., Balakumar, J., Grabinski, R., Roebert, J., . . . Kemp, J. L. (2022). Does the use of i-FACTOR bone graft affect bone healing in those undergoing periacetabular osteotomy (PAO) for developmental dysplasia of the hip (DDH)? A retrospective study. *J Hip Preserv Surg, 9*(3), 165-171. doi:10.1093/jhps/hnac027

Oh, J. Y., Kim, H., Lee, H. J., Lee, K., Barreda, H., Kim, H. J., . . . Lee, R. H. (2022). MHC Class I Enables MSCs to Evade NK-Cell-Mediated Cytotoxicity and Exert Immunosuppressive Activity. *Stem Cells, 40*(9), 870-882. doi:10.1093/stmcls/sxac043

Okubo, Y., Bessho, K., Fujimura, K., Iizuka, T., & Miyatake, S. I. (2001). In vitro and in vivo studies of a bone morphogenetic protein-2 expressing adenoviral vector. *J Bone Joint Surg Am, 83-A Suppl 1*(Pt 2), S99-104.

Pae, A., Lee, H., Noh, K., & Woo, Y. H. (2014). Cell attachment and proliferation of bone marrow-derived osteoblast on zirconia of various surface treatment. *J Adv Prosthodont, 6*(2), 96-102. doi:10.4047/jap.2014.6.2.96

Panzavolta, S., Torricelli, P., Bracci, B., Fini, M., & Bigi, A. (2009). Alendronate and Pamidronate calcium phosphate bone cements: Setting properties and in vitro response of osteoblast and osteoclast cells. *Journal of Inorganic Biochemistry, 103*(1), 101-106. doi:https://doi.org/10.1016/j.jinorgbio.2008.09.012

Patil, S., Gao, Y. G., Lin, X., Li, Y., Dang, K., Tian, Y., . . . Qian, A. R. (2019). The Development of Functional Non-Viral Vectors for Gene Delivery. *Int J Mol Sci, 20*(21). doi:10.3390/ijms20215491

Perić Kačarević, Z., Kavehei, F., Houshmand, A., Franke, J., Smeets, R., Rimashevskiy, D., . . . Barbeck, M. (2018). Purification processes of xenogeneic bone substitutes and their impact on tissue reactions and regeneration. *The International Journal of Artificial Organs, 41*(11), 789-800. doi:10.1177/0391398818771530

Perry, C., & Rayat, A. (2021). Lentiviral Vector Bioprocessing. *Viruses, 13*(2). doi:10.3390/v13020268

Peyrin, F. (2011). Evaluation of bone scaffolds by micro-CT. *Osteoporos Int, 22*(6), 2043-2048. doi:10.1007/s00198-011-1609-y

Pham, T., Najy, A. J., & Kim, H. C. (2022). E3 ligase HUWE1 promotes PDGF D-mediated osteoblastic differentiation of mesenchymal stem cells by effecting polyubiquitination of β-PDGFR. *J Biol Chem, 298*(6), 101981. doi:10.1016/j.jbc.2022.101981

Phothichailert, S., Samoun, S., Fournier, B. P., Isaac, J., Nelwan, S. C., Osathanon, T., & Nowwarote, N. (2024). MSCs-Derived Decellularised Matrix: Cellular Responses and Regenerative Dentistry. *Int Dent J*. doi:10.1016/j.identj.2024.02.011

Pietrzak, W. S., Woodell-May, J., & McDonald, N. (2006). Assay of bone morphogenetic protein-2, -4, and -7 in human demineralized bone matrix. *J Craniofac Surg, 17*(1), 84-90. doi:10.1097/01.scs.0000179745.91165.73

Poilliot, A., Gay-Dujak, M. H., & Müller-Gerbl, M. (2023). The quantification of 3D-trabecular architecture of the fourth cervical vertebra using CT osteoabsorptiometry and micro-CT. *J Orthop Surg Res, 18*(1), 297. doi:10.1186/s13018-023-03760-2

Poon, B., Kha, T., Tran, S., & Dass, C. R. (2016). Bone morphogenetic protein-2 and bone therapy: successes and pitfalls. *J Pharm Pharmacol, 68*(2), 139-147. doi:10.1111/jphp.12506

Poursamar, S. A., Hatami, J., Lehner, A. N., da Silva, C. L., Ferreira, F. C., & Antunes, A. P. M. (2015). Gelatin porous scaffolds fabricated using a modified gas foaming technique: Characterisation and cytotoxicity assessment. *Materials Science and Engineering: C, 48*, 63-70. doi:https://doi.org/10.1016/j.msec.2014.10.074

Prasopthum, A., Cooper, M., Shakesheff, K. M., & Yang, J. (2019). Three-Dimensional Printed Scaffolds with Controlled Micro-/Nanoporous Surface Topography Direct Chondrogenic and Osteogenic Differentiation of Mesenchymal Stem Cells. *ACS Appl Mater Interfaces, 11*(21), 18896-18906. doi:10.1021/acsami.9b01472

Pulix, M., Lukashchuk, V., Smith, D. C., & Dickson, A. J. (2021). Molecular characterization of HEK293 cells as emerging versatile cell factories. *Curr Opin Biotechnol, 71*, 18-24. doi:10.1016/j.copbio.2021.05.001

Qian, J. J., & Bhatnagar, R. S. (1996). Enhanced cell attachment to anorganic bone mineral in the presence of a synthetic peptide related to collagen. *Journal of Biomedical Materials Research, 31*(4), 545-554. doi:10.1002/(SICI)1097-4636(199608)31:4<545::AID-JBM15>3.0.CO;2-F

Qin, J. Y., Zhang, L., Clift, K. L., Hulur, I., Xiang, A. P., Ren, B. Z., & Lahn, B. T. (2010). Systematic comparison of constitutive promoters and the doxycycline-inducible promoter. *PLoS One, 5*(5), e10611. doi:10.1371/journal.pone.0010611

Qing, W., Guang-Xing, C., Lin, G., & Liu, Y. (2012). The osteogenic study of tissue engineering bone with BMP2 and BMP7 gene-modified rat adipose-derived stem cell. *J Biomed Biotechnol, 2012*, 410879. doi:10.1155/2012/410879

Quero, R. F., Domingos da Silveira, G., Fracassi da Silva, J. A., & Jesus, D. P. (2021). Understanding and improving FDM 3D printing to fabricate high-resolution and optically transparent microfluidic devices. *Lab Chip, 21*(19), 3715-3729. doi:10.1039/d1lc00518a

Rajendran Royan, N. R., Leong, J. S., Chan, W. N., Tan, J. R., & Shamsuddin, Z. S. B. (2021). Current State and Challenges of Natural Fibre-Reinforced Polymer Composites as Feeder in FDM-Based 3D Printing. *Polymers (Basel), 13*(14). doi:10.3390/polym13142289

Reddi, A. H., & Huggins, C. (1972). Biochemical sequences in the transformation of normal fibroblasts in adolescent rats. *Proc Natl Acad Sci U S A, 69*(6), 1601-1605. doi:10.1073/pnas.69.6.1601

Ripamonti, U. (2017). Biomimetic Functionalized Surfaces and the Induction of Bone Formation. *Tissue Eng Part A, 23*(21-22), 1197-1209. doi:10.1089/ten.tea.2017.0321

Rogers, M. B., Shah, T. A., & Shaikh, N. N. (2015). Turning Bone Morphogenetic Protein 2 (BMP2) on and off in Mesenchymal Cells. *J Cell Biochem, 116*(10), 2127-2138. doi:10.1002/jcb.25164

Safari, B., Davaran, S., & Aghanejad, A. (2021). Osteogenic potential of the growth factors and bioactive molecules in bone regeneration. *Int J Biol Macromol, 175*, 544-557. doi:10.1016/j.ijbiomac.2021.02.052

Samsonraj, R. M., Raghunath, M., Nurcombe, V., Hui, J. H., van Wijnen, A. J., & Cool, S. M. (2017). Concise Review: Multifaceted Characterization of Human Mesenchymal Stem Cells for Use in Regenerative Medicine. *Stem Cells Transl Med, 6*(12), 2173-2185. doi:10.1002/sctm.17-0129

Sarem, M., Moztarzadeh, F., Mozafari, M., & Shastri, V. P. (2013). Optimization strategies on the structural modeling of gelatin/chitosan scaffolds to mimic human meniscus tissue. *Mater Sci Eng C Mater Biol Appl, 33*(8), 4777-4785. doi:10.1016/j.msec.2013.07.036

Satoh, T., & Manel, N. (2013). Gene transduction in human monocyte-derived dendritic cells using lentiviral vectors. *Methods Mol Biol, 960*, 401-409. doi:10.1007/978-1-62703-218-6_30

Savolainen, S., Usenius, J. P., & Hernesniemi, J. (1994). Iliac crest versus artificial bone grafts in 250 cervical fusions. *Acta Neurochirurgica, 129*(1-2), 54-57. doi:10.1007/bf01400873

Selden, R. F. (2001). Transfection using DEAE-dextran. *Curr Protoc Immunol, Chapter 10*, 10.14.11-10.14.16. doi:10.1002/0471142735.im1014s03

Seshima, H., Yoshinari, M., Takemoto, S., Hattori, M., Kawada, E., Inoue, T., & Oda, Y. (2006). Control of bisphosphonate release using hydroxyapatite granules. *J Biomed Mater Res B Appl Biomater, 78*(2), 215-221. doi:10.1002/jbm.b.30446

Shard, A. G., & Tomlins, P. E. (2006). Biocompatibility and the efficacy of medical implants. *Regen Med, 1*(6), 789-800. doi:10.2217/17460751.1.6.789

Shi, X., He, L., Zhang, S. M., & Luo, J. (2021). Human iPS Cell-derived Tissue Engineered Vascular Graft: Recent Advances and Future Directions. *Stem Cell Rev Rep, 17*(3), 862-877. doi:10.1007/s12015-020-10091-w

Shi, Y., He, R., Deng, X., Shao, Z., Deganello, D., Yan, C., & Xia, Z. (2020). Three-dimensional biofabrication of an aragonite-enriched self-hardening bone graft substitute and assessment of its osteogenicity in vitro and in vivo. *Biomater Transl, 1*(1), 69-81. doi:10.3877/cma.j.issn.2096-112X.2020.01.007

Shi, Y., Pan, T., Zhu, W., Yan, C., & Xia, Z. (2020). Artificial bone scaffolds of coral imitation prepared by selective laser sintering. *J Mech Behav Biomed Mater, 104*, 103664. doi:10.1016/j.jmbbm.2020.103664

Shor, L., Güçeri, S., Chang, R., Gordon, J., Kang, Q., Hartsock, L., . . . Sun, W. (2009). Precision extruding deposition (PED) fabrication of polycaprolactone (PCL) scaffolds for bone tissue engineering. *Biofabrication, 1*(1), 015003. doi:10.1088/1758-5082/1/1/015003

Singh, A., Tiwari, A., Bajpai, J., & Bajpai, A. K. (2018). 3 - Polymer-Based Antimicrobial Coatings as Potential Biomaterials: From Action to Application. In A. Tiwari (Ed.), *Handbook of Antimicrobial Coatings* (pp. 27-61): Elsevier.

Singh, N., Qutub, S., & Khashab, N. M. (2021). Biocompatibility and biodegradability of metal organic frameworks for biomedical applications. *J Mater Chem B, 9*(30), 5925-5934. doi:10.1039/d1tb01044a

Siqueira, E. B., & Kranzler, L. I. (1982). Cervical interbody fusion using calf bone. *Surgical Neurology, 18*(1), 37-39. doi:10.1016/0090-3019(82)90010-6

Skog, M., Sivlér, P., Steinvall, I., Aili, D., Sjöberg, F., & Elmasry, M. (2019). The Effect of Enzymatic Digestion on Cultured Epithelial Autografts. *Cell Transplant, 28*(5), 638-644. doi:10.1177/0963689719833305

Stamnitz, S., & Klimczak, A. (2021). Mesenchymal Stem Cells, Bioactive Factors, and Scaffolds in Bone Repair: From Research Perspectives to Clinical Practice. *Cells, 10*(8). doi:10.3390/cells10081925

Stender, S., Murphy, M., O'Brien, T., Stengaard, C., Ulrich-Vinther, M., Søballe, K., & Barry, F. (2007). Adeno-associated viral vector transduction of human mesenchymal stem cells. *Eur Cell Mater, 13*, 93-99; discussion 99. doi:10.22203/ecm.v013a10

Suarez, C. E., & McElwain, T. F. (2010). Transfection systems for Babesia bovis: a review of methods for the transient and stable expression of exogenous genes. *Vet Parasitol, 167*(2-4), 205-215. doi:10.1016/j.vetpar.2009.09.022

Sum, C. H., Shortall, S. M., Wong, S., & Wettig, S. D. (2018). Non-viral Gene Delivery. *Exp Suppl, 110*, 3-68. doi:10.1007/978-3-319-78259-1_2

Sun, J., Lyu, J., Xing, F., Chen, R., Duan, X., & Xiang, Z. (2020). A biphasic, demineralized, and Decellularized allograft bone-hydrogel scaffold with a cell-based BMP-7 delivery system for osteochondral defect regeneration. *J Biomed Mater Res A, 108*(9), 1909-1921. doi:10.1002/jbm.a.36954

Szostakowski, B., & DeMaio, M. (2020). Ideal xenograft or a perfect bone substitute?-A retrospective review and analysis of the historical concept of ivory implants in orthopaedics. *Int Orthop, 44*(5), 1003-1009. doi:10.1007/s00264-020-04483-3

Takahashi, Y., & Tabata, Y. (2004). Effect of the fiber diameter and porosity of non-woven PET fabrics on the osteogenic differentiation of mesenchymal stem cells. *Journal of Biomaterials Science, Polymer Edition, 15*(1), 41-57. doi:10.1163/156856204322752228

Talbi, M., Carrie, F., & Meley, M. (2006). [Bisphosphonate-related bilateral mandibular osteochemonecrosis with pathological fracture of the horizontal ramus]. *Rev Stomatol Chir Maxillofac, 107*(5), 400-402. doi:10.1016/s0035-1768(06)77074-7

Tamm, C., Kadekar, S., Pijuan-Galitó, S., & Annerén, C. (2016). Fast and Efficient Transfection of Mouse Embryonic Stem Cells Using Non-Viral Reagents. *Stem Cell Rev Rep, 12*(5), 584-591. doi:10.1007/s12015-016-9673-5

Tanaka-Kamioka, K., Kamioka, H., Ris, H., & Lim, S.-S. (1998). Osteocyte Shape Is Dependent on Actin Filaments and Osteocyte Processes Are Unique Actin-Rich Projections. *Journal of Bone and Mineral Research, 13*(10), 1555-1568. doi:https://doi.org/10.1359/jbmr.1998.13.10.1555

Thavornyutikarn, B., Chantarapanich, N., Sitthiseripratip, K., Thouas, G. A., & Chen, Q. (2014). Bone tissue engineering scaffolding: computer-aided scaffolding techniques. *Prog Biomater, 3*, 61-102. doi:10.1007/s40204-014-0026-7

Tjempakasari, A., Suroto, H., & Santoso, D. (2021). Mesenchymal Stem Cell Senescence and Osteogenesis. *Medicina (Kaunas), 58*(1). doi:10.3390/medicina58010061

Truong, D. J., Kühner, K., Kühn, R., Werfel, S., Engelhardt, S., Wurst, W., & Ortiz, O. (2015). Development of an intein-mediated split-Cas9 system for gene therapy. *Nucleic Acids Res, 43*(13), 6450-6458. doi:10.1093/nar/gkv601

Tsuruga, E., Takita, H., Itoh, H., Wakisaka, Y., & Kuboki, Y. (1997). Pore Size of Porous Hydroxyapatite as the Cell-Substratum Controls BMP-Induced Osteogenesis1. *The Journal of Biochemistry, 121*(2), 317-324. doi:10.1093/oxfordjournals.jbchem.a021589

Turco, G., Porrelli, D., Marsich, E., Vecchies, F., Lombardi, T., Stacchi, C., & Di Lenarda, R. (2018). Three-Dimensional Bone Substitutes for Oral and Maxillofacial Surgery: Biological and Structural Characterization. *J Funct Biomater, 9*(4). doi:10.3390/jfb9040062

Tzameli, I., Fang, H., Ollero, M., Shi, H., Hamm, J. K., Kievit, P., . . . Flier, J. S. (2004). Regulated Production of a Peroxisome Proliferator-activated Receptor-γ Ligand during an Early Phase of Adipocyte Differentiation in 3T3-L1 Adipocytes*. *Journal of Biological Chemistry, 279*(34), 36093-36102. doi:https://doi.org/10.1074/jbc.M405346200

Ullah, M., Liu, D. D., & Thakor, A. S. (2019). Mesenchymal Stromal Cell Homing: Mechanisms and Strategies for Improvement. *iScience, 15*, 421-438. doi:10.1016/j.isci.2019.05.004

Urist, M. R. (1965). Bone: formation by autoinduction. *Science, 150*(3698), 893-899. doi:10.1126/science.150.3698.893

Vallejo, L. F., Brokelmann, M., Marten, S., Trappe, S., Cabrera-Crespo, J., Hoffmann, A., . . . Rinas, U. (2002). Renaturation and purification of bone morphogenetic protein-2 produced as inclusion bodies in high-cell-density cultures of recombinant Escherichia coli. *J Biotechnol, 94*(2), 185-194. doi:10.1016/s0168-1656(01)00425-4

Valtanen, R. S., Yang, Y. P., Gurtner, G. C., Maloney, W. J., & Lowenberg, D. W. (2021). Synthetic and Bone tissue engineering graft substitutes: What is the future? *Injury, 52 Suppl 2*, S72-s77. doi:10.1016/j.injury.2020.07.040

van der Linden, J. C., Birkenhäger-Frenkel, D. H., Verhaar, J. A., & Weinans, H. (2001). Trabecular bone's mechanical properties are affected by its non-uniform mineral distribution. *J Biomech, 34*(12), 1573-1580. doi:10.1016/s0021-9290(01)00146-4

Van Lieshout, E. M., & Alt, V. (2016). Bone graft substitutes and bone morphogenetic proteins for osteoporotic fractures: what is the evidence? *Injury, 47 Suppl 1*, S43-46. doi:10.1016/s0020-1383(16)30011-0

Verdera, H. C., Kuranda, K., & Mingozzi, F. (2020). AAV Vector Immunogenicity in Humans: A Long Journey to Successful Gene Transfer. *Mol Ther, 28*(3), 723-746. doi:10.1016/j.ymthe.2019.12.010

Vijayavenkataraman, S., Kuan, L. Y., & Lu, W. F. (2020). 3D-printed ceramic triply periodic minimal surface structures for design of functionally graded bone implants. *Materials & Design, 191*, 108602. doi:https://doi.org/10.1016/j.matdes.2020.108602

Viljanen, V. V., Gao, T. J., Marttinen, A., & Lindholm, T. S. (1996). Partial purification and characterization of bone morphogenetic protein from bone matrix of the premature moose (Alces alces): degradation of bone-inducing activity during storage. *Eur Surg Res, 28*(6), 447-460. doi:10.1159/000129490

Virk, M. S., Conduah, A., Park, S. H., Liu, N., Sugiyama, O., Cuomo, A., . . . Lieberman, J. R. (2008). Influence of short-term adenoviral vector and prolonged lentiviral vector mediated bone morphogenetic protein-2 expression on the quality of bone repair in a rat femoral defect model. *Bone, 42*(5), 921-931. doi:10.1016/j.bone.2007.12.216

Volarevic, V., Markovic, B. S., Gazdic, M., Volarevic, A., Jovicic, N., Arsenijevic, N., . . . Stojkovic, M. (2018). Ethical and Safety Issues of Stem Cell-Based Therapy. *Int J Med Sci, 15*(1), 36-45. doi:10.7150/ijms.21666

Wang, L., Xu, W., Chen, Y., & Wang, J. (2019). Alveolar bone repair of rhesus monkeys by using BMP-2 gene and mesenchymal stem cells loaded three-dimensional printed bioglass scaffold. *Scientific Reports, 9*. doi:10.1038/s41598-019-54551-x

Wang, S., Shi, Z. a., Liu, L., Zhou, X., Zhu, L., & Hao, Y. (2020). The design of Ti6Al4V Primitive surface structure with symmetrical gradient of pore size in biomimetic bone scaffold. *Materials & Design, 193*, 108830. doi:https://doi.org/10.1016/j.matdes.2020.108830

Wang, S., Zhao, S., Yu, J., Gu, Z., & Zhang, Y. (2022). Advances in Translational 3D Printing for Cartilage, Bone, and Osteochondral Tissue Engineering. *Small, 18*(36), e2201869. doi:10.1002/smll.202201869

Weaver, C. M., Bischoff-Ferrari, H. A., & Shanahan, C. J. (2019). Cost-benefit analysis of calcium and vitamin D supplements. *Arch Osteoporos, 14*(1), 50. doi:10.1007/s11657-019-0589-y

Wehrli, F. W., Song, H. K., Saha, P. K., & Wright, A. C. (2006). Quantitative MRI for the assessment of bone structure and function. *NMR Biomed, 19*(7), 731-764. doi:10.1002/nbm.1066

Wei, F., Zhou, Y., Wang, J., Liu, C., & Xiao, Y. (2017). The Immunomodulatory Role of BMP-2 on Macrophages to Accelerate Osteogenesis. *Tissue Engineering Part A, 24*(7-8), 584-594. doi:10.1089/ten.tea.2017.0232

White, A., & Wallis, G. (2001). Endochondral ossification: a delicate balance between growth and mineralisation. *Curr Biol, 11*(15), R589-591. doi:10.1016/s0960-9822(01)00359-1

Wilkinson, J. M., & Little, D. G. (2011). Bisphosphonates in orthopedic applications. *Bone, 49*(1), 95-102. doi:10.1016/j.bone.2011.01.009

Willershausen, I., Wolf, T., Kasaj, A., Weyer, V., Willershausen, B., & Marroquin, B. B. (2013). Influence of a bioceramic root end material and mineral trioxide aggregates on fibroblasts and osteoblasts. *Archives of Oral Biology, 58*(9), 1232-1237. doi:https://doi.org/10.1016/j.archoralbio.2013.04.002

Wilson, C. E., Dhert, W. J., Van Blitterswijk, C. A., Verbout, A. J., & De Bruijn, J. D. (2002). Evaluating 3D bone tissue engineered constructs with different seeding densities using the alamarBlue assay and the effect on in vivo bone formation. *J Mater Sci Mater Med, 13*(12), 1265-1269. doi:10.1023/a:1021139415528

Wozney, J. M., Rosen, V., Celeste, A. J., Mitsock, L. M., Whitters, M. J., Kriz, R. W., . . . Wang, E. A. (1988). Novel regulators of bone formation: molecular clones and activities. *Science, 242*(4885), 1528-1534. doi:10.1126/science.3201241

Wu, J., Matthias, N., Bhalla, S., & Darabi, R. (2021). Evaluation of the Therapeutic Potential of Human iPSCs in a Murine Model of VML. *Mol Ther, 29*(1), 121-131. doi:10.1016/j.ymthe.2020.09.012

Wu, Z., Yang, H., & Colosi, P. (2010). Effect of genome size on AAV vector packaging. *Mol Ther, 18*(1), 80-86. doi:10.1038/mt.2009.255

Xia, Z., Locklin, R. M., & Triffitt, J. T. (2008). Fates and osteogenic differentiation potential of human mesenchymal stem cells in immunocompromised mice. *Eur J Cell Biol, 87*(6), 353-364. doi:10.1016/j.ejcb.2008.02.013

Xia, Z., Ye, H., Locklin, R. M., Ferguson, D. J., Cui, Z., & Triffitt, J. T. (2005). Efficient characterisation of human cell-bioceramic interactions in vitro and in vivo by using enhanced GFP-labelled mesenchymal stem cells. *Biomaterials, 26*(29), 5790-5800. doi:10.1016/j.biomaterials.2005.02.018

Xiao, D., Yang, Y., Su, X., Wang, D., & Sun, J. (2013). An integrated approach of topology optimized design and selective laser melting process for titanium implants materials. *Bio-Medical Materials and Engineering, 23*, 433-445. doi:10.3233/BME-130765

Xiao, F., & Yin, X. (2016). Geometry models of porous media based on Voronoi tessellations and their porosity–permeability relations. *Computers & Mathematics with Applications, 72*(2), 328-348. doi:https://doi.org/10.1016/j.camwa.2015.09.009

Xin, Y., Li, N., Huang, Y., Cui, W., Liu, S., Xu, X., & Zhang, Z. (2013). [Primary culture and multiple differentiation potency of mesenchymal stem cells from human umbilical cord]. *Xi Bao Yu Fen Zi Mian Yi Xue Za Zhi, 29*(10), 1087-1093.

Xiong, Z., Yan, Y., Wang, S., Zhang, R., & Zhang, C. (2002). Fabrication of porous scaffolds for bone tissue engineering via low-temperature deposition. *Scripta Materialia, 46*(11), 771-776. doi:https://doi.org/10.1016/S1359-6462(02)00071-4

Yakar, S., Werner, H., & Rosen, C. J. (2018). Insulin-like growth factors: actions on the skeleton. *J Mol Endocrinol, 61*(1), T115-t137. doi:10.1530/jme-17-0298

Yan, C., Hao, L., Hussein, A., & Young, P. (2015). Ti–6Al–4V triply periodic minimal surface structures for bone implants fabricated via selective laser melting. *Journal of the Mechanical Behavior of Biomedical Materials, 51*, 61-73. doi:https://doi.org/10.1016/j.jmbbm.2015.06.024

Yang, X., Wen, X., Dai, J., Chen, Y., Ding, W., Wang, J., . . . Ruan, G. (2022). Probing the Intracellular Delivery of Nanoparticles into Hard-to-Transfect Cells. *ACS Nano, 16*(6), 8751-8765. doi:10.1021/acsnano.1c07648

Yin, H., Kanasty, R. L., Eltoukhy, A. A., Vegas, A. J., Dorkin, J. R., & Anderson, D. G. (2014). Non-viral vectors for gene-based therapy. *Nat Rev Genet, 15*(8), 541-555. doi:10.1038/nrg3763

Zhang, C., Han, X., Liu, J., Chen, L., Lei, Y., Chen, K., . . . Wang, Q. F. (2022). Single-cell Transcriptomic Analysis Reveals the Cellular Heterogeneity of Mesenchymal Stem Cells. *Genomics Proteomics Bioinformatics, 20*(1), 70-86. doi:10.1016/j.gpb.2022.01.005

Zhang, G., Li, J., Li, J., Zhou, X., & Wang, A. (2019). Structure and properties of a personalized bio-fixed implant prepared with selective laser melting. *Comput Methods Biomech Biomed Engin, 22*(13), 1034-1042. doi:10.1080/10255842.2019.1616085

Zhang, H., Tang, X., Wang, C., & Sun, L. (2018). AB0063 High-efficiency transduction of mesenchymal stem cells by aav2/dj vector for their potential use in autoimmune diseases. *Annals of the Rheumatic Diseases, 77*(Suppl 2), 1230-1230. doi:10.1136/annrheumdis-2018-eular.5014

Zhang, J., Wehrle, E., Rubert, M., & Müller, R. (2021). 3D Bioprinting of Human Tissues: Biofabrication, Bioinks, and Bioreactors. *Int J Mol Sci, 22*(8). doi:10.3390/ijms22083971

Zhang, X.-Y., Yan, X.-C., Fang, G., & Liu, M. (2020). Biomechanical influence of structural variation strategies on functionally graded scaffolds constructed with triply periodic minimal surface. *Additive Manufacturing, 32*, 101015. doi:https://doi.org/10.1016/j.addma.2019.101015

Zhang, Y., Cheng, N., Miron, R., Shi, B., & Cheng, X. (2012). Delivery of PDGF-B and BMP-7 by mesoporous bioglass/silk fibrin scaffolds for the repair of osteoporotic defects. *Biomaterials, 33*(28), 6698-6708. doi:https://doi.org/10.1016/j.biomaterials.2012.06.021

Zheng, S., Li, J., Jing, X., & Gong, Z. (2020). Parameterized design and fabrication of porous bone scaffolds for the repair of cranial defects. *Medical Engineering & Physics, 81*, 39-46. doi:https://doi.org/10.1016/j.medengphy.2020.05.002